^{229m}Th($3/2^+$, 3.5 eV) and a check of the exponentiality of the decay law

A. M. Dykhne[a)] and E. V. Tkalya[b)]
Scientific-Research Institute of Nuclear Physics, M. V. Lomonosov Moscow State University, 119899 Moscow, Russia

(Submitted 6 March 1998)
Pis'ma Zh. Éksp. Teor. Fiz. **67**, No. 8, 521–525 (25 April 1998)

A new object is proposed for checking the exponentiality of the decay law of an isolated metastable state at long times — the anomalously low-lying level $3/2^+(3.5\pm 0.5$ eV) in ^{229}Th. Highly efficient excitation of this level by laser radiation in combination with optimal collection of optical photons emitted in an isomeric transition make it possible to achieve measurement times longer than $50T_{1/2}$. © *1998 American Institute of Physics.* [S0021-3640(98)00108-X]

PACS numbers: 27.90.+b, 23.40.−s, 23.60.+e, 23.50.+z

Verification of the main predictions of quantum mechanics, including the exponentiality of the decay law of an isolated metastable state, is still an important problem of modern physics. This problem is of interest because, first, opinions about the temporal evolution of an isolated quasistationary state at long and very short times differ.[1–6] Second, the decay may be tied in with a number of fundamental phenomena, such as, in particular, decay of the proton,[7] double β decay,[8] tunneling,[9] the quantum Zeno effect, and others. Third, the behavior of the decay curve could be of critical importance for some physical theories, for example, Prigogine's evolutionary quantum mechanics[5] (see the discussion in Ref. 6) or Bohm's interpretation of quantum mechanics based on the idea of hidden variables.[10,3]

In the present letter we shall not be concerned with different controversial aspects of this problem. They are expounded in detail in numerous articles and reviews (see Refs. 6 and 11–13 and the references cited therein). The subject of the present letter is to present a new object for investigating the decay law at times longer than have been achieved experimentally to date.

Very long-time measurements of the decay curve have been performed since the discovery of radioactivity. The organization of each new experiment or the identification of a nucleus suitable for measurements of this type is of great interest.

The most prolonged measurements of the decay curve of an isolated quasistationary state have been performed on ^{222}Rn, ^{56}Mn, and ^{116}In nuclei. In 1911, while performing observations of α decay in ^{222}Rn(0^+, 0.0, 3.82 days), Rutherford[14] traced the exponentiality of the decay law up to $27T_{1/2}$ ($T_{1/2}$ is the half-life). In 1972 Butt and Wilson[15] performed measurements on ^{222}Rn up to $40T_{1/2}$. Two experiments were performed with the β^--decaying nucleus ^{56}Mn (3^+, 0.0, 2.58 h): In 1962 Winter[3] continued measurements up to $34T_{1/2}$, and in 1988 Norman *et al.*[16] performed measurements up to $45T_{1/2}$.

Finally, in 1984 Gopych *et al.*[17] reported observations of the β^- decay of ^{116m}In (5^+, 127 keV, 54.3 min) for $33T_{1/2}$. No deviations of the decay curve from exponentiality were found. The decays were measured by detecting high-energy γ rays ($\simeq 1-2$ MeV) from the daughter nuclei.

The problems which inevitably appear in experiments of this kind are described in detail in Ref. 6. They are mainly associated with the production of a high-activity sample in a nuclear reactor over a time of the order of $T_{1/2}$, the radiochemical purification of the sample, and the detection of radiation in the initial and final stages of the experiment. (Because the signal changes by more than 10 orders of magnitude over the measurement time, special measures must be taken in order to shield the detector and personnel from the intense radiation at the beginning of the experiment, and the sample must be ultrapure — no other radioactive impurities can be present — in order to distinguish the signal above the background at the final stage of the measurements.) A substantial advance in these directions can be made by using ^{229}Th with its unique isomeric state with excitation energy 3.5 ± 0.5 eV.[18,19]

Let us consider as an example a sample containing 10^{-3} g ^{229}Th ($\simeq 2.6\times 10^{18}$ nuclei) in the form of one of the possible chemical compounds which are transparent in the near-UV range. The excitation of a large number of isomers can be accomplished by using laser radiation with a suitable wavelength.[20] The reduced probability of a nuclear $M1$ transition from the ground to an isomeric state, calculated in Ref. 21 taking into account the Coriolis interaction of the rotational bands, equals $0.057\mu_N^2$, where μ_N is the nuclear magneton. The radiation width of the nuclear transition to an excited state with energy $\omega_N \approx 3.7$ eV (Ref. 19) equals 3.4×10^{-20} eV. Let us consider the simplest variant — direct photoexcitation of a nucleus by laser photons. The cross section σ of such a process using laser radiation with relative linewidth $\delta\omega_L/\omega_L \approx 10^{-5}$ and photon energy ω_L satisfying the condition $|\omega_L-\omega_N| \leqslant \delta\omega_L$ is of the order of 10^{-25} cm^2. The fraction ζ of excited nuclei can be calculated from the relation

$$\zeta = \frac{\sigma\phi}{\lambda+\sigma\phi}(1-\exp(-(\lambda+\sigma\phi)t)), \tag{1}$$

where ϕ is the laser-photon flux density, $\lambda = \ln 2/T_{1/2}$ is the isomeric decay constant, and t is the irradiation time.

In the case of exponential decay the number of counts $\mathcal{N}$ over an accumulation time of $T_{1/2}$ from the time $t_1 = nT_{1/2}$ to the time $t_2 = (n+1)T_{1/2}$, where n is an integer, can be estimated from the formula

$$\mathcal{N} = \int_{nT_{1/2}}^{(n+1)T_{1/2}} Q_0 \exp^{-\lambda t} dt = N_0^*/2^n, \tag{2}$$

where $Q_0 = \lambda N_0^*$ is the initial activity and N_0^* is the number of excited nuclei at the start of the measurements.

The principal decay channels for the state $3/2^+$ (3.5 ± 0.5 eV) are direct nuclear emission with photon energy equal to the isomeric transition energy (about 3.7 eV)[19] and an inelastic electronic bridge, in which a nucleus decays via an atomic shell in a third-order process and softer photons are emitted.[19,22] The decay channel and the lifetime of the low-lying level can be regulated by varying the chemical state of the thorium atoms.

The maximum lifetime, as was shown in Ref. 21, equals about 2.5 h for an isomeric transition having an energy of 3.7 eV and with the decay channel via the electronic bridge completely shut off. In the experiment of Ref. 19 the electronic bridge in one sample was approximately four times stronger the direct nuclear emission, while in another experiment the probabilities were comparable. Accordingly, the lifetimes of low-lying isomers in the samples should have values of 30 min and 1–1.5 h, respectively. Our estimates below will be based on these lifetimes.

If a laser with average power $P \approx 10$ W whose radiation is focused into a spot approximately 1 mm in diameter is used, it is possible to excite over a time $t \approx T_{1/2} \approx 1$ h approximately 20% of the ^{229}Th nuclei in 1 mg of matter. The activity produced in this manner will equal $\sim 10^{14}$ Bq. Even after $50T_{1/2}$ the activity of the sample will be 0.1 Bq, which over an accumulation time $t \approx T_{1/2}$ will give, according to Eq. (2), several hundreds of counts.

The obvious advantages of ^{229}Th over other nuclei include the following: 1) There is no need to use a reactor to produce a high-activity sample; 2) it is possible to obtain with laser irradiation much higher activities than have been achieved thus far; 3) it is safe to work with the sample at all stages of the measurements; 4) there is no background; 5) it is possible to work with the same sample from the beginning to the end of the measurements.

The first three points are obvious. Let us elucidate the last two. The useful signal in the decay of the isomeric state $3/2^+$ $(3.5 \pm 0.5$ eV) comes in the form of near-UV photons from the direct nuclear transition and visible and near-IR photons accompanying decay via the electronic bridge.[22,19] The ground state of ^{229}Th with respect to α-decay has a lifetime of 7880 yr. For the first few weeks after radiochemical purification there will be no α, β, or γ background from daughter products. The optical background, produced by stopping of α particles from the decay of the ^{229}Th can be easily eliminated by using a special target construction. The target can be in the form of a thin-walled optical waveguide (lightguide) filled with the active material. The lightguide wall must either be transparent to α particles or must be made of a material that does not fluoresce when α particles are stopped in it. The second variant is a target in the form of a ''sandwich'' in which the active layer is located between thin walls (for example, made of pure quartz) or films. The latter must meet the requirement is that the photons emitted in an isomeric transition in ^{229}Th must undergo total internal reflection. Such a construction makes it possible to achieve virtually complete accumulation of the useful signal at the ends of the lightguide or on the faces of the sandwich, which is very important at the final stages of the measurements. If the lightguide wall or film is transparent to α particles, then one can monitor the change in activity in the initial stage of the experiment according to the decrease in the number of 4.930 MeV α-particles,[23] which are absent in the α-decay spectrum of the ground state of ^{229}Th but are present in large numbers in the α-decay spectrum of the isomer ^{229m}Th ($3/2^+$, 3.5 eV).[23] The α decay of the low-lying state itself has no effect on the number of isomeric nuclei, since the expected lifetime for this channel exceeds 1000 yr.[23]

It is important to note that direct photoexcitation is not an optimal method for obtaining the low-lying isomer ^{229m}Th ($3/2^+$, 3.5 eV). As was shown in Ref. 20, it is possible to find a laser photon energy $\omega_L \geqslant \omega_N$ such that the cross section for excitation via a system of atomic levels, in this case acting as a sort of electronic bridge between the

laser photons and the nucleus, will be several orders of magnitude larger. The relation between λ and $\sigma\phi$ in Eq. (1) assumes the form $\lambda \ll \sigma\phi$. Accordingly, the fraction of excited nuclei becomes of the order of 1 even over a time much shorter than $T_{1/2}$. The use of just such a regime has been suggested for the production of a population inversion in a system of isomeric nuclei.[20] As far as experiments investigating the exponentiality of the decay law at long times are concerned, here this regime affords a truly unique opportunity: with the aforementioned 1 mg of Th-229, measurements can be performed up to $55T_{1/2}$, while with 10 mg it is possible to approach $60T_{1/2}$.

We underscore that we do not expect any deviations from exponentiality in the decay law at the times indicated above. According to the formulas of Ref. 2, effects of this kind in the decay of the state $3/2^+(3.5\pm 0.5$ eV) can exist at times in the range $270–290T_{1/2}$, with $T_{1/2}\simeq 0.5–2.5$ h. Nonetheless, investigations with ^{229}Th are undoubtedly of interest, since they make it possible to advance the study of the problem touched upon here on the basis of an experimental technology that is completely different from the conventional technology.

This work was supported in part by the Russian Fund for Fundamental Research under Grant 98-02-16070a, a grant from the State Scientific and Technical Program ''Physics of Quantum and Wave Processes,'' and Grant 96-15-96481 in Support of the Leading Scientific Schools.

[a)]Troitsk Institute of Innovational and Thermonuclear Studies
[b)]e-mail: tkalya@ibrae.ac.ru

[1] N. S. Krylov and V. A. Fok, Zh. Éksp. Teor. Fiz. **17**, 93 (1947).
[2] L. A. Khalfin, Zh. Éksp. Teor. Fiz. **33**, 1371 (1957) [Sov. Phys. JETP **6**, 1053 (1958)].
[3] R. G. Winter, Phys. Rev. **126**, 1152 (1962).
[4] M. I. Shirokov, Yad. Fiz. **21**, 674 (1975) [Sov. J. Nucl. Phys. **21**, 347 (1975)].
[5] I. Prigogine, *From Being to Becoming*, Freeman, San Francisco, 1980 [Russian translation, Nauka, Moscow, 1985].
[6] P. M. Gopych and I. I. Zalyubovksiĭ, Fiz. Élement. Chastitsy Atom. Yadra **19**, 785 (1988) [Sov. J. Part. Nucl. **19**, 338 (1988)].
[7] L. A. Khalfin, Phys. Lett. B **112**, 233 (1982).
[8] K. Grotz and H. V. Klapdor, Phys. Rev. C **30**, 2098 (1984).
[9] D. Bohm, Phys. Rev. **85**, 166 (1952).
[10] L. A. Khalfin, Usp. Fiz. Nauk **166**, 688 (1996).
[11] R. G. Newton Ann. Phys. **14**, 333 (1961).
[12] M. V. Terent'ev, Ann. Phys. **74**, 1 (1972).
[13] L. Fonda, G. C. Ghirardi, and A. Rimini, Rep. Prog. Phys. **41**, 587 (1978).
[14] E. Rutherford, Stizungsber. Akad. Wiss. Wien, Math.-Naturwiss, Kl., Abt. **2A 120**, 303 (1911).
[15] D. K. Butt and A. R. Wilson, J. Phys. A **5**, 1248 (1972).
[16] E. B. Norman, S. B. Gazes, S. G. Grane, and D. A. Bennett, Phys. Rev. Lett. **60**, 2246 (1988).
[17] P. M. Gopych, I. I. Zalyubovskiĭ, V. V. Sotnikov *et al.*, Yad. Fiz. **39**, 257 (1984) [Sov. J. Nucl. Phys. **39**, 159 (1984)].
[18] R. G. Helmer and C. W. Reich, Phys. Rev. C **49**, 1845 (1994).
[19] G. M. Irwin and K. H. Kim, Phys. Rev. Lett. **79**, 990 (1997).
[20] E. V. Tkalya, V. O. Varlamov, V. V. Lomonosov, and S. A. Nikulin, Phys. Scr. **53**, 296 (1996).
[21] A. M. Dykhne and E. V. Tkalya, JETP Lett. **67**, 251 (1998).
[22] V. F. Strizhov and E. V. Tkalya, Zh. Éksp. Teor. Fiz. **99**, 697 (1991) [Sov. Phys. JETP **72**, 387 (1991)].
[23] A. M. Dykhne, N. V. Eremin, and E. V. Tkalya, JETP Lett. **64**, 345 (1996).

Translated by M. E. Alferieff

Vortex dynamics in classical non-Abelian spin models

O. A. Borisenko[a)]
N. N. Bogolyubov Institute of Theoretical Physics, NASU, 252143 Kiev, Ukraine

M. N. Chernodub[b)] and F. V. Gubarev[c)]
Institute of Theoretical and Experimental Physics, 117259 Moscow, Russia

(Submitted 25 December 1997; resubmitted 16 March 1998)
Pis'ma Zh. Éksp. Teor. Fiz. **67**, No. 8, 526–530 (25 April 1998)

We discuss the Abelian vortex dynamics in the Abelian projection approach to non-Abelian spin models. We show numerically that in the three-dimensional $SU(2)$ spin model in the maximal Abelian projection the Abelian off-diagonal vortices, unlike the diagonal vortices, are not responsible for the phase transition. A generalization of the Abelian projection approach to $SU(N)$ spin models is briefly discussed. © *1998 American Institute of Physics.* [S0021-3640(98)00208-4]

PACS numbers: 12.10.−g

One of the important phenomena in spin models is mass-gap generation. This phenomenon has been intensively studied for the Abelian spin models in various space dimensions. The classic papers by Berezinskii, Kosterlitz, and Thouless[1] show that in the 2D XY model the mass-gap generation is due to the condensation of topological excitations called vortices. In a massive phase the vortices are condensed, and this leads to exponential falloff of the two-point correlation function, while for weak coupling the vortices form a dilute gas with a logarithmic long-range interaction (see Ref. 2 for a rigorous proof). In the three-dimensional XY model the condensation of vortices also leads to mass-gap generation.[3,4] In this case the situation is somewhat simpler, since one has a spontaneous breaking of the global $U(1)$ symmetry in the weak coupling phase, and vortices interact via the short-range Coulomb potential above the critical point.

The nature of mass gap in non-Abelian spin systems is still an open question despite numerous attempts to attack this problem.[5] The non-Abelian models, like to their gauge counterparts, possess a number of excitations (instantons, merons, thin and thick vortices), and it is a delicate problem to estimate their contribution to the mass gap reliably. Nevertheless, one can handle the problem, at least partially, using the gauge fixing procedure and calculating the contribution to the mass gap from configurations which the gauge fixing leaves untouched. This idea came up in an obvious way in lattice gauge models, where it has been successfully applied for studying the confinement mechanism. We put forward recently such an approach in Ref. 6, making use of the Abelian projection method.[7] After Abelian projection the non-Abelian spin system possesses Abelian symmetries and Abelian topological excitations (vortices). It is important to stress at this point that, precisely as in gauge models, the Abelian projection does not mean the restriction of the configuration space of the original non-Abelian model. The original non-

Abelian global symmetry is broken up to its maximal Abelian subgroup by appropriate gauge fixing procedure. In general, the global gauge fixing procedure is a powerful tool for investigating non-Abelian models in different regimes. Also, it has been understood for quite a long time now that this is a necessary condition for construction of the correct perturbation theory of non-Abelian models in the weak-coupling region.[8] We would like to argue that this method is also very fruitful for studying nonperturbative phenomena such as mass-gap generation.

Following this avenue, we have found the Abelian dominance[9] in the Maximal Abelian (MaA) projection[d)] of the $SU(2)$ spin model: the full mass gap (i.e., calculated from full correlation function) in the classical non-Abelian $SU(2)$ spin model is dominated by the Abelian mass gap calculated from the projected correlation function.[6] We have concluded that the Abelian degrees of freedom seem to play an important role in the mass-gap generation phenomena.

The next important question is, what is the role of Abelian topological excitations in the phenomena of the Abelian dominance? The 3D $SU(2)$ spin model possesses two types of Abelian vortices (''diagonal'' and ''off-diagonal''). The diagonal vortices were shown to be condensed in the massive phase and to form a dilute gas in the massless phase.[6] This picture is very similar to the vortex dynamics in the Abelian XY model. In this paper we study the behavior of the off-diagonal vortices across the phase transition. The generalization of the Abelian projection approach to the $SU(N)$ spin models is discussed at the end of the paper.

We study the three-dimensional $SU(2)$ spin model with the following action:

$$S=-\frac{\beta}{2}\sum_x\sum_{\mu=1}^{3}\mathrm{Tr}\,U_x U_{x+\mu}^{+}, \tag{1}$$

where U_x are the spin fields, which take values in the $SU(2)$ group, and β is the coupling constant. Action (1) is invariant under $SU_L(2)\times SU_R(2)$ global transformations, $U_x \to U_x^{(\Omega)}=\Omega_L^{+}U_x\Omega_R$, where $\Omega_{L,R}$ are the $SU(2)$ matrices.

The MaA projection for the $SU(2)$ spin theory is defined by the following maximization condition:[6]

$$\max_{\{\Omega\}} R[U^{(\Omega)}], \quad R[U]=\sum_x \mathrm{Tr}(U_x\sigma^3 U_x^{+}\sigma^3). \tag{2}$$

The functional $R[U]$ is invariant under $U_L(1)\times U_R(1)$ global transformations, $U_x \to U_x^{(\tilde{\Omega})}=\tilde{\Omega}_L^{+}U_x\tilde{\Omega}_R$, where $\tilde{\Omega}_{L,R}=e^{i\sigma^3\omega_{L,R}}$ and $\omega_{L,R}\in[0,2\pi)$. Due to the invariance of the functional R under Abelian gauge transformations, the condition (2) fixes the $SU_L(2)\times SU_R(2)$ global symmetry group up to the $U_L(1)\times U_R(1)\sim O_L(2)\times O_R(2)$ global group.

In order to fix the MaA gauge in the path integral approach we substitute the Faddeev–Popov (FP) unity

$$1=\Delta_{FP}[U;\lambda]\int D\Omega\,\exp\{\lambda R[U]\}, \quad D\Omega=D\Omega_L D\Omega_R \tag{3}$$

into the partition function of $SU(2)$ spin model. Here Δ_{FP} is the FP determinant and the limit $\lambda \to +\infty$ is assumed. The functional $R[U]$ is defined in (2). Shifting the fields $U_x \to U_x^{\Omega^+}$ and using the invariance of the FP determinant $\Delta_{FP}[U;\lambda]$, the action $S[U]$ and the Haar measure DU, we get the product of the gauge orbit volume $\int D\Omega$ and the partition function with the fixed gauge:

$$Z_{\mathrm{MaA}} = \int DU \, \exp\{-S[U] + \lambda R[U]\} \Delta_{FP}[U;\lambda]. \tag{4}$$

The limit $\lambda \to \infty$ should guarantee that all the saddle points of the invariant integral in (4) lie in the Abelian subgroup.

Let us parametrize the $SU(2)$ spin field U in the standard way: $U_x^{11} = \cos\varphi_x e^{i\theta_x}$; $U_x^{12} = \sin\varphi_x e^{i\chi_x}$; $U_x^{22} = U_x^{11,*}$; $U_x^{21} = -U_x^{12,*}$; $0 \leqslant \varphi \leqslant \pi/2$, $0 < \theta, \chi \leqslant 2\pi$. Under the $U_L(1) \times U_R(1)$ transformations defined above, the components of the field U transform as

$$\theta_x \to \theta_x' = \theta_x + \omega_d \bmod 2\pi, \quad \chi_x \to \chi_x' = \chi_x + \omega_o \bmod 2\pi, \tag{5}$$

where $\omega_{d,o} = -\omega_L \mp \omega_R$. It is convenient to decompose the residual symmetry group, $O_L(2) \times O_R(2) \sim O_d(2) \times O_o(2)$. The diagonal (off-diagonal) component θ (χ) of the $SU(2)$ spin U transforms as a spin variable with respect to the $O_d(2)$ ($O_o(2)$) symmetry group.

It is useful to consider the one-link spin action S_l in terms of the angles φ, θ, χ:

$$S_{l_{x,\mu}} = -\beta[\cos\varphi_x \cos\varphi_{x+\hat{\mu}} \cos(\theta_x - \theta_{x+\hat{\mu}}) + \sin\varphi_x \sin\varphi_{x+\hat{\mu}} \cos(\chi_x - \chi_{x+\hat{\mu}})]. \tag{6}$$

The action consists of two parts which correspond to the self-interaction of the spins θ and χ, respectively. The $SU(2)$ component φ does not behave as a spin field, and its role is to provide the interaction between the θ and χ spins. Thus the $SU(2)$ spin model in the Abelian projection reduces to two interacting copies of the XY model, with fluctuating couplings due to the dynamics of the field φ.

The phases $\theta = \arg U^{11}$ and $\chi = \arg U^{12}$ behave as $O(2)$ spins under the Abelian gauge transformation.[6] In the Abelian projection the $SU(2)$ spin model possesses two types of Abelian vortices due to the compactness of the residual Abelian group. These vortices correspond to the diagonal (θ) and to the off-diagonal (χ) Abelian spins (''diagonal'' and ''off-diagonal'' vortices, respectively).

We expect that in the MaA projection the diagonal vortices may be more dynamically important then the off-diagonal vortices. The reason for this expectation is simple. In our representation for $SU(2)$ spin field the maximizing functional (2) has the form: $R = 4\Sigma_x \cos^2\varphi_x + \mathrm{const}$. Therefore, in the MaA projection the effective coupling constant in front of the action for the θ spins is maximized, while the effective self-coupling for χ spins is minimized. Thus we may expect that the diagonal vortices may be more relevant to the dynamics of the system than the off-diagonal vortices.

The behavior of the diagonal vortices was studied numerically in Ref. 6. The diagonal Abelian vortices are condensed in the massive phase and form a dilute gas of vortex–antivortex pairs in the Coulomb phase. This behavior is very similar to the behavior of the Abelian vortices in 3D XY model,[3,4] where the vortices are known to be responsible

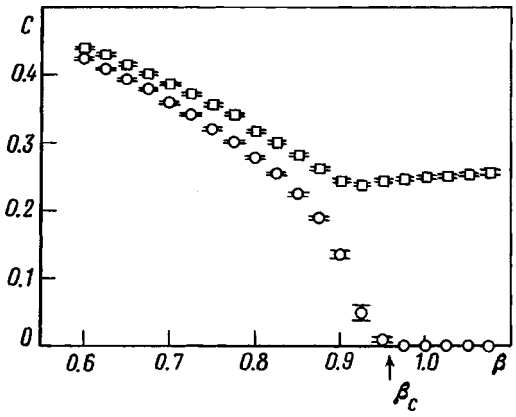

FIG. 1. The percolation probability for the diagonal (circles) and anti-diagonal (squares) Abelian vortex trajectories versus β on the 16^3 lattice. The data for diagonal vortex trajectories are taken from Ref. 6.

for the mass-gap generation. This similarity allows to conclude that the diagonal Abelian vortices in the MaA projection of the $SU(2)$ spin model are relevant degrees of freedom for the mass-gap generation.[6]

Now we proceed to study the condensation properties of the off-diagonal vortices in the MaA projection across the phase transition. First, we construct the off-diagonal vortex trajectory ${}^*j_o$ from the spin variables χ using the standard formula:[11,12] ${}^*j_o = (2\pi)^{-1} {}^*d[d\chi]$, where the square brackets stand for ''modulo 2π'' and the operator d is the lattice derivative. In three dimensions the vortex trajectories are loops which are closed by virtue of the property $d^2=0$.

The condensation of the vortex trajectories can be studied by measuring of the so-called percolation probability[4] C:

$$C = \lim_{r\to\infty} \left(\sum_{x,y,i} \delta_{x\in {}^*j_i} \delta_{y\in {}^*j_i} \delta(|x-y|-r) \right) \left(\sum_{x,y} \delta(|x-y|-r) \right)^{-1}, \tag{7}$$

where the summation is over all the vortex trajectories j_i and over all the points x,y of the lattice.

If there is a nonzero probability for two infinitely separated points to be connected by a vortex trajectory, then the quantity C is nonzero. This means that the entropy of the vortex trajectories dominates over the energy of the vortices, which means in turn that the vortex condensate exists in the vacuum. If the vortex trajectories form an ensemble of small loops (the gas of vortex–antivortex pairs) then the quantity C is obviously zero.

We studied the quantity C by numerical methods on a 16^3 lattice with periodic boundary conditions. In our numerical simulations the Wolff cluster algorithm[13] was used. To thermalize the spin fields at each value of the coupling constant β we performed a number of thermalization sweeps much greater than measured autocorrelation time.

We show the percolation probability C for both the diagonal (taken from Ref. 6) and off-diagonal vortex trajectories in Fig. 1. One can see that the percolation probability of the off-diagonal vortex trajectories does not vanish in the massless phase, unlike that of

the diagonal vortices. This allows us to conclude that the off-diagonal vortices do not play a significant role in the mass-gap generation[e)] and that the only the diagonal sector of the $SU(2)$ spin model in the MaA projection can be responsible for the mass gap.

The generalization of the MaA projection to the $SU(N)$ spin models is quite straightforward. The maximization functional is

$$R[U]=\sum_x \sum_h \mathrm{Tr}(U_x \lambda_h U_x^+ \lambda_h), \tag{8}$$

where the index h runs over the Cartan subgroup of the $SU(N)$ group, and λ_a are the generators of the $SU(N)$ group. The functional R is invariant under the $[U(1)]_L^{N-1} \times [U(1)]_R^{N-1}$ global symmetry group. The gauge-fixed partition function has the form (4). where one has to take the corresponding $SU(N)$ action and the functional $R[U]$. Now, there are $N(N+1)/2-1$ independent Abelian spin fields: $N-1$ diagonal fields and $N(N-1)/2$ off-diagonal spin fields. Therefore there are $(N-1)$ species of diagonal vortices and $N(N-1)/2$ species of off-diagonal vortices. In analogy with the $SU(2)$ spin model one can expect that the phase transition in the $SU(N)$ spin model is accompanied by the condensation of the $N-1$ species of diagonal vortices. The off-diagonal vortices should show a random distribution and should not be relevant for mass-gap generation in the $SU(N)$ spin model.

Authors are grateful to M. I. Polikarpov for fruitful discussions. M. N. C. and F. V. G. were supported by the JSPS Program on Japan—FSU Scientists Collaboration, by Grants INTAS-94-0840, INTAS–RFBR-95-0681, and by Grant No. 93-02-03609, financed by the Russian Fund for Fundamental Research.

[a)]e-mail: oleg@ap3.gluk.apc.org
[b)]e-mail: chernodub@vxitep.itep.ru
[c)]e-mail: gubarev@vxitep.itep.ru
[d)]The MaA projection was first used for study of the lattice non-Abelian gauge theories in Ref. 10.
[e)]The properties of the diagonal and off-diagonal vortices in the $SU(2)$ spin model are very similar to the properties of the monopoles and minopoles, respectively, in the MaA projection of the $SU(2)$ gluodynamics.[14]

[1] V. L. Berezinskii, Zh. Éksp. Teor. Fiz. **59**, 907 (1970) [Sov. Phys. JETP **32**, 493 (1971); J. M. Kosterlitz, D. J. Thouless, Physica C **6**, 1181 (1973).
[2] J. Fröhlich and T. Spencer, Commun. Math. Phys. **81**, 527 (1981).
[3] G. Kohring, R. E. Shrock and P. Wills, Phys. Rev. Lett. **57**, 1358 (1986).
[4] A. V. Pochinsky, M. I. Polikarpov and B. N. Yurchenko, Phys. Lett. A **154**, 194 (1991); A. Hulsebos, preprint LTH-324, http://xxx.lanl.gov/abs/hep-lat/9406016; A. Hulsebos, Nucl. Phys. B (Proc. Suppl.) **34** (Proc. Suppl.), 695 (1994); http://xxx.lanl.gov/abs/hep-lat/9311042.
[5] T. G. Kovács, Thesis of PhD Dissertation, University of California, Los Angeles, 1996; Nucl. Phys. B **482**, 613 (1996) and references therein.
[6] O. A. Borisenko, M. N. Chernodub and F. V. Gubarev, preprint KANAZAWA-97-05, http://xxx.lanl.gov/abs/hep-lat/9705010 to appear in Phys. Lett. B.
[7] G. 't Hooft, Nucl. Phys. B: Field Theory Stat. Syst. **190**[FS3], 455 (1981).
[8] P. Hasenfratz, Phys. Lett. B **141**, 385 (1984).
[9] T. Suzuki and I. Yotsuyanagi, Phys. Rev. D **42**, 4257 (1990).
[10] A. S. Kronfeld, M. L. Laursen, and G. Schierholtz, Phys. Lett. B **198**, 516 (1987); A. S. Kronfeld, G. Schierholz and U. J. Wiese, Nucl. Phys. B **293**, 461 (1987).
[11] T. Banks, R. Myerson and J. Kogut, Nucl. Phys. B **129**, 493 (1997).

[12] R. Savit, Phys. Rev. B **17**, 1340 (1978).
[13] U. Wolff, Phys. Rev. Lett. **62**, 361 (1989).
[14] M. N. Chernodub, M. I. Polikarpov and A. I. Veselov, Phys. Lett. B **342**, 303 (1995).

Published in English in the original Russian journal. Edited by Steve Torstveit.

Temporal evolution of the hydrodynamic instability of the boundary between the dense core and the plasma corona during nanosecond explosion of wires

S. Yu. Gus'kov, G. V. Ivanenkov, A. R. Mingaleev, S. A. Pikuz, and T. A. Shelkovenko
P. N. Lebedev Physical Institute, Russian Academy of Sciences, 117924 Moscow, Russia

D. A. Hammer
Laboratory of Plasma Studies, 369 Upson Hall, Cornell University, Ithaca, NY 14853 USA.

(Submitted 23 February 1998; resubmitted 7 April 1998)
Pis'ma Zh. Éksp. Teor. Fiz. **67**, No. 8, 531–536 (25 April 1998)

We report the results of investigations of the interaction of a plasma corona with a dense, cold core formed on the discharge axis in the initial stage of the nanosecond electrical explosion of metal wires. The internal structure of the dense core and the dynamics of processes occurring in it were studied by a specially developed method of multiframe x-ray shadow photography. The large observed amplitudes of the disturbances of the boundary between the dense core and the *Z*-pinch corona, which are comparable to the core radius, are attributed to the development of Rayleigh–Taylor and Kelvin–Helmholtz hydrodynamic instabilities. © *1998 American Institute of Physics.* [S0021-3640(98)00308-9]

PACS numbers: 52.80.Qj, 52.35.Bj

Despite numerous investigations of wire explosions in high-current nanosecond electrical in connection with the development of intense x-ray sources, the mechanism leading to the formation of bright plasma regions, known as hot spots, remains unclear. Existing ideas about the dynamics of the neck formed in the pinch, in the first place, do not explain the substantially different character of the discharge through an initially cold wire as compared with a discharge through a plasma channel prepared beforehand[1] and, in the second place, do not describe at all the complicated internal structure of the hot spot, which under improved resolution transforms, as a rule, into a group of several microdots $\ll 10$ μm in size, arranged along the discharge axis with a 10–100 μm spacing.[2] The existing experimental data[3] for a discharge through a wire also show a dense and relatively cold core, which exists for a quite long time.

In the present work we were able not only to observe the dense core directly but also to investigate its internal structure and the dynamics of the processes occurring during the explosion of Ti, Fe, Ni, and Cu wires. The plasma of the exploding wires was investigated by shadow photography in x-rays emitted by a small source. The 1.5–4 Å radiation sources were Pd and Mo *X* pinches, connected in series in the discharge circuit and

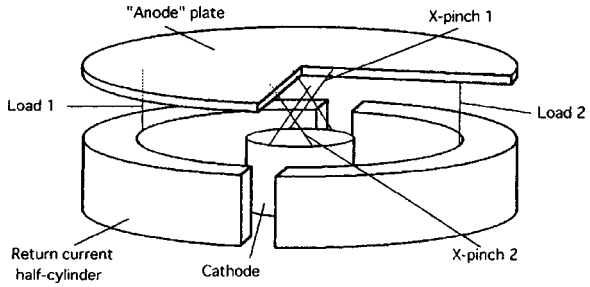

FIG. 1. Diagram of the experiment.

giving high spatial ($<1-5$ μm) and temporal (<1 ns) resolutions. The picture obtained turned out to look very much like the classic Rayleigh–Taylor instability of hydrodynamics. The instability appeared at the boundary between the dense core and the plasma corona, when the MHD shock wave formed during plasma compression interacted with the core. The macrostructure of the instability corresponded to the pinch structure of the plasma corona, while the microstructure corresponded to the fine structure of the hot spots. Theoretical estimates of the growth rate of the Rayleigh–Taylor instability agreed quite well with the observed growth rate of the nonuniformities.

1. The experiments, a diagram of which is displayed in Fig. 1, were performed on the XP pulser at Cornell University, with an output current of 480 kA and a pulse duration of 100 ns. Ordinarily, an *X* pinch[4] from molybdenum wires 17.5–25 μm in diameter was used as the radiation source for the shadow photography. The multispot nature of the emitting region[5] was greatly suppressed by placing in the diode not one but two parallel *X* pinches. The experimental wires were inserted in the return-current circuit in the gap between an insulated common anode and separate grounded half-cylinders. The currents through the wires were measured with Rogowski loops, placed on the half-cylinders. Two successive (in time) images of both wires could be obtained in each shot. For this, wires either with different diameters (for example, Mo, 25 and 17.5 μm) or made of different materials (Mo, 25 μm and Pd, 20 μm) were used in the *X* pinches. This made it possible to fix the sequence of x-ray bursts and the interval between them. Images were recorded with a magnification from 7 to 15 on Kodak RAR 2497 or Kodak GWL photographic films, which were covered with a set of Be and Ti filters. The spatial resolution was checked in reference to an image of gold grids with a 17 μm period and an opaque part 6 μm wide. The pulse duration was measured with a photoconducting diamond detector and a Tektronix 684 oscillograph with a 1 GHz bandwidth and a 5 GHz digitization frequency. In most experiments, at least one *X* pinch had a strictly one-spot structure, giving a spatial resolution of not worse than 2 μm with exposure time $<0.7-2$ ns.

Figure 2 shows images of the plasma of exploded Ti wires having an initial diameter of 50 μm. The images correspond to two points in time: 55 and 66 ns from the onset of current. The choice of material was motivated by the fact that Ti has a transmission window near the *K* absorption edge (2.5–4.0 Å) — the range of minimum sizes of the emitting region of the *X* pinch. A knot tied in the wire was used as a reference for lining up the two images in space. Developing nonuniformities in the core shape can be clearly

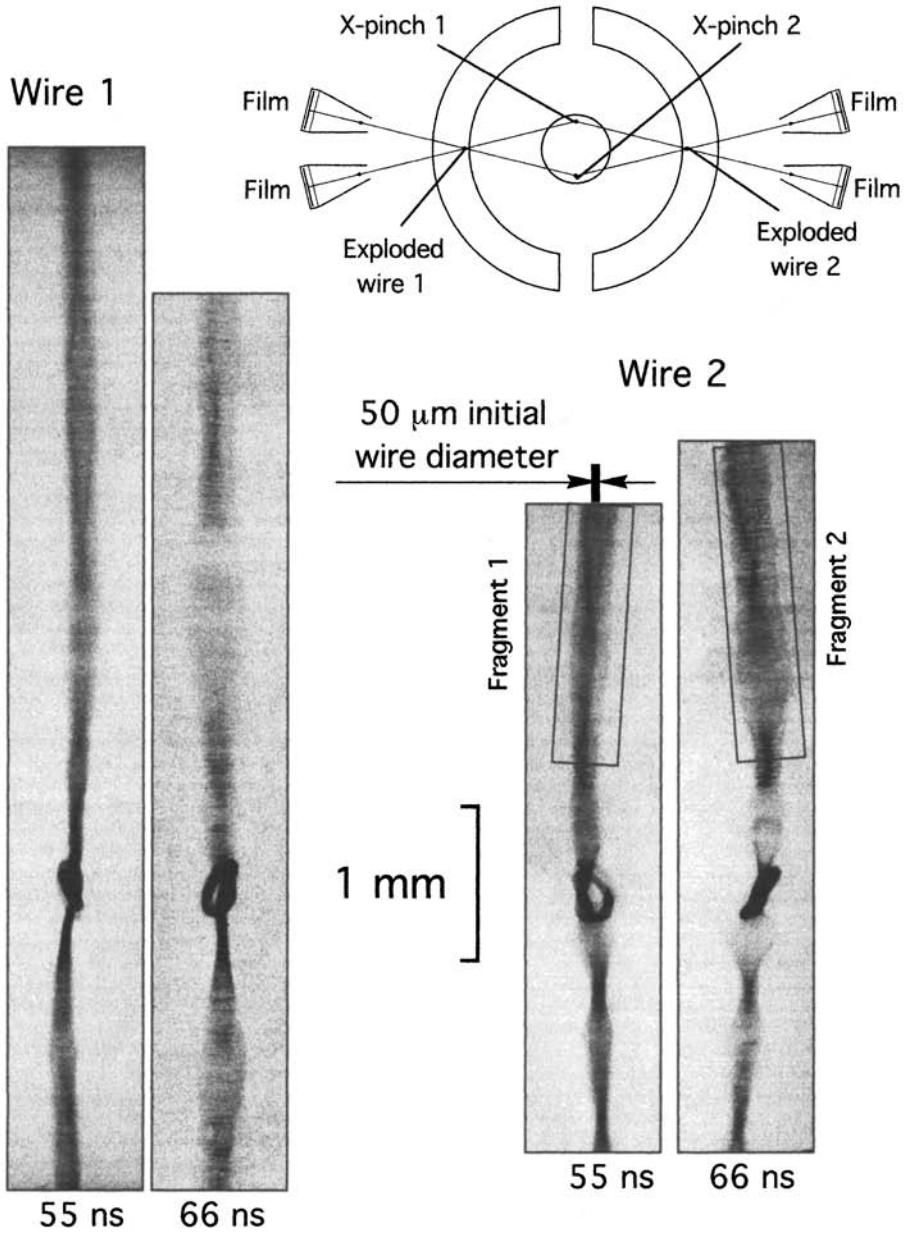

FIG. 2. Shadowgrams of exploded Ti wire plasma: cores against a background of the corona at successive times — 55 and 60 ns from current onset.

seen on both sides of the knot. The existence of two different spatial components can be easily discerned in these nonuniformities: large-scale — with a period of $\simeq 2$ mm, and small-scale — with a characteristic size of 20–30 μm. Enlarged fragments of the images are given in Fig. 3. Both the cores and their internal structure are can be clearly seen in

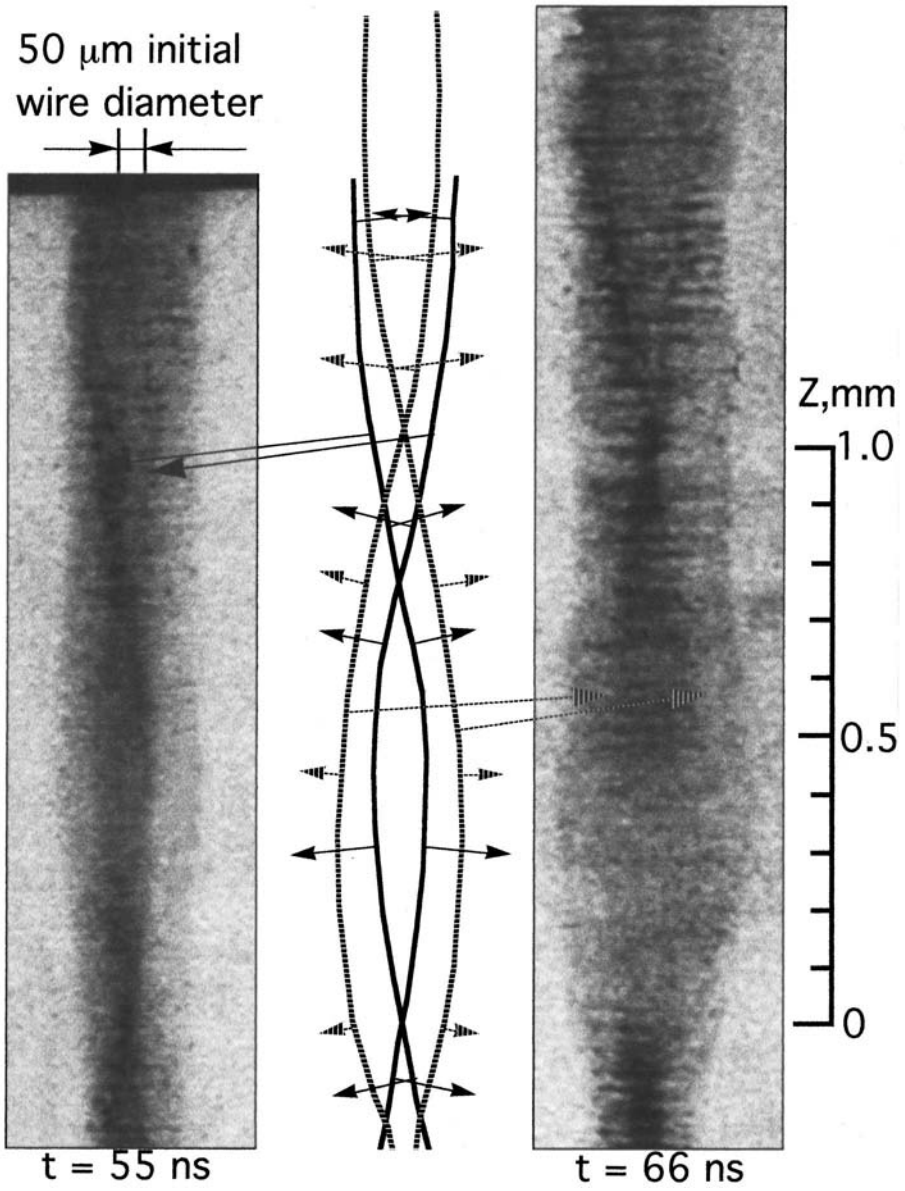

FIG. 3. Enlarged fragments of images in Fig. 2 for successive positions of the core shock fronts.

them. In the first place, a strong irregularity of the sharp (the width of the transition layer is much less than 10 μm) core–corona interface is visible; it is caused by deep penetration of narrow jets of hot plasma into the dense matter. This small-scale structure is modulated by large-scale variation of the outer ''envelope'' of the interface and a shock front propagating toward the axis. The nodes of this front, moving along the axis with time, can be clearly seen. Two fixed positions of the front, according to which the

velocity of the front can be measured — primarily the radial velocity $\simeq 5\times 10^5$ cm/s and the phase velocity of the node 2×10^6 cm/s, are shown separately at the center of the figure. A periodic succession of the sections in which the front moves toward and away from the axis can be clearly seen, and the ''choppy'' structure is pronounced only in the regions of focusing of the front, while in the expanded regions of the opposite type it is pronounced only near the nodes. This suggests that driving does not occur and that the small-scale disturbances ultimately degenerate after the shock front reflects from the axis.

2. The inevitability of the formation of a heterogeneous radial structure of the matter of an exploded fine (10–50 μm in diameter) metal wire follows directly from an analysis[1] of the initial stage of the electric explosion of a conductor whose superheated metal core undergoes intense vaporization. The estimates made in the present work show that when voltage is applied rapidly ($\simeq 10$ ns) there is enough time for the vaporization front to penetrate to the axis only if the initial diameter is very small (<5 μm). On the other hand, this diameter is limited (<50 μm) by the skin effect in the metal, and in the intermediate region one can justifiably assume that the current distribution is uniform over the cross section. Under these conditions the unvaporized metal core becomes superheated above the boiling point, creating a large Ohmic resistance. As the critical point is approached, rapid bulk ebullition occurs. In this region of parameters the conductivity of the hot metal at the center is very low (for a standard length $\simeq 1$ cm the resistance to the flow of current reaches several kΩ) and the surrounding low-density vapor, ionizing in the course of breakdown, starts to tap off current. This, together with confinement of the current in the skin layer in the subsequent expansion of the plasma formed, stops the further heating of the center, and after that the center remains relatively cold up until the arrival of the shock wave formed during compression. Ultimately, there arises a heterogeneous distribution of matter over the cross section — a central core, where the temperature does not exceed the Fermi energy, surrounded by a plasma corona.

This structure does not appear at all until the shock wave formed during the the MHD compression of the corona approaches the core. The subsequent interaction of this wave with the core, which has hitherto remained beyond the scope of existing models, in our opinion plays an important role in the formation of the hot spots. The complicated structure of the shock front in the plasma is also manifested in the core; this structure is characterized by a strong difference in the electron and ion temperatures and the existence of a wave of electron and radiational heating preceding the front.[6]

The interaction starts with the collision of the coronal plasma, undergoing compression, with the dense matter of the core, slowly expanding by inertia from the initial explosion. In hydrodynamics such a process can be described in terms of the decay of an arbitrary discontinuity:[6] Rather than having a shock wave incident from the corona side, a shock wave passing into the core and a back-reflected shock wave arise at the interface, and the interface transforms into a contact discontinuity moving toward the axis. A wave of radiation and electronic heat conduction propagates into the interior of the dense core ahead of the shock front, while the shock (which is much narrower in the dense medium of the core than in the corona) is initially still too weak and slow to be seen against the overall background of events. However, further current growth accompanied by heating of the matter in the path of the front by the heat wave converging toward the axis and by compression of the plasma by the shock wave reflected into the corona gradually intensify and accelerate the shock. The thermal pressure of the compressed corona, reaching

$\simeq 1$ Mbar, becomes sufficient for hydrodynamic compression of the central dense region. Thus, under current growth conditions all matter in the region between the shock waves in both the corona and the core is brought into accelerated motion. This creates conditions for the development of the classic Rayleigh–Taylor hydrodynamic instability of the interface, wherein the corona carrying the main current plays the role of the ''heavy'' liquid and the core plays the role of the ''light'' liquid.

The situation described above is completely analogous to the acceleration of a target by a laser pulse, when the corona heated and evaporated from the target surface accelerates the interior cold part[7] and conditions arise which support the driving of the Rayleigh–Taylor and Richtmyer–Meshkov instabilities. The appreciable smearing of the shock front in the corona suggests a quite uniform pressure distribution in the part of the corona next to the boundary. Therefore our conditions are more likely to give rise to Rayleigh–Taylor instability (quasimonotonic acceleration of higher-density matter by low-density matter) than the Richtmyer–Meshkov instability (passage of a shock wave through the boundary between media with different densities). As the experiment and calculations show, an electrical explosion of a thin wire results in the formation of a very sharp boundary between a corona with a density of 10^{-2}–10^{-1} g/cm^3 and a core with a density of about 1 g/cm^3. The Atwood number $A=(\rho_c-\rho_k)/(\rho_c+\rho_k)$, where ρ_c and ρ_k are, respectively, the core and corona densities, is close to 1, and according to Ref. 7 the linear growth rate of the Rayleigh–Taylor instability is

$$\gamma_{RT}\simeq k_z\sqrt{p_k/\rho_c} \quad \text{or} \quad \sqrt{gk_z} \tag{1}$$

(p_k is the pressure in the corona, g is the acceleration of the flow between the shock waves, and k_z is the wave number of the disturbance), depending on whether the instability is of the long- or short-wavelength type.

Let us now discuss the possible sources of the spectrum of the initial disturbances in such a hydrodynamic compression of the core matter. Possible sources are all kinds of irregularities of the initial shape of the wire, which can be estimated by the dimensions of the transverse cross section (tens of μm). A nonuniformity of the pressure distribution in the corona can arise during the vaporization and bulk ebullition of the matter at the start of the discharge (same order of magnitude) and finally during development of current instabilities of the plasma during compression of the corona (nonuniformities $\simeq 0.1$–1 mm). Thus the shortest-wavelength and most rapidly growing (see Eq. (1)) mode is associated with a wavelength of the order of the initial diameter of the wire, 20–50 μm. The wavelength $p_k/(\rho_c g)$ at which the changeover of the dependences (1) takes place also lies in this range (the values employed $(p_k/\rho_c)^{1/2}\simeq(3-8)\times 10^5$ cm/s and $g\simeq(2-5)\times 10^{13}$ cm/s^2 were taken from a numerical experiment performed with a 2D MHD code[8]). Hence we estimate the growth rate of the Rayleigh–Taylor instability as $\gamma_{RT}\simeq(2-5)\times 10^8$ s^{-1}. This shows that the boundary disturbances develop into the volume of the core over a time 2–5 ns which is quite short compared with the discharge duration, allowing them to reach depths comparable to the transverse size of the core. Ultimately, disturbances accompanied by collisions of the hot plasma flows can be expected to reach the axis. We can thereby explain the fine structure of the emission of hot plasma spots that is observed near the axis of the discharge in laboratory experiments and numerical simulations.

Let us examine this phenomenon in greater detail, assuming that the Rayleigh–Taylor instability reaches a profoundly nonlinear stage of development, where the coronal plasma jets which are formed can fall into the dense core all the way to the axis itself near the nodes of focusing of the shock wave. We characterize the flow in the jets of relatively slowly moving coronal matter by the velocity u. Under these conditions a Kelvin–Helmholtz instability with growth rate $\gamma_{KH} \simeq u k_r (\rho_k/\rho_c)^{1/2}$ can develop on the side boundaries of the jets. Taking account of the cumulation occurring as a jet moves toward the axis of a cylindrical core, the velocity can be estimated as $u \simeq r_c \gamma_{RT} (r_c/r)^2$, where $r_c \simeq 100$ μm is the initial radius of the core. Hence we find a relation between the growth rates of the instabilities

$$\gamma_{KH} \simeq \gamma_{RT} k_r r_c (\rho_k/\rho_c)^{1/2} (r_c/r)^2. \tag{2}$$

It is easy to see that the growth rates become equal to one another when a jet travels over a distance equal to approximately 2/3 of the core radius. Thus a transverse structure of the jets, vortices, and bursts of hydrodynamic turbulence can be expected to develop in regions where the coronal matter penetrates deep into the volume of the core. The induction dynamo effect engendered by these motions is capable of substantially restructuring the distribution of the magnetic field in the plasma. This and other consequences of the phenomena described require further investigation, but they undoubtedly should contribute important corrections to existing ideas about processes occurring in exploding wires.

3. The results of the present work show that the heterogeneous structure transforms exploding wires into a very interesting object for studying hydrodynamic instabilities, distinguishing it in the general class of dense pinches with the conventional ''sausage'' instability. The parameters of the matter formed are close to those of the plasma produced when a target is irradiated with intense fluxes of laser radiation, but in contrast to targets with a planar or spherical geometry, the cylindrical symmetry of a Z pinch facilitates diagnostics of the region of instability development. Pinches win over shock tubes because pinch temperatures, which are close to those in a laser experiment, make it possible to investigate the physics of instability under conditions of intense transport of heat by electrons and radiation.

The experiments performed demonstrate the strongly nonlinear character of the instability of the core–corona boundary, especially in the late stage of pinch formation. Further investigations in this direction could be very important for studying turbulent mixing, which, besides being of fundamental importance in itself, is a key problem of the plasma compression dynamics in inertial thermonuclear fusion. The results of the present work not only contribute to a deeper understanding of the processes occurring in a nanosecond wire explosion, but they also require a new formulation of the problem of MHD modeling of dense pinches.

This work was supported in part by the Sandia National Laboratory (Albuquerque, New Mexico, USA) under contract AJ-6400.

[1] G. V. Ivanenkov, A. R. Mingaleev, T. A. Novikova *et al.*, Zh. Tekh. Fiz. **65**(4), 40 (1995) [Tech. Phys. **40**, 312 (1995)].
[2] A. Bartnik, G. V. Ivanenkov, L. Karpinski *et al.*, Kvantovaya Élektron. (Moscow) **21**, 181 (1994).
[3] S. M. Zakharov, G. V. Ivanenkov, A. A. Kolomenskiĭ *et al.*, Fiz. Plazmy **9**, 469 (1983) [Sov. J. Plasma Phys. **9**, 271 (1983)]; L. E. Aranchuk, S. L. Bogolyubskiĭ, G. S. Volkov *et al.*, Fiz. Plazmy **12**, 1324 (1986) [Sov. J. Plasma Phys. **12**, 765 (1986)]; D. H. Kalantar and D. A. Hammer, Phys. Rev. Lett. **71**, 3806 (1993).

[4] T. A. Shelkovenko, S. A. Pikuz, A. R. Mingaleev, and D. A. Hammer, Bull. Am. Phys. Soc. **42**, 2051 (1997).
[5] S. A. Pikuz, B. A. Bryunetkin, G. V. Ivanenkov *et al.*, J. Quant. Spectrosc. Radiat. Transf. **51**, 291 (1994); S. A. Pikuz, T. A. Shelkovenko, V. M. Romanova *et al.*, in *Proceedings of the Fourth International Conference on Dense Z Pinches*, Vancouver, AIP, New York, 1997, p. 429.
[6] Ya. B. Zel'dovich and Yu. P. Raĭzer, *Physics of Shock Waves and High-Temperature Hydrodynamic Phenomena*, Academic Press, New York, Vols. 1 and 2, 1966, 1967 [Russian original, Nauka, Moscow, 1966].
[7] V. B. Rozanov, C. P. Verdon, V. Decroisette *et al.*, in *Energy from Inertial Fusion*, IAEA, Vienna, 1995, p. 21.
[8] G. V. Ivanenkov, A. R. Mingaleev, S. A. Pikuz *et al.*, in *Proceedings of the Fourth International Conference on Dense Z Pinches*, Vancouver, AIP, New York, 1997, p. 253.

Translated by M. E. Alferieff

Thermodiffusional stratification of a continuous microwave discharge plasma

A. L. Vikharev, A. M. Gorbachev,[a)] O. A. Ivanov, A. L. Kolysko, and O. Yu. Kuznetsov

Institute of Applied Physics, Russian Academy of Sciences, 603600 Nizhniĭ Novgorod, Russia

(Submitted 2 March 1998)
Pis'ma Zh. Éksp. Teor. Fiz. **67**, No. 8, 537–542 (25 April 1998)

We report the results of investigations of a continuous microwave discharge ignited in a quasioptical resonant cavity. We study a new phenomenon for such a discharge: a small-scale stratification of the plasma in the direction perpendicular to the electric field vector. This stratification is observed in a plasma with electron density higher than the critical density at the microwave frequency and is due to the development of a thermocurrent instability. © *1998 American Institute of Physics.* [S0021-3640(98)00408-3]

PACS numbers: 52.80.Pi, 52.35.−g

A freely localized microwave discharge in gases is attracting attention as an object of study in nonlinear physics owing to the diversity of small-scale (compared with the wavelength) structures arising as a result of the development of various instabilities in the discharge plasma.[1] A pulsed-discharge plasma is subject to ionizational (ionization–field and ionization–overheating) instabilities, while a continuous discharge is subject to an attachment instability.[2]

In the present letter we report the results of investigations of a freely localized discharge ignited in a quasioptical cavity. This scheme for producing a continuous microwave discharge makes it possible to avoid contact between the discharge plasma and the metal walls, is quite easily implemented, and makes it possible to control the plasma parameters over wide limits. We have investigated experimentally and theoretically a type of small-scale stratification of plasma in the direction perpendicular to the electric field vector that is new for microwave discharges. In contrast to the conditions for the development of the well-known ionization-field instability,[1] this stratification is observed in plasma with electron density above the critical density for the microwave radiation and, as will be shown below, is due to the appearance of a thermodiffusional electron flow.

A detailed description of the experimental apparatus is given in Ref. 3. A quasioptical cavity with $Q_0 \approx 5\times 10^3$ was excited by microwave radiation from a continuous-wave magnetron (wavelength $\lambda \approx 3$ cm, power $P_0 = 10$–200 W) in the TEM_{00q} mode. The electron density N_e was measured by the resonant-cavity method according to the shift induced in the resonance frequency of the cavity by the appearance of plasma in it.[4]

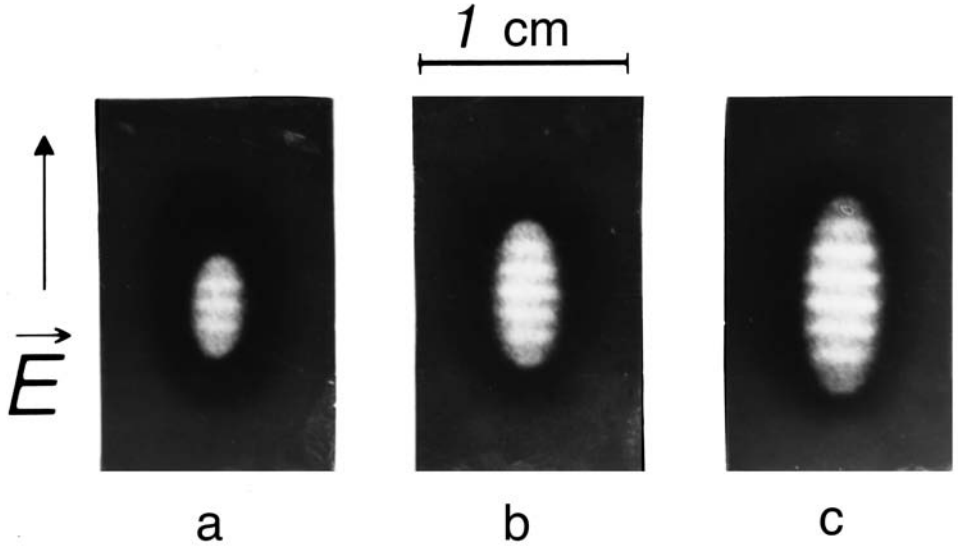

FIG. 1. Photograph of a stratified form of a contracted discharge in ammonia under pressure $p=6$ Torr and different microwave power fed to the resonant cavity: a — 6, b — 13, and c — 21 W.

An 8-mm range quasioptical cavity with spherical mirrors ($Q_0 \approx 7\times 10^3$), positioned on both sides of the axis of a three-centimeter cavity, was used as a diagnostic cavity. A discharge was ignited in different gases and gas mixtures: air, oxygen O_2, nitrogen N_2, water vapor H_2O, ammonia NH_3, carbon dioxide CO_2, and helium He.

It was observed in the first experiments[2] that such a discharge exists in two basic forms: diffuse and contracted. The diffuse discharge burned at one or several antinodes of the field, the dimensions of the discharge were close to those of the localization region of the field, and the interface was diffuse. As the microwave power fed to the cavity increased, the discharge passed into a contracted state. In this form the discharge consisted of an ellipsoid slightly prolate in the direction of the electric field vector and much smaller in size than the diffuse discharge and the wavelength of the electromagnetic wave.

Further investigations established that besides these two forms another unusual form was observed in some gases, such as NH_3, H_2O, and CO_2, in the pressure range $p=3-20$ Torr — a contracted discharge stratified in the direction perpendicular to the electric field vector (Fig. 1). The discharge had the form of an ellipsoid slightly prolate in the direction of the electric field vector and consisted of alternating light and dark disks. Such a stratification was not observed in the other gases investigated (air, N_2, O_2, and He). The distance between two disks (stratification scale) equals 1–2 mm in all cases. As the power fed to the cavity increased, the ellipsoid increased in size and the distance between the disks increased while their number remained constant. At a certain power level the number of disks increased by one and the stratification scale decreased abruptly.

The addition of several percent nitrogen to the ammonia resulted in suppression of

the stratification. This, together with the fact that the stratification was observed in only some gases, attests to the kinetic nature of the phenomenon.

Measurements of N_e performed with the aid of the diagnostic cavity showed that the average electron density in the contracted form of the discharge, in both the stratified and uniform forms, was approximately the same in the different gases and greater than the critical value: $N_e \approx (1-3)N_c$, where $N_c = m_e(\omega^2+\nu^2)/4\pi e^2$ is the critical electron density, ω is the angular frequency of the electromagnetic wave, and ν is the elastic electron–neutral collision frequency.

Let us now analyze the reasons for the appearance of plasma stratification. We shall study the one-dimensional case, i.e., we shall assume that the plasma parameters vary only along an axis parallel to the electric field vector **E**. In a layer perpendicular to the **E** vector the relation between the electric field and N_e is algebraic:

$$E = E(N_e) = \frac{E_0}{|\varepsilon|}, \quad \varepsilon = 1 - \frac{N_e}{N_c}\left(1 + i\frac{\nu}{\omega}\right), \tag{1}$$

where ε is the complex permittivity of the plasma. For $N_e > N_c$ a local increase of N_e decreases the field and vice versa. At the same time, as the field increases, the electron temperature increases, and in a stratified discharge T_e and N_e should vary in antiphase. For this reason, we shall conduct our analysis on the basis of a system of one-dimensional heat-conduction and diffusion equations for T_e and N_e, respectively.

We shall obtain the equation for T_e in the case of ambipolar electron transport from the general equation (see, for example, Ref. 5) by dropping in it terms containing the ambipolar electron velocity:

$$\frac{\partial T_e}{\partial t} = \frac{2}{3}\frac{\sigma E^2(N_e)}{N_e} - \nu_u(T_e)T_e + \frac{1}{N_e}\frac{\partial}{\partial x}\left(\frac{5}{3}N_e D_e(T_e)\frac{\partial T_e}{\partial x}\right). \tag{2}$$

Here $\sigma = e^2 N_e \nu / m_e(\omega^2+\nu^2)$ is the high-frequency conductivity of the plasma, ν_u is the relaxation rate of the electron temperature, and D_e is the electron free diffusion coefficient.

In the equation for N_e we neglect the role of negative ions. This approximation is admissible in the dense plasma of a contracted discharge, where as a result of the accumulation of a large number of active particles the detachment frequency is high, the negative-ion density is low, and attachment is compensated by detachment:[5]

$$\frac{\partial N_e}{\partial t} + \frac{\partial}{\partial x}(u_a N_e) = \nu_i(T_e)N_e - \alpha N_e^2, \tag{3}$$

where $\nu_i(T_e)$ is the ionization rate and α is the recombination coefficient.

The ambipolar electron velocity u_a, taking account of the spatial nonuniformity of the distribution of T_e, is given by the expression[6]

$$u_a = -\frac{D_a}{N_e}\frac{\partial N_e}{\partial x} - \frac{D_a^T}{T_e}\frac{\partial T_e}{\partial x}. \tag{4}$$

The ambipolar diffusion coefficient D_a and thermal diffusion coefficient D_a^T for a strongly nonequilibrium plasma, where $T_e \gg T_i$, equal[6]

$$D_a \approx D_i\left(1+\frac{T_e}{T_i}\right), \quad D_a^T \approx D_i\frac{T_e}{T_i}(1-g)\approx D_a(1-g), \tag{5}$$

where D_i is the positive-ion diffusion coefficient and the coefficient $g \approx \partial \ln \nu/\partial \ln T_e$ takes into account the effect of the thermal force.[6]

We shall now apply to Eqs. (2) and (3) the standard procedure of linearization with respect to a uniform stationary state. To simplify the calculations we set $g=0$, and we also assume that an electron temperature is established over a characteristic distance much shorter than the electron diffusion distance: $D_e/\nu_u \ll D_a/\nu_i$, which holds under the conditions considered here. For disturbances of the form $\exp(i\kappa x+\gamma t)$ we obtain the following dependence of the growth rate γ of the disturbances on the wave number κ:

$$\gamma = \frac{-(5/3)\kappa^4 D_a D_e + \kappa^2 D_a \nu_u (2a-1-c) - \nu_i \nu_u (1+c+2ab)}{(5/3)\kappa^2 D_e + (1+c)\nu_u}, \tag{6}$$

where $a=-\partial \ln E/\partial \ln N_e$, $b=\partial \ln \nu_i/\partial \ln T_e$, and $c=\partial \ln \nu_u/\partial \ln T_e$. The maximum value of γ obtains at

$$\kappa_m^2 = \frac{3}{5}\frac{\nu_u}{D_e}[((1+c)^2+(2a-1-c)(1+c))^{1/2}-(1+c)], \tag{7}$$

whence we can see that the uniform state is unstable if $2a-1-c>0$. The parameter c can be expressed in terms of the dependence $T_e(E)$ in the stationary case, using Eq. (2), and the instability condition can be put into the form

$$-\frac{\partial \ln T_e}{\partial \ln E}\frac{\partial \ln E}{\partial \ln N_e} > 1. \tag{8}$$

For $N_e > N_c$, in the gas pressure range where $\nu \leqslant \omega$, the dependence $E(N_e)$ is a descending function. If the function $T_e(E)$ varies sufficiently rapidly, so that the condition (8) holds, then an instability whose physical mechanism consists of the following can develop. A decrease of N_e in a layer perpendicular to the **E** vector increases the field. When the dependence $T_e(E)$ is sharp the electrons are strongly heated, and the thermodiffusional electron flow out of this region due to the nonuniformity of T_e is greater than the reverse flow due to the nonuniformity of the electron density. As a result, N_e decreases further.

For a glow discharge such an instability, called a thermocurrent instability, was predicted in Ref. 7, where a criterion similar to (8) for the onset of instability was obtained. This instability in a glow discharge has been studied experimentally and theoretically.[8–11]

Comparing $T_e = D_e/\mu_e$ as a function of the reduced field E/p for different gases[5,12,13] shows the following. For gases such as air, N_2, O_2, and He, where stratification of the contracted form is not observed, the function $T_e(E)$ is smooth ($\partial \ln T_e/\partial \ln E < 1/2$) over the entire range of fields for which the discharge is maintained. For NH_3, H_2O, and CO_2, on the contrary, the dependence $T_e(E)$ possesses a quite steep section where the condition (8) can be satisfied.

It is important to note that the sharp dependence $T_e(E)$ is observed for electric fields less than the breakdown value E_c determined from the condition $\nu_i(E_c)=\nu_a(E_c)$, where

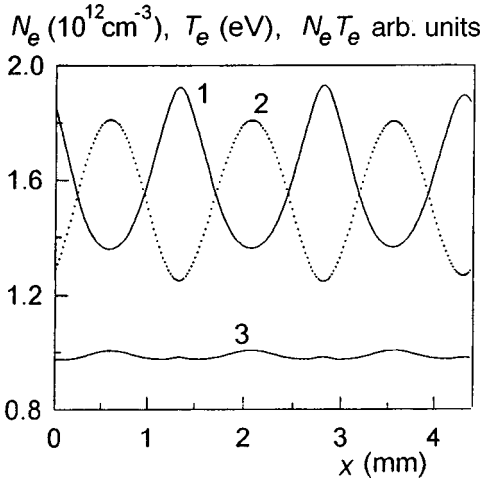

FIG. 2. Spatial distribution of the electron density (1) and electron temperature (2) and the parameter $\eta = N_eT_e$ (inhibitor) (3) in ammonia under pressure $p = 6$ Torr.

ν_a is the attachment rate.[13] For this reason, the instability described can be observed only in quasistationary discharges with above-critical plasma densities, where in electronegative gases the electron loss due to attachment is compensated by detachment as a result of the accumulation of active particles, and the field required to maintain the discharge is appreciably less than the breakdown field.[3] In short-pulse discharges the field is strong, the dependence $T_e(E)$ is weak, and the thermodiffusional flow makes a very small contribution to the total electron flow. In stationary discharges with electron density less than the critical value, $N_e < N_c$, thermodiffusion in the case of an ascending function $E(N_e)$ does not change the direction of electron flow.

The theory of nonuniform stationary states in nonequilibrium dissipative systems described by a system of two nonlinear differential equations of the diffusion type is expounded in detail in Ref. 14. Members of a certain class of such systems have come to be called active systems with diffusion in the sense that positive feedback obtains in one parameter, the activator θ, and is gives rise to an instability of the uniform state of the system. The other parameter, the inhibitor η, suppresses activator growth.

According to the ideas of Ref. 14, for our case it is convenient to take $\theta = T_e$ and $\eta = N_eT_e$ and to switch from the system of equations (2), (3) to a system of equations for θ and η. It is easy to show that for $\eta =$ const the uniform stationary solution of the equation for θ is unstable when the condition (8) holds, while for $\theta =$ const the uniform stationary solution of the equation for η is stable. The characteristic electron-production diffusion length $L = (D_a/\nu_i)^{1/2}$ characterizes the scale of variation of the inhibitor $\eta = N_eT_e \propto N_eD_a$, while $l = (D_e/\nu_u)^{1/2}$is the characteristic spatial scale of the variation of the activator θ. In Ref. 14 it is shown that when $L \gg l$ in the present system nonuniform stationary solutions materialize in the form of thermodiffusion autosolitons and striations with characteristic scale $l < \Lambda < L$.

The system of equations (2), (3) was also solved numerically. Figure 2 shows a stationary solution of Eqs. (2), (3) with $E(N_e)$ of the form (1) for ammonia. In the

numerical calculations no assumptions were made (of the type $g=0$), and the values of the coefficients and rates appearing in Eqs. (1)–(3) were chosen on the basis of the data given in Ref. 13. The magnitude of the electric field was chosen so as to ensure a plasma electron density above the critical value. As one can see, the stratification period obtained in the calculation agrees well with the experimentally observed period. The distribution of the inhibitor $\eta=N_eT_e$ is virtually uniform, in complete agreement with the theoretical ideas of Ref. 14. We note that η is essentially the partial pressure of the electron gas.

In summary, we have discovered in the present work a new small-scale stratification of a continuous microwave discharge. The phenomenon is observed in only some gases. It can be explained by the development of a thermocurrent instability, which is responsible for the formation of the stratified structure of the discharge.

This work was supported by the Civilian R & D Fund (USA) under Grant RE1–352.

[a)]e-mail: gorb@appl.sci-nnov.ru

[1] A. L. Vikharev, V. V. Gil'denburg, A. V. Kim *et al.*, in *High-Frequency Discharge in Wave Fields* [in Russian], Institute of Applied Physics, Soviet Academy of Sciences, Gor'kiĭ, 1988, p. 41.
[2] A. L. Vikharev, O. A. Ivanov, O. Yu. Kuznetsov *et al.*, Dokl. Akad. Nauk SSSR **295**, 358 (1987) [Sov. Phys. Dokl. **32**, 581 (1987)].
[3] A. L. Vikharev, O. A. Ivanov, O. Yu. Kuznetsov *et al.*, Fiz. Plazmy **13**, 1124 (1987) [Sov. J. Plasma Phys. **13**, 648 (1987)].
[4] V. E. Golant, *Microwave Methods for Plasma Diagnostics* [in Russian], Nauka, Moscow, 1968.
[5] Yu. P. Raĭzer, *Physics of Gas Discharges* [in Russian], Nauka, Moscow, 1987.
[6] V. E. Golant, A. P. Zhilinskiĭ, and I. E. Sakharov, *The Fundamentals of Plasma Physics* [in Russian], Atomizdat, Moscow, 1977.
[7] A. V. Timofeev, Zh. Tekh. Fiz. **40**, 192 (1970) [Sov. Phys. Tech. Phys. **15**, 140 (1970)].
[8] N. L. Aleksandrov, A. M. Konchakov, A. P. Napartovich *et al.*, in *Plasma Chemistry* [in Russian], Énergoatomizdat, Moscow, 1984, No. 11, p. 3.
[9] Yu. S. Akishev, N. A. Dyatko, I. N. Lopatkin *et al.*, in *Proceedings of the 7th All-Union Conference on the Physics of Low-Temperature Plasma* [in Russian], Tashkent, 1987, Vol. 1, p. 261.
[10] V. A. Shveĭgert, Fiz. Plazmy **14**, 1263 (1988) [Sov. J. Plasma Phys. **14**, 739 (1988)].
[11] N. L. Aleksandrov and A. M. Okhrimovskiĭ, Fiz. Plazmy **23**, 77 (1997) [Plasma Phys. Rep. **23**, 71 (1997)].
[12] E. W. McDaniel, *Collision Phenomena in Ionized Gases*, John Wiley, New York, 1964 [Russian translation, Mir, Moscow, 1967].
[13] M. Yousfi and M. D. Benabdessadok, J. Appl. Phys. **80**, 6619 (1996).
[14] B. S. Kerner and V. V. Osipov, *Autosolitons: Localized, Strongly Nonequilibrium Regions in Homogeneous Dissipative Systems* [in Russian], Nauka, Moscow, 1991.

Translated by M. E. Alferieff

Exact solution of the problem of quasineutral expansion into vacuum of a localized collisionless plasma with cold ions

D. S. Dorozhkina[a)] and V. E. Semenov
Institute of Applied Physics, Russian Academy of Sciences, 603600 Nizhniĭ Novgorod, Russia

(Submitted 10 March 1998)
Pis'ma Zh. Éksp. Teor. Fiz. **67**, No. 8, 543–547 (25 April 1998)

An analytical solution of the Vlasov equation for the electrons and the hydrodynamic equations for the ions in a self-consistent electric field is constructed in the quasineutral approximation. This solution is valid for a finite electron-to-ion mass ratio. It permits describing the expansion into vacuum of a collisionless plasma with cold ions and arbitrary initial electron velocity distribution, forming a plasmoid that is bounded and, in the general case, spherically asymmetric in space. [S0021-3640(98)00508-8]

PACS numbers: 52.25.Wz, 52.30.−q

The problem of the expansion of plasma into vacuum has long been attracting the attention of both astrophysicists and investigators working in the field of controlled thermonuclear fusion (see, for example, the review in Ref. 1 and the literature cited therein). In the last few years, rapidly developing investigations of dusty plasmas have also stimulated interest in this problem.[2–5] In the thirty years since the publication of Gurevich's pioneering paper[6] the question of the expansion of a semibounded collisionless plasma into vacuum has been studied in detail by theorists.[6–16] A characteristic feature arising in this problem on account of the infinite store of energy in the initial plasma is the ''unbounded'' acceleration of ions all the way up to velocities corresponding to the thermal velocity of the electrons. It is obvious that when a real, spatially bounded plasmoid expands into vacuum, only a very small fraction of all ions in the plasma can attain such high velocities. For most of the ions the kinetic energy can increase only by an amount of the order of the thermal energy of the electrons in the initial plasmoid. A correct description of the expansion of a plasmoid requires taking into account the self-consistent cooling of the electrons. Until recently, this process has been studied only on the basis of a hydrodynamic description.[1] The corresponding kinetic problem was formulated in Refs. 17 and 18 and was analyzed in those studies by numerical methods. The numerical investigations showed that the plasma expansion process asymptotically settles into a quasineutral self-similar regime. In the present work it is shown that a self-similar solution of the problem of the expansion into vacuum of a spatially localized plasmoid with cold ions can be constructed analytically in the quasineutral approximation. The solution is obtained for an arbitrary initial electron velocity distribution and describes the dynamics of spherically asymmetric plasmoids. Thus

it can be used as a basic model for investigating the expansion of a quite arbitrary plasmoid into vacuum.

The complete system of equations describing the plasma dynamics in the approximations studied includes the following:

a) The equations of hydrodynamics for cold ions:

$$\frac{\partial n_i}{\partial t}+\nabla\cdot(n_i\mathbf{u})=0,$$
$$\frac{\partial \mathbf{u}}{\partial t}+(\mathbf{u}\cdot\nabla_{\mathbf{r}})\mathbf{u}=-\frac{Ze}{M}\nabla_{\mathbf{r}}\varphi(\mathbf{r},t), \tag{1}$$

b) the Vlasov equation for electrons:

$$\frac{\partial f_e}{\partial t}+(\mathbf{v}\cdot\nabla_{\mathbf{r}})f_e+\left(\frac{e}{m}\nabla_{\mathbf{r}}\varphi\cdot\nabla_{\mathbf{v}}\right)f_e=0\,, \tag{2}$$

c) the quasineutrality condition:

$$Zn_i=n_e\equiv\int f_e(\mathbf{v},\mathbf{r},t)d^{\nu}\mathbf{v}, \tag{3}$$

where $n_i(\mathbf{r},t)$ and $\mathbf{u}(\mathbf{r},t)$ are the ion density and velocity, $f_e(\mathbf{v},\mathbf{r},t)$ is the electron velocity distribution function, $n_e(\mathbf{r},t)$ is the electron density, m and $-e$ are the electron mass and charge, Z and M are the ion atomic number and mass, $\varphi(\mathbf{r},t)$ is the electric field potential arising as a result of charge separation during the expansion of the plasma, and $\nu=1$, 2, and 3 corresponds to the dimension of the space in the problem under study.

A broad spectrum of self-similar solutions of Eqs. (1)–(3) can be constructed with a quadratic dependence of the ambipolar electric field potential φ on the spatial coordinates $\mathbf{r}$:

$$\varphi(\mathbf{r},t)=-\frac{m}{2e}\sum_{k=1}^{\nu}\omega_k^2(t)x_k^2\,, \tag{4}$$

where x_k are the components of the radius vector $\mathbf{r}$ and ω_k corresponds to the frequency of the harmonic oscillations of one electron along the direction x_k in the electric field under study. The time dependences $\omega_k(t)$ are found in the course of the solution.

A self-similar solution of the equations of hydrodynamics (1) in the field (4) with arbitrary $\omega_k(t)$ can be represented in the form

$$n_i=N(\mathbf{R})\prod_{k=1}^{\nu}\frac{l_k(0)}{l_k(t)}, \tag{5}$$

$$u_k=X_k\dot{l}_k(t), \tag{6}$$

where u_k are the corresponding components of the hydrodynamic velocity $\mathbf{u}$ of the ions, $\mathbf{R}$ is a vector with the components R_k, $X_k=x_k/l_k(t)$ are self-similar variables, $N(\mathbf{R})$ is an arbitrary function of its arguments, $\dot{l}_k(t)=dl_k/dt$, and the functions $l_k(t)$ satisfy the differential equations

$$\ddot{l}_k - \frac{Zm}{M}\omega_k^2(t) l_k = 0\,. \tag{7}$$

The solution of the kinetic equation (2) can also be represented in the form of an arbitrary function F of a set of arguments G_k:

$$f_e(\mathbf{v},\mathbf{r},t) = F(\mathbf{G}); \quad G_k = \Omega_k^2 \beta_k(t) x_k^2 + \beta_k^{-1}(t)(v_k - \Omega_k \gamma_k(t) x_k)^2, \tag{8}$$

where Ω_k are arbitrary constants, and the functions $\beta_k(t)$ and $\gamma_k(t)$ satisfy the ordinary differential equations

$$\dot{\beta}_k(t) = -2\Omega_k \gamma_k(t)\beta_k(t),$$

$$\dot{\gamma}_k(t) = \Omega_k \beta_k^2(t) - \frac{\omega_k^2(t)}{\Omega_k} - \Omega_k \gamma_k^2(t) \tag{9}$$

with the initial conditions $\beta_k(0) = 1$ and $\gamma_k(t) = 0$.

The quasineutrality condition (3) can be satisfied, using the solutions (5) and (9), by taking

$$\beta_k(t) = l_k^2(0)/l_k^2(t). \tag{10}$$

In this case Eqs. (7), (9), and (10) form a closed system with respect to the as yet unknown functions $l_k(t)$, $\beta_k(t)$, $\gamma_k(t)$, and $\omega_k(t)$. Integrating these equations for an initially stationary plasma ($\dot{l}_k(0) = 0$) we find

$$\Omega_k = \sqrt{1 + \frac{Zm}{M}}\,\omega_k(0),$$

$$\beta_k(t) = \left(1 + \frac{Zm}{M}\omega_k^2(0) t^2\right)^{-1},$$

$$\Omega_k \gamma_k(t) = \frac{Zm\omega_k^2(0) t}{M + Zm\omega_k^2(0) t^2} = \frac{u_k(x_k,t)}{x_k},$$

$$\omega_k = \omega_k(0)\beta_k(t). \tag{11}$$

Thus expressions (5), (6), (8), (10), and (11) represent the solution of the problem posed for an arbitrary function $F(\mathbf{G})$, which depends on ν arguments, and ν arbitrary parameters $\omega_k(0)$. The function $N(\mathbf{R})$ describing the dynamics of the spatial distribution of the plasma density cannot be arbitrary in this case. In accordance with the quasineutrality condition it is determined by the function F and the set of parameters $\omega_k(0)$:

$$N(X_1, \ldots, X_\nu) = \int F(\Omega_1^2 l_1^2(0) X_1^2 + w_1^2, \ldots, \Omega_\nu^2 l_\nu^2(0) X_\nu^2 + w_\nu^2) \prod_{k=1}^{\nu} dw_k\,. \tag{12}$$

For a prescribed electron velocity distribution the parameters $\omega_k(0)$ determine the characteristic scales of the initial plasma density distribution along the corresponding coordinate axes. Specifically, if the second moments of the electron velocity distribution are taken as these scales

$$l_k^2(t)\equiv\langle x_k^2\rangle=\int\int x_k^2 f_e(\mathbf{v},\mathbf{r},t)d^\nu\mathbf{v}d^\nu\mathbf{r}\Big/\int\int f_e(\mathbf{v},\mathbf{r},t)d^\nu\mathbf{v}d^\nu\mathbf{r}, \tag{13}$$

then the relation of their initial values with $\omega_k(0)$ can be represented as

$$\left(1+\frac{Zm}{M}\right)\omega_k^2(0)l_k^2(0)=\langle v_k^2\rangle_0\equiv\frac{\int\int v_k^2 f_e(\mathbf{v},\mathbf{r},t=0)d^\nu\mathbf{v}d^\nu\mathbf{r}}{\int\int f_e(\mathbf{v},\mathbf{r},t=0)d^\nu\mathbf{v}d^\nu\mathbf{r}}. \tag{14}$$

Proceeding to a discussion of the results, we note first that a plasma with an arbitrary electron distribution function expands, as expected, with the characteristic ion-sound velocity. This result follows from the law of variation of the localization scales of the plasma density, which are determined by relations (13):

$$l_k^2(t)=l_k^2(0)+c_k^2t^2,\quad c_k^2=\frac{Zm}{M+Zm}\langle v_k^2\rangle_0. \tag{15}$$

As the plasma expands, the ions are accelerated while the electrons cool down, in the process acquiring a hydrodynamic velocity equal to the local value of the ion velocity:

$$\langle v_k\rangle\equiv\int\int v_k f_e(\mathbf{v},\mathbf{r},t)d^\nu\mathbf{v}d^\nu\mathbf{r}\int\int f_e(\mathbf{v},\mathbf{r},t)d^\nu\mathbf{v}d^\nu\mathbf{r}=u_k(x_k,t). \tag{16}$$

The electrons cool down according to an adiabatic law, i.e., the rms velocity of the electrons along each coordinate axis decreases inversely as the corresponding size of the plasmoid,

$$\langle(v_k-u_k)^2\rangle\equiv\frac{\int\int(v_k-u_k)^2 f_e(\mathbf{v},\mathbf{r},t)d^\nu\mathbf{v}d^\nu\mathbf{r}}{\int\int f_e(\mathbf{v},\mathbf{r},t)d^\nu\mathbf{v}d^\nu\mathbf{r}}\propto\frac{l_k^2(0)}{l_k^2(t)}. \tag{17}$$

The integral electron velocity distribution $\phi_e(v_1^2,\ \ldots,\ v_\nu^2,t)$ will be similar at each moment in time to the initial distribution:

$$\phi_e(v_1^2,\ldots,v_\nu^2,t)\equiv\int f_e(\mathbf{v},\mathbf{r},t)d^\nu\mathbf{r}$$
$$=\prod_{k=1}^{\nu}\sqrt{\frac{Zm+M}{Zm+M\beta_1(t)}}\phi_0\left(\frac{Zm+M}{Zm+M\beta_1(t)}v_1^2,\ldots,\frac{Zm+M}{Zm+M\beta_\nu(t)}v_\nu^2\right). \tag{18}$$

This is also true of the integral ion velocity distribution formed as the plasma expands — it is also similar to $\phi_0=\phi_e(v_1^2,\ \ldots,\ v_\nu^2,t=0)$:

$$\phi_i(v_1^2,\ldots,v_\nu^2,t)\equiv\int f_i(\mathbf{v},\mathbf{r},t)d^\nu\mathbf{r}$$

$$= \prod_{k=1}^{\nu} \sqrt{\frac{Zm+M}{Zm(1-\beta_1(t))}} \phi_0\left(\frac{Zm+M}{Zm(1-\beta_1(t))} v_1^2, \ldots, \frac{Zm+M}{Zm(1-\beta_\nu(t))} v_\nu^2 \right), \tag{19}$$

where $f_i(\mathbf{v},\mathbf{r},t) = n_i(\mathbf{r},t)\,\delta(\mathbf{v}-\mathbf{u}(\mathbf{r},t))$ is the ion velocity distribution function. Therefore the unbounded ion acceleration characteristic for the previously studied case of expansion of a semibounded plasma does not occur during the expansion of a spatially localized plasmoid.

The solution constructed above corresponds to the presence of a uniform electric charge density, proportional to $\Sigma_{k=1}^{\nu}\omega_k^2(t)$, in space. This means that the model of quasineutral expansion of a plasmoid is, generally speaking, incorrect in regions of low plasma density. Therefore the solution found cannot give an absolutely accurate description of the expansion of a plasma into vacuum.

It should be noted, however, that for a sufficiently dense plasma, where the plasma frequency $\omega_p$is much higher than the characteristic frequencies ω_k, i.e.,

$$\omega_p^2 \gg \sum_{k=1}^{\nu} \frac{\langle (v_k - u_k)^2 \rangle}{l_k^2}, \tag{20}$$

the quasineutrality condition breaks down only at the periphery of the plasmoid at large distances from the region of localization of the main plasma. We note that on the basis of the solution found, as a result of the cooling of the electrons the right-hand side of relation (20) decreases with time more rapidly than the plasma density. Therefore in the region of localization of the plasmoid the quasineutral description of the expansion of the plasma does not become invalid over time. This shows that the solution constructed in the present letter can adequately describe the real situation.

This work was supported by the Russian Fund for Fundamental Research under Grant 98-02-17052.

[a)]e-mail: dorozh@appl.sci-nnov.ru

[1]Ch. Sack and H. Schamel, Phys. Rep. **156**, 311 (1987).
[2]M. Y. Yu and H. Luo, Phys. Lett. A **161**, 506 (1992).
[3]H. Luo and M. Y. Yu, Phys. Fluids B **4**, 1122 (1992).
[4]H. Luo and M. Y. Yu, Phys. Fluids B **4**, 3066 (1992).
[5]M. Y. Yu and H. Luo, Phys. Plasmas **3**, 591 (1995).
[6]A. V. Gurevich, L. V. Pariĭskaya, and L. P. Pitaevskiĭ, Zh. Éksp. Teor. Fiz. **49**, 647 (1965) [Sov. Phys. JETP **21**, 449 (1966)].
[7]L. M. Wickens, J. E. Allen, and P. T. Rumsby, Phys. Rev. Lett. **41**, 243 (1978).
[8]B. Bezzerides, D. W. Forslund, and E. L. Lindman, Phys. Fluids **21**, 2179 (1978).
[9]P. Mora and R. Pellat, Phys. Fluids **22**, 2300 (1979).
[10]A. Gurevich, D. Anderson, and H. Wilhelmsson, Phys. Rev. Lett. **42**, 769 (1979).
[11]A. V. Gurevich and L. P. Pitaevskiĭ, in *Problems of Plasma Theory* [in Russian], edited by M. A. Leontovich, Atomizdat, Moscow, 1980, No. 10.
[12]A. V. Gurevich and A. P. Mishcherkin, Zh. Éksp. Teor. Fiz. **80**, 1810 (1981) [Sov. Phys. JETP **53**, 937 (1981)].
[13]A. V. Gurevich and A. P. Mishcherkin, Zh. Éksp. Teor. Fiz. **81**, 1295 (1981) [Sov. Phys. JETP **54**, 688 (1981)].
[14]Ch. Sack and H. Schamel, Plasma Phys. Controlled Fusion **27**, 717 (1985).

[15] M. K. Srivastava, S. V. Lawande, and B. K. Sinha, Plasma Phys. Controlled Fusion **32**, 359 (1990).
[16] Y. El-Zein, A. Amin, H. S. Kim *et al.*, Phys. Plasmas **2**, 1073 (1995).
[17] G. Manfredi, S. Mola, and M. R. Feix, Phys. Fluids B **5**, 388 (1993).
[18] L. G. Garcia, J. Goedert, H. Figua *et al.*, Phys. Plasmas **4**, 4240 (1997).

Translated by M. E. Alferieff

Influence of nonlinear effects on whistler emission in magnetoactive plasma

A. V. Kostrov,[a] A. I. Smirnov, M. V. Starodubtsev, and A. A. Shaĭkin[b]
Institute of Applied Physics, Russian Academy of Sciences, 603600 Nizhniĭ Novgorod, Russia

(Submitted 13 March 1998)
Pis'ma Zh. Éksp. Teor. Fiz. **67**, No. 8, 548–551 (25 April 1998)

The influence of thermal and strictional nonlinear effects on the whistler emission in magnetoactive plasma is studied experimentally. It is established that a nonlocal thermal nonlinearity determines the directional pattern of the antenna, while a strictional nonlinearity, which is strongest near the antenna surface, is responsible for the matching of the emitter with the surrounding plasma. © *1998 American Institute of Physics.* [S0021-3640(98)00608-2]

PACS numbers: 52.35.Mw, 52.25.Sw

The emission of intense electromagnetic wave fields in plasmas is often accompanied by the development of various nonlinear processes (strictional, ionization, thermal) that strongly alter the electrodynamic characteristics of the surrounding medium. The nonlinear effects are strongest near antennas, where, as a rule, the electric and magnetic field intensities reach their maximum values. They influence the radiator–plasma matching and, generally speaking, the structure of the near (quasistatic) and radiation fields.[1–4]

The nonuniformities arising in a magnetoactive plasma as a result of heating of the electrons in the near fields of antennas stretch along the magnetic field and can maintain spatially localized electromagnetic modes, which are emitted into the surrounding space as the nonuniformities vanish. As a result, in the absence of a nonuniformity the directional pattern becomes substantially narrower. In the direct proximity of an antenna, strictional processes give rise to small-scale nonuniformities (of the order of the characteristic transverse dimensions of the conductors) which determine the input impedance of the radiators. It is a very attractive idea to use this effect to match antennas and plasma. In the present work the effects listed above were studied experimentally.

The experiments were performed in a decaying argon plasma with neutral gas pressure $p_0 = 5 \times 10^{-3}$ torr. The apparatus consisted of a vacuum chamber 150 cm long and 80 cm in diameter. The plasma was produced by a high-frequency pulsed discharge in a uniform magnetic field $H_0 = 100$ Oe. The density reached $N = 10^{13}$ cm^{-3} and then (after the plasma source was switched off) decayed with characteristic time $\tau_N \approx 2$ ms. The main experiments were performed with plasma density 10^{12} cm^{-3}; the electron temperature was equal to 0.5 eV.

The density of the background plasma was monitored with a microwave interferometer ($\lambda = 8$ mm), while local density disturbances were measured with mobile dual and

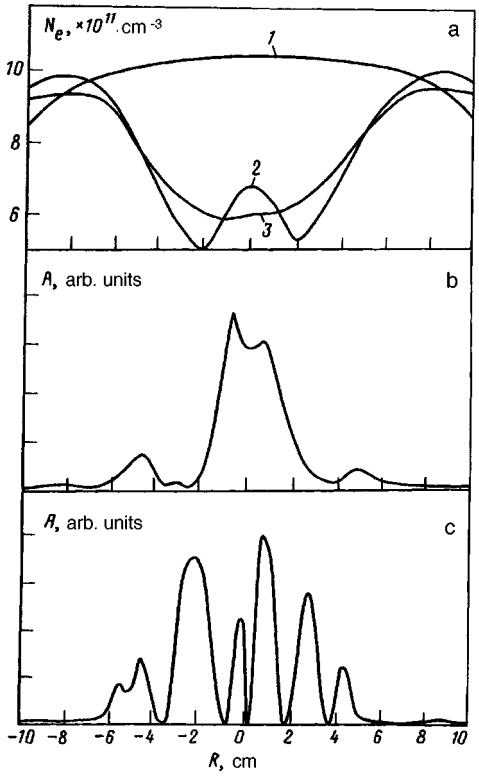

FIG. 1. Transverse distributions: a — Plasma density (*1* — unperturbed, *2* — during the pump pulse, *3* — 100 μs after the pump pulse ends); amplitude of the H_2 component of the probe wave field in the channel: b — during the pump pulse, c — 100 μs after the pump pulse ends.

microwave probes.[5] The spatial distribution of the electromagnetic fields was investigated by means of a mobile frame antenna with a diameter of 0.7 cm, which was electrostatically shielded and insulated from the plasma by a layer of a dielectric material.

Two signals were simultaneously introduced into the transmitting antenna section, which consisted of a frame with a diameter of 5 cm, which was electrostatically shielded but not insulated from the plasma: The first signal consisted of a continuous low-power ($P \simeq 0.2$ W) probe signal whose frequency could be varied in a band from 10 to 500 MHz, covering the entire whistler range; the second signal was a pump pulse ($P_0 \simeq 100$ W, $f_0 = 60$ MHz) with duration $\tau_i = 1.25$ ms (hatched region in Fig. 2a).

The pump signal strongly modified the parameters of the surrounding plasma and influenced the efficiency of emission of probe waves and their directional pattern. As a result of the heating of the electrons near the antenna by the pump field and further thermal diffusion processes, a low-density channel stretching strongly along the magnetic field forms in the plasma.[1] The probe waves are trapped in the plasma waveguide formed and propagate over large distances from the radiating antenna. The plasma nonuniformities thereby arising as a result of thermal nonlinearity form the directional pattern of the radiator for both the pump and the probe waves.

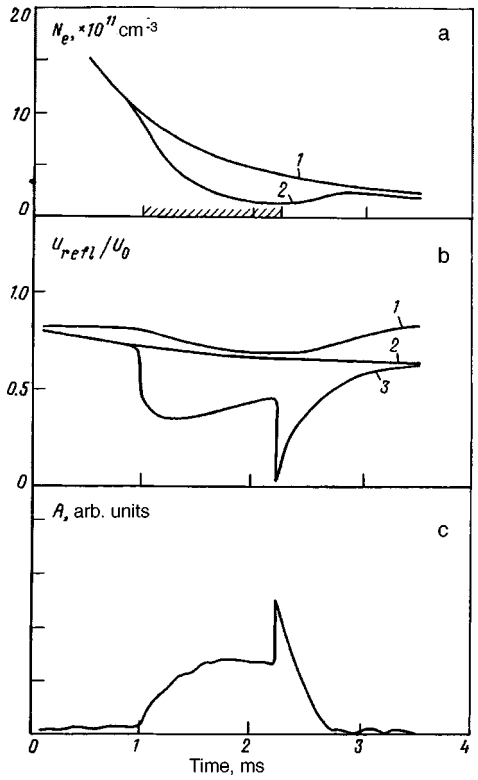

FIG. 2. a — Plasma density as a function of time: *1* — Undisturbed plasma and *2* — plasma disturbed by the pump pulse; b — oscillograms of the reflected wave in the feeder section at the probe frequency $f=90$ MHz: *1* — antenna coated with a layer of insulating material in the presence of the pump pulse; *2* — uninsulated antenna without a pump wave, *3* — in the presence of a pump pulse, c — typical oscillogram of the H_z component of the field of the probe wave with $f=90$ MHz in the plasma channel at a distance $z=35$ cm from the transmitting antenna.

The structure of the high-frequency fields of the probe waves propagating in the plasma channel is interesting. It is known that at frequencies $\omega_0 < \omega_{He}/2$ quasilongitudinal whistlers with longitudinal wave number $k \approx \omega_{pe}(\omega/\omega_{He})^{1/2}/c)$, where ω_0 is the frequency of the probe wave and ω_{pe} and ω_{He} are, respectively, the plasma frequency and gyrofrequency of the electrons and c is the speed of light in vacuum, can propagate in the high-density channel, while oblique whistlers propagate (conical-refraction waves with transverse wave number $k_\perp \approx \omega_{pe}/c$) in channels with low plasma density.

Figure 1a shows the plasma density distribution over the transverse cross section of the channel at the moment the pump wave operates (curve *2*) and 100 μs after it is switched off (curve *3*). The central maximum in the curve *2* is due to the structure of the vortex electric field of the wave. The transverse spatial scale of the thermal conductivity $L_{T\perp} \approx \rho_{eH}/(2m/M)^{1/2} \approx 2$ cm (m and M are the electron and ion masses, respectively, ρ_{eH} is the gyroradius of an electron) is of the order of the frame dimensions ($2a \approx 5$ cm). Under such conditions the transverse nonuniformity of the electron temperature results in a nonuniform plasma density distribution in the channel. After the pump pulse is

switched off, the maximum density at the center relaxes over a time $\tau_\perp \approx L_{T\perp}^2/(2.6)^2\rho_{eH}^2\nu_{ei} \approx 10^{-5}$ s (ν_{ei} is the electron–ion collision frequency), i.e., much more rapidly than the entire channel with a radius of 6 cm is filled up (see Fig. 2a, curve *2*).

One can see that when a density maximum is present at channel center the field H_z is localized only at this maximum (Fig. 1b). This attests to excitation of a quasilongitudinal whistler mode. After the pump pulse is switched off and the channel becomes quasiuniform (curve *3* in Fig. 1a), whistler waves with shorter wavelengths can propagate in it (specifically, conical-refraction waves (Fig. 1c)).

Therefore whistler waves with different transverse wavelengths can be efficiently separated and then emitted into the surrounding plasma, i.e., the directional pattern of a frame radiator can be controlled by varying the shape of the plasma waveguide.[c)]

Information about matching of the antenna with the surrounding plasma was extracted by analyzing oscillograms of the reflected signal in the feeder section. Such an oscillogram for the probe wave is presented in Fig. 2b. One can see from this oscillogram that the amplitude of the reflected signal changes sharply when the pump wave is switched on or off. Such a rapid change in the input parameters of the antenna (occurring over times much shorter than the characteristic thermal-diffusion redistribution times of the plasma) attests to a strictional mechanism of the action on the plasma. This action is strongest in direct proximity to the antenna surface, where the electric fields are strong. It follows from the experimental data that almost complete antenna–feeder matching is observed after the pump pulse is switched off.[d)] The thermal channel relaxes to a uniform state over times $\tau_{\rm rel} \approx 10^{-3}$ s, much longer than the characteristic matching time $\tau_{\rm match} \approx 10^{-4}$ s. It should be noted that no sharp changes in the amplitude of the reflected signal of the probe waves and no matching effect after the pump pulse was switched off were observed in the case of a frame coated with a layer of insulating material much thicker than a double layer (curve *1* in Fig. 2b), though a thermal channel of the same shape and characteristic size as for an antenna without an insulator did form in the plasma.

In summary, the strictional and thermal effects accompanying the whistler-range operation of a frame radiator in a magnetoactive plasma were investigated experimentally. It was shown that the feed and radiation characteristics of a frame antenna can be controlled by feeding a powerful high-frequency voltage pulse to the antenna. Strictional effects appreciably influence the input impedance of the antenna. Specifically, they can substantially improve the antenna–plasma matching, while the large-scale plasma nonuniformities formed as a result of heating change the directional pattern of the frame antenna.

The authors are grateful to are grateful to the Russian Fund for Fundamental Research for funding under Grants 96-02-16471-a (A. V. Kostrov and M. V. Starodubtsev) and 96-02-17473 (A. I. Smirnov and A. A. Shaĭkin).

[a)]e-mail: kstr@appl.sci-nnov.ru
[b)]e-mail: shaykin@appl.sci-nnov.ru

[c)]During the HF pulse harmonics with sum and difference combinations of the pulse frequency and the working frequency of the transmitted signal appeared in the emission spectrum. The intensities of the harmonics were sometimes comparable to that of the transmitted signal.

[d)]This effect is due to the retardation of the high-frequency current flowing along a conductor surrounded by the low-density channel formed under the action of the strictional displacement of plasma away from the conduc-

tor surface. Current retardation results in the appearance of an electric dipole moment of the frame antenna. This moment explains the efficient radiation of quasilongitudinal whistler waves by a frame oriented with its plane perpendicular to the external static field.

[1] G. Yu. Golubyatnikov, S. V. Egorov, A. V. Kostrov *et al.*, Fiz. Plazmy **14**, 482 (1988) [Sov. J. Plasma Phys. **14**, 285 (1988)].
[2] H. C. Koons and D. A. McPherson, Radio Sci. **9**, 547 (1974).
[3] I. P. Shkarofsky, Radio Sci. **7**, 503 (1972).
[4] Yu. N. Agafonov, V. S. Bazhanov, V. Ya. Isyakaev *et al.*, JETP Lett. **52**, 530 (1990).
[5] R. L. Stenzel, Rev. Sci. Instrum. **47**, 603 (1976).

Translated by M. E. Alferieff

A new quasi-Ising magnet

A. S. Lagutin, G. E. Fedorov, and A. V. Kopylov
Institute of Molecular Physics, Kurchatov Institute Russian Science Center, 123182 Moscow, Russia

J. Vanacken and F. Herlach
Laboratory of Solid-State Physics and Magnetism, Catholic University of Leuven, B-3001 Leuven, Belgium

(Submitted 24 December 1997; resubmitted 24 February 1998)
Pis'ma Zh. Éksp. Teor. Fiz. **67**, No. 8, 552–556 (25 April 1998)

We have performed measurements of the magnetization and differential magnetic susceptibility of $Dy_{0.62}Y_{2.38}Fe_5O_{12}$ single crystals in pulsed magnetic fields up to 45 T at liquid-helium temperature for three orientations of the external field: $\mathbf{H} \parallel [100]$, $\mathbf{H} \parallel [110]$, and $\mathbf{H} \parallel [111]$. It was found that the magnetization reversal in the rare-earth magnetic subsystem occurs via several phase transitions, whose number depends on the direction of the external field, as is characteristic for Ising magnets. The anomalies in the field dependences of the magnetization are interpreted on the assumption of quasi-Ising ordering of the rare-earth ions. © *1998 American Institute of Physics.*
[S0021-3640(98)00708-7]

PACS numbers: 75.30.Cr, 75.60.Ej, 75.10.Hk

In the rare-earth iron garnet (REIG) family the compounds $R_xY_{3-x}Fe_5O_{12}$ containing dysprosium ions (R=Dy) have been least studied. Investigations of the isomorphic compounds $R_xY_{3-x}Al_5O_{12}$ have shown that the magnetic properties of Dy^{3+} ions in these crystals can be described well in the Ising approximation.[1–3] The ground state of such ions in $Dy_xY_{3-x}Al_5O_{12}$ is a doublet, separated from the excited states by approximately 100 K, with a strongly anisotropic g factor ($g_{zz} \cong 18$, $g_{xx} \cong g_{yy} \cong 0$). For this reason, the Dy^{3+} ions in aluminum garnets at $T \ll 100$ K can be regarded as Ising ions with anisotropy axes corresponding for different nonequivalent positions to the axes [100], [010], and [001] axes of a cubic crystal.[4] The easy axes (EAs) are directions of the type [111].

It was found that at temperatures $T > 78$ K $Dy_3Fe_5O_{12}$ possesses the same EAs,[5] but at $T = 4.2$ K none of the principal crystallographic directions of REIGs ([111], [110], and [100]) serves as an EA.[6–8] Investigation of the spin reorientation process in $Dy_xY_{3-x}Fe_5O_{12}$ has shown that reorientation of the type $\langle 111 \rangle \Leftrightarrow \langle uuv \rangle$ arises at $T \cong 13$ K on account of a change in the state of the rare-earth (RE) subsystem of the crystal.[9] Calculations of the ground state of Dy^{3+} in the crystal field of a REIG have confirmed this conclusion.[10] Up to now, detailed experimental information about the magnetic properties of the RE subsystem of $Dy_xY_{3-x}Fe_5O_{12}$ at low temperatures has

been unavailable. For this reason, our main goals in the present work were to obtain reliable information about the magnetization and magnetic-field-induced phase transitions in mixed dysprosium–yttrium iron garnets at low temperatures and to determine one of the most important parameters: the magnitude of the $3d$–$4f$ exchange interaction.

EXPERIMENTAL PROCEDURE AND SAMPLES

The measurements of the magnetization and differential magnetic susceptibility were performed at liquid-helium temperature in strong pulsed magnetic fields with amplitude up to 45 T.[11] A 7-mm-long, high-precision, four-coil induction magnetic pickup with an inner diameter of 4 mm was used. A DataLab–1200 four-channel single-process detector with 12-bit amplitude resolution and maximum frequency of digitization of the analog signal of 500 kHz was used to convert the analog voltages $U_1 \cong dM/dt$, $U_2 \simeq dH/dt \cdot dM/dH$, and $U_3 \simeq dH/dt$ into digital form, store the digital data files, and transfer the data to a personal computer. The magnetic-moment sensitivity of the measuring circuit reached 10^{-4} G·cm^3 in fields up to 10 T and slid to 10^{-2} G·cm^3 at the maximum field amplitude.

The $Dy_{0.62}Y_{2.38}Fe_5O_{12}$ samples were grown at M. V. Lomonosov Moscow State University by the method of spontaneous crystallization from a fluxed melt. The chemical composition of the samples was determined by mass-spectrometric analysis on a Perkin-Elmer Plasma-1000 ICP–AES spectrometer. Samples in the form of 5–7 mm long rectangular parallelepipeds with a cross section of 1.5×1.5 mm were used for measurements in pulsed fields.

EXPERIMENTAL RESULTS AND DISCUSSION

The field dependences of the magnetization obtained for $Dy_{0.62}Y_{2.38}Fe_5O_{12}$ single crystals at $T = 4.2$ K with external magnetic field orientation along the crystallographic directions [100], [110], and [111] are presented in Fig. 1. Three characteristic sections can be clearly distinguished on all magnetization curves. In the first range of fields ($H = 0$–8 T) the magnetization M is virtually independent of H. In the second range, starting at $H_1 \simeq 8$ T, substantial changes in the magnetization occur in fields up to $H_2 \cong 30$–34 T. For the third field range ($H > 30$–34 T) the sample magnetizations once again change very little with increasing H. Since for all magnetic field directions the quantity $(H_1 + H_2)/2$ is virtually constant and equals 20 T, the second field range can be unequivocally associated with the region of magnetization reversal of the rare-earth magnetic subsystem of REIG. Here $H_{\text{eff}} = (H_1 + H_2)/2$ is the effective $3d$–$4f$ exchange interaction field. Anomalies of the differential magnetic susceptibility, which were observed only for $H_1 < H < H_2$ (Fig. 2), attest to the existence of several phase transformations in this region of fields. This is characteristic for quasi-Ising REIGs.[4,12]

The theoretical magnetization curves were calculated in a quasi-Ising approximation neglecting the magnetic anisotropy of the iron subsystem. A seven-sublattice model of the REIG, including one iron and six rare-earth sublattices, formed by Fe^{3+} and Dy^{3+} ions with magnetic moments $5\mu_B$ and $10\mu_B$, respectively, was used. It was assumed that the local anisotropy axes of the RE ions are oriented in directions of the type [110], which agrees with the experimental data to within the error limits. The thermodynamic potential per molecule for the system $Dy_xY_{3-x}Fe_5O_{12}$ without allowance for the anisotropy of the iron subsystem was used in the form[4]

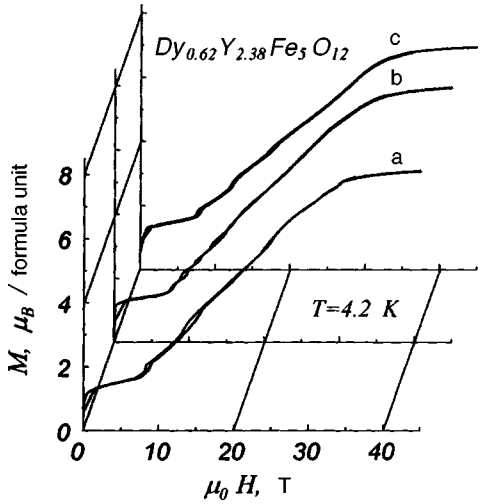

FIG. 1. Magnetization curves of $Dy_{0.62}Y_{2.38}Fe_5O_{12}$ single crystals at $T=4.2$ K for three different orientations of the external field: a — $\mathbf{H}\|[100]$, b — $\mathbf{H}\|[110]$, c — $\mathbf{H}\|[111]$.

$$\Phi = -\mathbf{M}_{\mathrm{Fe}}\cdot\mathbf{H} - \frac{1}{T}\frac{x}{6}\sum_{i=1}^{6} \ln 2\cosh\left(\frac{\Delta_i}{T}\right), \tag{1}$$

where $\mathbf{M}_{\mathrm{Fe}}$ is the magnetization of the iron matrix, $\mathbf{M}_{\mathrm{R}}^{i}$ is the magnetization of a RE ion at the ith site ($i=1\ldots6$), $\mathbf{H}$ is the magnetic field, x is the concentration of RE ions, T is the temperature,

$$\Delta^{(i)} = \left(\sum_{\alpha} g^2{}_{\alpha\alpha}(\lambda M_{\mathrm{Fe}\alpha}^{(i)} + H_{\alpha}^{(i)})^2\mu_B^2\right)^{1/2}$$

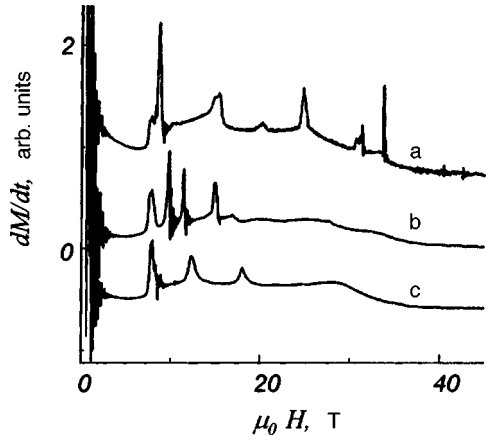

FIG. 2. Differential magnetic susceptibility of $Dy_{0.62}Y_{2.38}Fe_5O_{12}$ single crystals versus the external field at $T=4.2$ K for three different orientations of the external field: a — $\mathbf{H}\|[100]$, b — $\mathbf{H}\|[110]$, c — $\mathbf{H}\|[111]$.

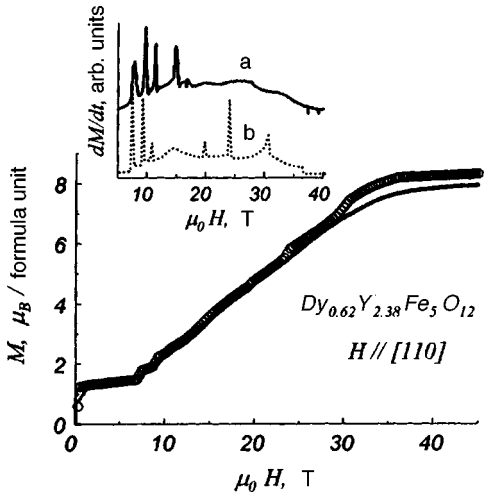

FIG. 3. Magnetization curves of $Dy_{0.62}Y_{2.38}Fe_5O_{12}$ single crystals at $T=4.2$ K with $\mathbf{H} \parallel [110]$: solid line — experiment; circles — calculations. Inset: Theoretical (dots) and experimental (solid line) curves $dM/dt(H)$.

is the energy splitting of the RE ion at the ith site as a result of exchange and Zeeman interactions, and $\alpha = x,y,z$. The equilibrium state was determined by minimizing the thermodynamic potential taking account of all possible states of the REIG that differ by the signs of the projections of the magnetic moments of the ions Dy^{3+} on the local Ising axes, after which the total magnetization of the crystal was calculated according to the formula $\mathbf{M} = -\partial\Phi/\partial\mathbf{H}$.

The computational results, which will be described in detail in a separate publication, can be summarized as follows. In magnetic fields less than H_1 the RE moments form a noncoplanar structure with an EA of the type [012], and the angle between the vectors $\mathbf{M}_{Fe}$ and $\mathbf{M}_R$ exceeds 90°. Such a structure also materializes for $H > H_2$ but with the difference that the angle between the vectors $\mathbf{M}_{Fe}$ and $\mathbf{M}_R$ is now less than 90°. In intermediate fields ($H_1 < H < H_2$) a transformation of the initial magnetic structure of the iron garnet occurs. This transformation is due to successive 180° flips of the magnetic moments of the REs in nonequivalent positions, accompanied by a deflection of the magnetic moment of the iron matrix away from the direction of the field (magnetic analog of the Jahn–Teller effect[4]). Both the number and amplitude of the magnetization jumps observed in the field range $H_1 < H < H_2$ depend on the orientation of the external magnetic field, as is characteristic for Ising magnets. The best quantitative agreement between the calculations and the experimental data was obtained for $g_{xx} = 10$, $g_{yy} = 3$, and $g_{zz} = 0$ (Fig. 3). We underscore especially that the form of the experimental and theoretical magnetization curves for $Dy_xY_{3-x}Fe_5O_{12}$ crystals differ substantially from that of the $M(H)$ curves of $Ho_xY_{3-x}Fe_5O_{12}$ compounds,[13] where the local Ising axes are aligned in directions of the type [100].

The smoother character of the magnetization curves for $Dy_{0.62}Y_{2.38}Fe_5O_{12}$ samples (see Fig. 1) as compared with $Ho_xY_{3-x}Fe_5O_{12}$ is due mainly to two factors. First, the number of degenerate magnetic phases is large, since in $Dy_{0.62}Y_{2.38}Fe_5O_{12}$ the local Ising axes are aligned in directions of the type [110] and not [100] as in $Ho_xY_{3-x}Fe_5O_{12}$.

Second, there is more than one nonzero component of the g factor of the Dy^{3+} ion, as indicated in Ref. 9. Of course, smoothing of the $M(H)$ curve can also appear as a result of a nonuniform distribution of the rare earth over the volume of the sample. Our analysis of Eq. (1), taking account of the statistical distribution of the Dy^{3+} ions in $Dy_{0.62}Y_{2.38}Fe_5O_{12}$, did not produce any qualitative or significant quantitative changes in the form of the computed curves $M(H)$.

In summary, the experimental and theoretical results in aggregate show that the iron garnet investigated is indeed a quasi-Ising magnet. The magnetization reversal of its rare-earth subsystem occurs by means of successive flips of the magnetic moments of the RE ions in nonequivalent positions (just as in Ising magnets). Since not only $g_{xx} \neq 0$ but also $g_{yy} \neq 0$, small rotations of the rare-earth magnetic moments toward the direction of the external field occur between flips of the moments, which is not observed in purely Ising systems (which is why we have used the term ''quasi-Ising'' in this paper).

In closing, we wish to express our sincere appreciation to R. Z. Levitin and A. S. Markosyan for providing the samples.

[1] W. P. Wolf, B. Schneider, D. P. Landau, and B. E. Keen, Phys. Rev. B **5**, 4472 (1972).
[2] D. P. Landau and B. E. Keen, Phys. Rev. B **19**, 4805 (1979).
[3] B. Schneider, D. P. Landau, B. E. Kenn, and W. P. Wolf, Phys. Lett. **23**, 210 (1966).
[4] A. K. Zvezdin, V. M. Matveev, A. A. Mukhin, and A. I. Popov, *Rare-Earth Ions and Magnetically Ordered Crystals* [in Russian], Nauka, Moscow, 1985.
[5] R. F. Pearson, J. Appl. Phys. **33** (Suppl), 1236 (1962).
[6] A. E. Clark and E. J. Callen, J. Appl. Phys. **39**, 5972 (1968).
[7] G. Aubert, J. Magn. Magn. Mater. **31-34**, 811 (1983).
[8] V. A. Borodin, V. D. Doroshev, and T. N. Tarasenko, Fiz. Met. Metalloved. **56**, 220 (1983).
[9] G. A. Babushkin, V. A. Borodin, V. D. Doroshev *et al.*, Zh. Éksp. Teor. Fiz. **87**, 989 (1984) [Sov. Phys. JETP **60**, 564 (1984)].
[10] V. Nekvasil and J. Veltrusky, J. Magn. Magn. Mater. **86**, 315 (1990).
[11] V. I. Ozhogin, K. G. Gurtovoi, and A. S. Lagutin, in *High Field Magnetism*, edited by M. Date, London, North-Holland, 1983, p. 267.
[12] K. P. Belov, A. K. Zvezdin, A. M. Kadomtsevs, and R. Z. Levitin, *Orientational Phase Transitions in Rare-Earth Magnets* [in Russian], Nauka, Moscow, 1985.
[13] V. I. Silant'ev, A. I. Popov, R. Z. Levitin, and A. K. Zvezdin, Zh. Éksp. Teor. Fiz. **78**, 640 (1980) [Sov. Phys. JETP **51**, 323 (1980)].

Translated by M. E. Alferieff

The electronic spectrum of a three-dimensional quasicrystal

D. V. Olenev,[a] E. I. Isaev, P. V. Slobodianiuk, and Yu. Kh. Vekilov
Moscow State Institute of Steel and Alloys, Theoretical Physics Department, 117936 Moscow, Russia

(Submitted 24 February 1998)
Pis'ma Zh. Éksp. Teor. Fiz. **67**, No. 8, 557–562 (25 April 1998)

The electronic spectrum of an icosahedral quasicrystal with a central-atom decoration of the Amman–Mackay network is investigated in the tight-binding approximation. The quasicrystal is described as a structural limit of the optimal cubic approximants with increasing period. The electronic spectra for the first four optimal cubic approximants do not contain the hierarchical gap structure which is typical for the Cantor set of the spectrum of a one-dimensional quasicrystal. At the same time, as the order of the approximant increases, the spectrum becomes singular throughout the entire energy scale. © *1998 American Institute of Physics.* [S0021-3640(98)00808-1]

PACS numbers: 71.23.Ft

Quasicrystals are objects which have non-crystallographic symmetry and positional long-range order (i.e., they coherently scatter electrons or x rays).[1] Quasicrystals exhibit unusual physical properties. They have a linear temperature contribution to the electronic heat capacity which is a bit smaller than that in simple metals.[2] Recent experiments show that below 4 K, with increasing structural order of the quasicrystal the temperature dependence of $c_v(T)$ becomes exponential (this indicates the presence of a gap in the electronic spectrum).[3] The resistivity of quasicrystals is anomalously high (it reaches nearly 2 $\Omega \cdot$cm at 0.5 K in the stable icosahedral phase of the system AlPdRe).[4] It depends strongly on the phase stoichiometry. It decreases when the temperature increases and increases with increasing structural order as well as with annealing of defects.[2,5] The Hall constant of quasicrystals is large and strongly temperature dependent, the optical conductivity does not follow Drude's law, and the thermoelectric power is also strongly temperature-dependent.[2,6] In weak magnetic fields a negative magnetoresistance is observed.[2] Most quasicrystalline phases (even alloys with transition elements) are weak diamagnets over a wide temperature interval.[6] It is obvious that all the specific properties mentioned are closely connected with electronic spectra of the quasicrystals.

The electronic spectra of quasiperiodic objects have been studied in detail for the cases of one- and two-dimensional quasicrystals.[7–10] The energy spectrum of a one-dimensional quasilattice (two-fragment Fibonacci chain) consists of a Cantor set of Lebesgue measure zero with a self-similar gap structure, and the wave functions are critical, being neither localized nor delocalized.[7,8] In the two-dimensional case the energy spec-

trum contains a singular (non smooth) part and the most wave functions are critical.[9,10] As a consequence of the exotic electronic structure of one- and two-dimensional quasicrystals there is a power-law dependence of the resistivity on the object size.[9] The character of the electronic spectrum and the wave functions of three-dimensional quasicrystals with the Amman–Mackay network structure have not been studied enough. Many investigators are inclined to think that this system does not contain any anomalies in the behavior of the wave functions and energy spectrum (see, for instance Ref. 11). For example, Marcus in his work on the electronic properties of the three-dimensional quasicrystal in the tight-binding approximation has not found any fundamental differences between the electronic properties of quasicrystals and crystals. He has concluded that the energy spectrum is smooth and the wave functions are delocalized.[12] On the other hand, Niizeki and Akamatsu have proposed that in the three-dimensional case ''critical'' wave functions do exist and that the energy spectrum has an exotic, singular continuous form.[13] The same results were obtained in the Refs. 14–16. Recently a structural model of three-dimensional icosahedral quasicrystals has been proposed wherein the quasicrystal is made with the help of a set of four tetrahedra.[11] The electronic spectrum of the three-dimensional quasicrystal with such a structure reveals strong oscillations of the density of states (DOS) throughout the entire energy range and the localization of selective states on special topological configurations.[11] So the existing results are contradictory and new investigations are needed.

In the present work the electronic energy spectrum of icosahedral quasicrystal is investigated in the tight-binding approximation. As quasicrystals do not possess translational symmetry and the traditional methods for calculations of the band structure of solids based on Bloch's theorem are no longer applicable, the objects of study are optimal cubic approximants of the icosahedral quasicrystal. The quasicrystal is regarded as the structural limit of a sequence of optimal cubic approximants with an increasing period, and the electronic properties of the approximants are investigated in the tight-binding approximation. The approximants are constructed by the projection method.[17] A Hamiltonian with constant transfer integrals for the nearest neighbors has been used to minimize the number of free parameters (the results for one- and two-dimensional quasicrystals show that this type of Hamiltonian makes it possible to reproduce the characteristic features of the quasicrystalline object and to consider qualitatively the influence of quasiperiodicity on the electronic structure of quasicrystals of the corresponding dimension.[2,7–10,18])

We have considered a ''central'' decoration of the approximants: atoms with one *s* orbital per atom are located at the centers of rhombohedra. In this case one can write the Hamiltonian of the system as

$$H=\sum_{j,j\neq i}|i\rangle t_{ij}\langle j|,$$

where the transfer integrals are chosen equal to a nonzero constant ($t_{ij}=-1$) only for the nearest neighbors, i.e., for atoms belonging to rhombohedra which have a common face (since the next-nearest neighbors do not introduce anything qualitatively new and only complicate the calculations). The projection method has been used to study the first four optimal cubic approximants of the icosahedral quasicrystals, namely the 1/1, 2/1, 3/2, and 5/3 approximants. The approximant f_{n+1}/f_n (where f_n is the Fibonacci sequence with

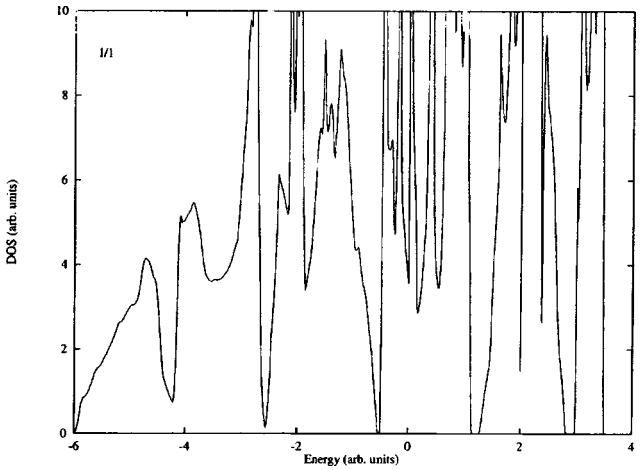

FIG. 1.

$f_0=f_1=1$, $f_n=f_{n-1}+f_{n-2}$ and $\lim_{n\to\infty} f_{n+1}/f_n=(1+\sqrt{5})/2=\tau$) involves the replacement of the irrational number $\tau=(1+\sqrt{5})/2$ describing the incommensurability of the icosahedral structure by a rational number f_{n+1}/f_n and is used for constructing the aforementioned approximants. With increasing number n of atoms in the basis, the period of the f_{n+1}/f_n approximant increases, and the approximant more accurately ''approximates'' the icosahedral quasicrystal. The case $n\to\infty$ describes the icosahedral quasicrystal. The unit cells of the approximants considered contained 32, 136, 576, and 2440 atoms in the basis, respectively.

The results of DOS calculations are presented in the figures. The calculations for the first three approximants, 1/1, 2/1, and 3/2 (Figs. 1, 2, and 3) have been done by the tetrahedra method using the values of energy levels at 40 **k**-points of the irreducible part

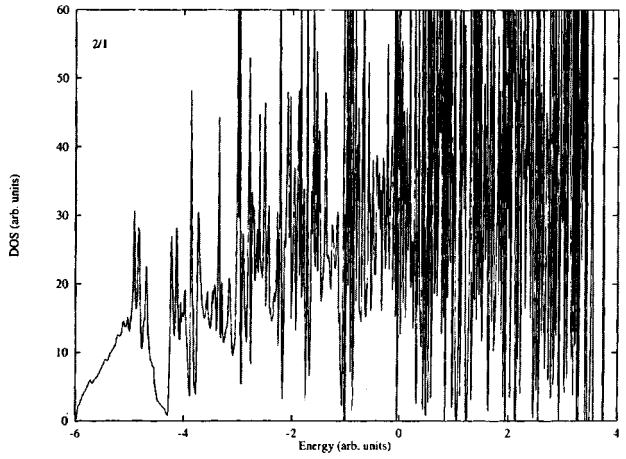

FIG. 2.

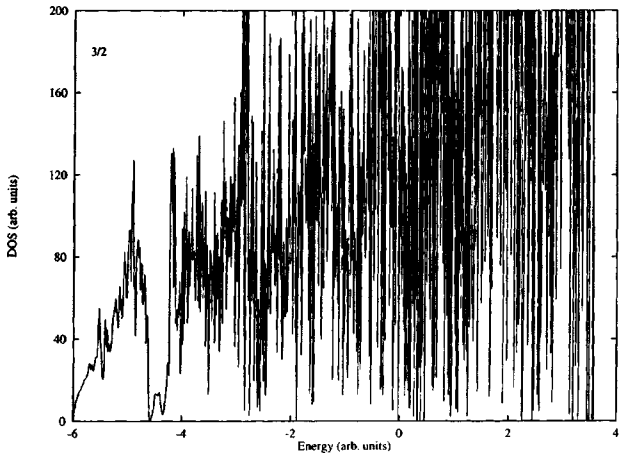

FIG. 3.

of the Brillouin zone of the corresponding approximant. For the 5/3 (Fig. 4) approximant we used only the four **k**-points in the irreducible part of the Brillouin zone. Because of a rather small volume of the Brillouin zone for the 5/3 approximant (as compared to the volume of the Brillouin zone for the first approximant), increasing the number of **k**-points in a calculation should only weakly influence the calculated DOS. One can see from figures that with increasing order of the periodic optimal approximant the DOS curves become less smooth and more ''spiky.'' This confirms the conclusion obtained by the method of level statistics.[14,16] that the energy spectrum of the icosahedral quasicrystal contains a singular (nonsmooth) part. In the opposite case (without a singular part) the DOS is a smooth curve. Besides, one can see from the figures that the smoothness of the spectrum depends on the energy range: the spectrum is smoother at low energies, and strong oscillations are present mostly in the high-energy range. However, with increasing

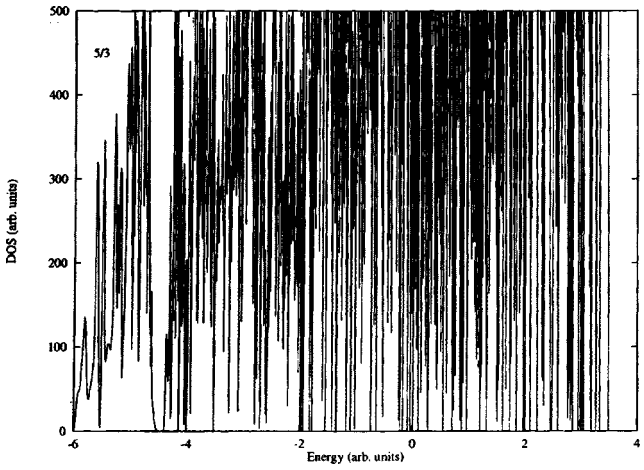

FIG. 4.

order of the approximant the length of the smooth region of the energy spectrum decreases. For this reason it seems reasonable that in the thermodynamic limit ($n \to \infty$, i.e., the case of a quasicrystal), strong DOS oscillations (a singular part of the spectrum) will be present throughout the entire energy range, including the long-wavelength part of the spectrum; this demonstrates that the energy bands in the quasicrystal are flat and practically dispersionless (this obviously influences the optical properties of quasicrystals). The plots in the figures are in good agreement with the DOS calculations for the first four periodic approximants, carried out by Carlson in the nearly-free-electron approximation:[19] a gap is seen in the region of small energies of the spectrum of the 5/3 approximant, though the energy spectrum of the lower-order approximants do not have such gaps.

Using the calculated DOS we determined the Lebesgue measure of the energy spectra of the investigated approximants. The Lebesgue measure of a one-dimensional set S is defined as an exact lower bound on the length sum of the finite or countable set of intervals which cover S. The Lebesgue measure of the energy spectrum was calculated as the total length of the admissible regions in the energy range $[-6;6]$ (according to the well-known theorem on spectrum boundaries[20] the energy levels of the investigated system belong to the interval $-6 \leqslant E \leqslant 6$). The Lebesgue measures of the energy spectra for the 1/1, 2/1, 3/2, and 5/3 approximants, normalized to the total bandwidth B (because of the fast convergence of the integrated DOS for the approximants considered, the B value for the 5/3 approximant was chosen), turned out to be equal to 0.95, 0.98, 0.98, and 0.97, respectively. For this reason one may conclude that for a three-dimensional quasicrystal the dependence of the Lebesgue measure of the energy spectrum on the order of the approximant is weak, in contrast with the case of a one-dimensional quasicrystal, where the Lebesgue measure of the energy spectrum of the periodic approximant decreases with system size according to a power law.[7,8] The rather small difference of the Lebesgue measures of the energy spectra of the last two approximants shows that the energy spectrum of three-dimensional quasicrystal occupies a region of finite width on the energy scale. Besides that, the values of the normalized Lebesgue measures of the energy spectra of the approximants considered (which close to 1) and the tendency of the results to converge show that the spectrum of the icosahedral quasicrystal does not have large energy gaps. Thus the energy spectrum of the three-dimensional quasicrystal has a ''non-Cantor'' (non-self-similar) character. This has to have an influence on the dependence of the conductance on the specimen length and the related properties of the three-dimensional quasicrystal.

In conclusion, the results show that the electronic spectrum of a three-dimensional icosahedral quasicrystal with Amman–Mackay network structure differs significantly from the electronic spectrum of a one-dimensional quasicrystal. As in the case of the one-dimensional quasicrystal, the energy spectrum of the three-dimensional quasicrystal contains a singular part. However, because of the different topology the structure of the energy spectrum of the icosahedral quasicrystal is non-self-similar, and for this reason the Lebesgue measure of the electronic energy spectrum of a three-dimensional quasiperiodic object is nonzero. Besides that, the energy spectrum of the investigated model of the icosahedral quasicrystal does not contain big gaps, and the quasiperiodicity of the structure results in very strong oscillations of the DOS throughout the entire energy range, including the long-wavelength part of the spectrum (the same is obviously true for the

other excitation spectra of quasicrystals — phonons, etc.). As a consequence, the energy bands in a quasicrystal are flat and practically dispersionless, the electrons are quasi-bound and have zero group velocity; this is obviously the cause of the anomalously low electrical conductivity, the low excitation energies of quasiparticles at the Fermi level, amd tje unusual magnetic properties (diamagnetism) of quasicrystalline alloys[21].

The authors acknowledge P. A. Korzhavyi and D. V. Livanov for their interest in this work and for a number of valuable remarks. This work was performed as part of Grant 96-02-16143 from the Russian Fund for Fundamental Research.

[a)]e-mail: olenev@trf.misa.ac.ru

---

[1] D. Shechtman, I. Blech, D. Gratias, and J. W. Cahn, Phys. Rev. Lett. **53**, 1951 (1984).
[2] S. J. Poon, Adv. Phys. **41**, 303 (1992).
[3] A. Inaba, S. Ishida, T. Matsuo *et al.*, Philos. Mag. Lett. **74**, 381 (1996);P. Archambault and C. Janot, MRS Bulletin/November **48** (1997).
[4] F. S. Pierce, S. J. Poon, and Q. Guo, Science **261**, 737 (1993); C. Berger, T. Grenet, P. Lindqvist *et al.*, Solid State Commun. **87**, 977 (1993).
[5] H. Akiyama, Y. Honda, T. Hashimoto *et al.*, Jpn. J. Appl. Phys., Part 2 **7**, L1003 (1993); Y. Honda, K. Edagava, A. Yoshika *et al.*, Jpn. J. Appl. Phys., Part 1 **9**, 4929 (1994).
[6] Z. M. Stadnik, G. W. Zhang, A.-P. Tsai, and A. Inoue, Phys. Rev. B **51**, 11358 (1995).
[7] P. A. Kalugin, A. Yu. Kitaev, and L. S. Levitov, JETP Lett. **41**, 145 (1985); Zh. Éksp. Teor. Fiz. **91**, 692 (1986) [Sov. Phys. JETP **64**, 410 (1986)].
[8] M. Kohmoto, B. Sutherland, and C. Tang, Phys. Rev. B **35**, 1020 (1987).
[9] H. Tsunetsugu, T. Fujiwara, K. Ueda, and T. Tokihiro, Phys. Rev. B **43**, 8879 (1991).
[10] H. Tsunetsugu, T. Fujiwara, K. Ueda, and T. Tokihiro, J. Phys. Soc. Jpn. **55**, 1420 (1986).
[11] G. Kasner, H. Schwabe, and H. Böttger, Phys. Rev. B **51**, 10454 (1995).
[12] M. A. Marcus, Phys. Rev. B **34**, 5981 (1986).
[13] K. Niizeki and T. Akamatsu, J. Phys.: Condens. Matter **2**, 2759 (1990).
[14] D. V. Olenev and Yu. Kh. Vekilov, JETP Lett. **63**, 113 (1996).
[15] D. V. Olenev and Yu. Kh. Vekilov, JETP Lett. **64**, 612 (1996).
[16] D. V. Olenev, E. I. Isaev, and Yu. Kh. Vekilov, JETP Lett. **113**, 1009 (1998).
[17] V. Elser, Phys. Rev. B **32**, 4892 (1985).
[18] L. Yamamoto and T. Fujiwara, Phys. Rev. B **51**, 8841 (1995).
[19] A. E. Carlsson, Phys. Rev. B **47**, 2515 (1993).
[20] H. Ehrenreich and L. Schwartz, *The Electronic Structure of Alloys*, New York, Academic Press, 1976.
[21] Yu. Kh. Vekilov, P. A. Korzhavii, and D. V. Olenev, JETP Lett. **62**, 372 (1995).

Published in English in the original Russian journal. Edited by Steve Torstveit.

Magnetic-field-induced hybridization of electron subbands in a coupled double quantum well

V. T. Dolgopolov, G. E. Tsydynzhapov, A. A. Shashkin, and E. V. Deviatov
Institute of Solid State Physics Russian Academy of Sciences, 142432 Chernogolovka, Moscow Region, Russia

F. Hastreiter, M. Hartung, and A. Wixforth
Ludwig-Maximilians-Universität D-80539 München, Germany

K. L. Campman and A. C. Gossard
Materials Department and Center for Quantized Electronic Structures, University of California, 93106 Santa Barbara, California, USA

(Submitted 13 March 1998)
Pis'ma Zh. Éksp. Teor. Fiz. **67**, No. 8, 563–568 (25 April 1998)

We employ a magnetocapacitance technique to study the spectrum of the soft two-subband (or double-layer) electron system in a parabolic quantum well with a narrow tunnel barrier at the center. In this system, when unbalanced by gate depletion, two sets of quantum oscillations are observed at temperatures $T \gtrsim 30$ mK: one originates from the upper electron subband in the closer-to-the-gate part of the well, and the other indicates the existence of common gaps in the spectrum at integer fillings. For the lowest filling factors $\nu=1$ and $\nu=2$, both the presence of a common gap down to the point of the one- to two-subband transition and their nontrivial magnetic field dependences point to magnetic-field-induced hybridization of electron subbands. © *1998 American Institute of Physics.* [S0021-3640(98)00908-6]

PACS numbers: 73.20.Dx, 73.40.Hm

A soft two-subband electron system, or electron double layer, is the simplest system having a degree of freedom, which is associated with the third dimension, in the integer (IQHE) and fractional (FQHE) quantum Hall effects. As compared to a conventional two-subband electron system with vanishing distance d between electron density maxima, such as the one in single heterojunctions, in the double layer the energy spacing between subbands is very sensitive to intersubband electron transfer because of the large $d \gtrsim a_B = \varepsilon\hbar^2/me^2$. Since the pioneering papers of Refs. 1 and 2, much attention has been paid to the investigation of balanced systems with symmetric electron density distributions. While in this case the origin of the IQHE at even integer filling factors is trivial, the symmetric–antisymmetric level splitting caused by tunneling gives rise to the IQHE at odd integer filling factors. The absence of certain IQHE states at low odd integer fillings[1,2] was interpreted in Refs. 3 and 4 as being due to the Coulomb-interaction-induced destruction of symmetric–antisymmetric splitting in high magnetic fields. There have been reported observations of both the bilayer many-body IQHE at filling factor

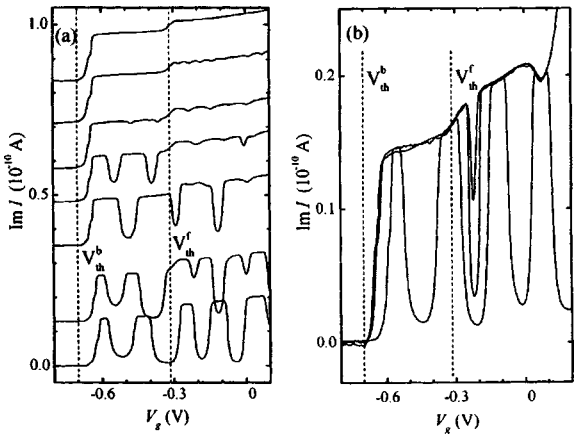

FIG. 1. Imaginary current component versus gate voltage at $f=110$ Hz at different temperatures and magnetic fields. a: $B=0$, 0.67, 1.34, 1.84, 2.51, 3.68, and 4.34 T at $T=30$ mK, the lines are shifted proportionally to steps in B; b: $T=30$, 620, and 880 mK at $B=6$ T.

$\nu=1$ (Refs. 5 and 6) and the FQHE (Refs. 7–10), whose origin, alternatively, has been attributed to interlayer correlation effects (Refs. 11–14). The case of an unbalanced system with strongly asymmetric electron density distributions was studied in Ref. 15. At relatively high filling factors the authors[15] observed an interplay between ''single- and double-layer behavior'' and explained this in terms of charge transfer between two electron subbands, without appealing to exchange and correlation effects.

Here, using a capacitive spectroscopy method, we investigate the spectrum of two-dimensional electrons in a quantizing magnetic field in a parabolic quantum well that contains a narrow tunnel barrier for the electron systems on either side. In the gate-depletion-unbalanced double-layer system, new gaps with unusual magnetic field dependences have been detected at filling factors $\nu=1$ and $\nu=2$. We argue that these emerge as a result of magnetic-field-induced hybridization of electron subbands.

The sample is grown by molecular beam epitaxy on semi-insulating GaAs substrate. The active layers form a 760 Å wide parabolic well. In the center of the well a 3 monolayer thick $Al_xGa_{1-x}As$ ($x=0.3$) sheet is grown which serves as a tunnel barrier between the two parts on either side. The symmetrically doped well is capped by 600 Å AlGaAs and 40 Å GaAs layers. The sample has two Ohmic contacts (each of them is connected to both electron systems in the two parts of the well) and a gate on the crystal surface with area 120×120 μm^2. The presence of the gate electrode makes it possible to tune the carrier density in the well and to measure the capacitance between the gate and the well. For capacitance measurements we apply an ac voltage $V_{ac}=2.4$ mV at frequencies f in the range 3 to 600 Hz between the well and the gate and measure both current components as a function of gate bias V_g, using a home-made I–V converter and a standard lock-in technique. Our measurements are performed in the temperature interval between 30 mK and 1.2 K at magnetic fields of up to 16 T.

The dependence of the imaginary current component on the gate voltage at different magnetic fields is shown in Fig. 1a. In zero magnetic field at $V_{\rm th}^b=-0.7$ V$<V_g<V_{\rm th}^f=-0.31$ V electrons fill only one subband in the back part of the well, relative to the

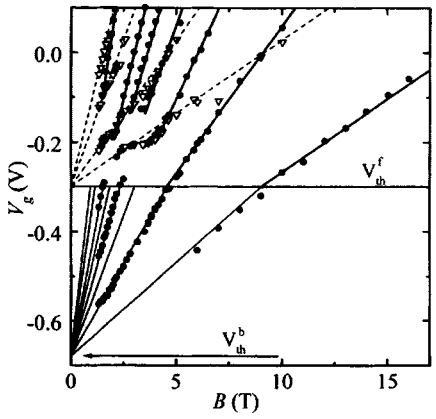

FIG. 2. Landau level fan chart as found from the minima of the density of states in the upper electron subband (open symbols, dashed lines) and of the conductivity of the lower electron subband (filled symbols, solid lines) and of the conductivity of the double-layer electron system (filled symbols, bold lines). The bold line disruptions signify the absence of common gaps. At crossing points of the dashed and bold lines the corresponding minima trigger with changing temperature.

gate. With increasing $V_g > V_{\rm th}^f$ a second electron subband starts to collect electrons in the front part of the well, as is indicated by an increase of the capacitance. In magnetic fields of about 1.3 T at low temperatures we observe two sets of quantum oscillations: first, the oscillations at $V_g > V_{\rm th}^f$ are due to the modulation of the thermodynamic density of states in the upper electron subband. They are typical of a three electrode system (see, e.g., Refs. 16 and 17) and depend only weakly on temperature in the regime investigated. Second, the oscillations at $V_g < V_{\rm th}^f$ originate from the conductivity oscillations in the lower electron subband, and so these are accompanied by peaks in the real current component. With increasing magnetic field, one more set of oscillations emerges, formed by additional minima at $V_g > V_{\rm th}^f$ (Fig. 1a). The small values of capacitance at the oscillation minima and the nonzero active current component indicate that the conductivity σ_{xx} vanishes for both electron subbands. Since they arerelated to σ_{xx}, these common oscillations are strongly temperature-dependent, whereas the measured capacitance in between the deep minima depends weakly on temperature. As seen from Fig. 1b, the weak oscillations reflecting the thermodynamic density of states in the upper subband persist after the appearance of the common oscillations. In particular, when located between deep minima, these do not change at all as the latter develop. For coincident positions, the minima for the two kinds of oscillations trigger with changing temperature.

Figure 2 presents a Landau level fan diagram in the (B, V_g) plane for our sample. Positions of the density of states minima in the upper electron subband are shown by open symbols. These minima correspond to the filling factors $\nu_2 = 1, 2, 4, 6$ in the upper subband. The conductivity minima are marked in Fig. 2 by solid symbols. In the gate voltage interval $V_{\rm th}^b < V_g < V_{\rm th}^f$ we see the filling factors $\nu_1 = 1, 2, 4, 6$ in the lower subband. Furthermore, for $V_g > V_{\rm th}^f$ the common oscillations define a third Landau level fan. The straight lines of this fan are parallel to those for the upper electron subband and correspond to $\nu = 1, 2, 3, 4, 5, 6, 8, 10$, which is the filling factor defined in terms of the electron density N_s in the quantum well. In the (B, V_g) plane the different slopes of the

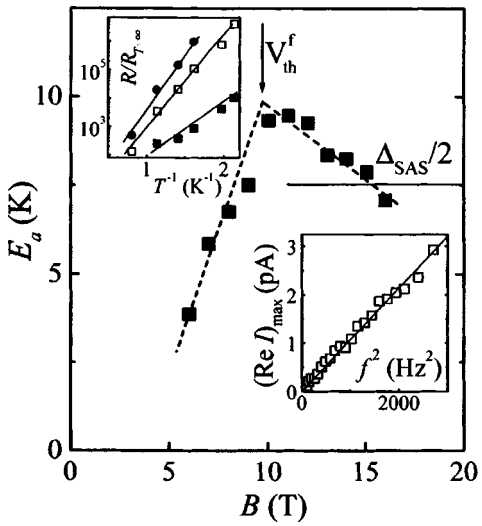

FIG. 3. Activation energy as a function of magnetic field at filling factor $\nu=1$. The insets display the frequency dependence of the active current component peak (bottom) and Arrhenius plot of the peak amplitude for $B=6$, 10, and 14 T (top).

fan lines below and above $V_g=V_{\rm th}^f$ (Fig. 2) correspond to the capacitance values before and after the jump near $V_g=V_{\rm th}^f$ (Fig. 1). One can see from Fig. 2 that despite the fact that upon variations in the gate voltage $V_g>V_{\rm th}^f$ the electron density changes substantially in the front part of the well, as is indicated by the fan line slopes, it is for integer ν that common gaps are observed in the double-layer system.

The activation energy in the common oscillation minima is found from the temperature dependence of peaks in the active current component, which accompany capacitance minima. In the limit of vanishing active current component the peak amplitude is expected to be proportional to $f^2\sigma_{xx}^{-1}$. To make sure that the measuring frequency is sufficiently low, we investigate the frequency dependence of the active current component (see the bottom inset to Fig. 3). In the frequency range where the above relation holds, the activation energy is simply determined from Arrhenius plot of the peak amplitude (the top inset to Fig. 3). Figure 3 displays the magnetic field dependence of the activation energy for filling factor $\nu=1$. This dependence is quite nontrivial: the activation energy is a maximum at about $V_g=V_{\rm th}^f$, where a second electron subband starts to be filled, and then it monotonically decreases with magnetic field up to the balance point. A similar behavior is found also for filling factor $\nu=2$. Although the gaps at filling factors $\nu>2$ are also maximal near the threshold voltage $V_{\rm th}^f$, at higher fields, unlike the gaps at $\nu=1$ and $\nu=2$, they vanish in some intervals of B (or V_g). This is indicated by disruptions of the fan lines in Fig. 2.

The band structure of our sample in the absence of magnetic field is known from far-infrared spectroscopy and magnetotransport investigations on samples fabricated from the same wafer.[18,19] It agrees with the result of self-consistent Hartree calculation of energy levels in a coupled double quantum well (Fig. 4). In the calculation one reasonably assumes that all electron subbands have a common electrochemical potential which

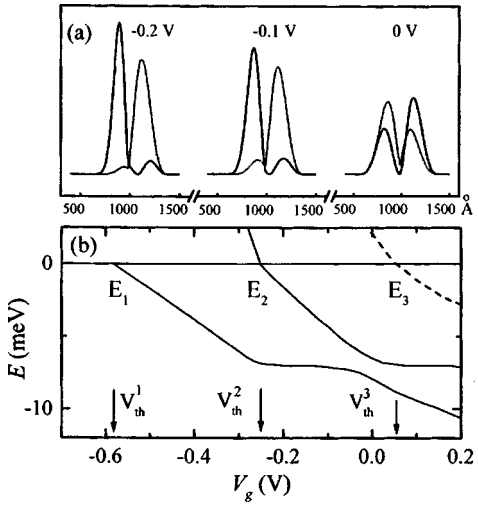

FIG. 4. Calculated at $B=0$, electron density distributions for the two lower energy bands in the quantum well (a) and positions of the energy band bottoms as a function of the gate voltage (b). The dotted and solid lines in case (a) correspond to E_1 and E_2, respectively.

corresponds to the zero-point on the energy scale in Fig. 4b. In agreement with experiment, only one energy band is occupied by electrons in the range $V_{\rm th}^1<V_g<V_{\rm th}^2$, two energy bands are filled at $V_{\rm th}^2<V_g<V_{\rm th}^3$, and three of them are filled above $V_g=V_{\rm th}^3$. The band splitting at a zero gate voltage is symmetric–antisymmetric splitting $\Delta_{SAS}=1.3$ meV. Figure 4a shows the electron density profiles for the two lower energy bands in the quantum well at three different gate voltages. We note that for both energy bands, even far from the balance, the wave function is not completely localized in either part of the quantum well.

Experimentally, the possibility of all the electrons collecting in one part of the quantum well (so-called broken-symmetry states)[20] is excluded because of the coexistence of the Landau level fan for the upper subband and the one determined by common oscillations (Fig. 2).

One can tentatively expect that the experimental data find their interpretation in terms of a relative shift of the Landau level ladders corresponding to two electron subbands. At fixed integer ν, the conductivity σ_{xx} of a bilayer system should tend to zero in the close vicinities of Landau-level-fan crossing points in the (B,V_g) plane, at which both individual filling factors ν_f,ν_b are integers, as long as the Fermi level remains in a gap between quantum levels for two electron subbands. Obviously, in between the crossing points the common gap closes as soon as the Fermi level pins to both of the quantum levels. Such behavior is indeed observed in the experiment at filling factors $\nu>2$ (see Fig. 2). We note that the presence (absence) of common gaps was identified in Ref. 15 as ''single (double) layer behavior.'' In contrast, for a conventional two-subband electron system with vanishing distance between electron density maxima, common gaps at integer ν are expected to close in negligibly narrow intervals on the Landau-level-fan lines where both quantum levels from two electron subbands cross the Fermi level.

However, such simple considerations fail to account for the common gaps at filling factors $\nu=1,2$ which do not disappear in the entire range from the threshold $V_{\rm th}^f$ to the balance point (Figs. 2 and 3). We explain this behavior as a result of magnetic-field-induced hybridization of the wave functions of two electron subbands, which gives rise to the creation of new gaps in the bilayer spectrum.

In a soft two-subband electron system, the quantum level energies for two Landau level ladders can become equal only if the corresponding wave functions are orthogonal, i.e., if the Landau level numbers are different. Apparently, this is not the case for $\nu=1,2$ or for higher $\nu\neq 4m$ (m is an integer) near the balance point. The absence of orthogonality implies that the bilayer system is described by a hybrid wave function that is a linear combination of the wave functions of two electron subbands. The appearance of new gaps, as a result, is crucially determined by intersubband charge transfer in magnetic field to make the band bottoms coincident. We note that this process is impossible in the conventional two-subband system as discussed above. Although in our soft two-subband system the distance between electron density maxima (Fig. 4) is close to the in-plane distance between electrons, the amount of charge transferred is estimated to be small. This is confirmed experimentally by the absence of appreciable deviations of the data points from the upper-subband-fan lines (Fig. 2) as determined by zero-magnetic-field capacitance at $V_g>V_{\rm th}^f$ (Fig. 1). It is clear that the magnetic-field-induced hybridization generalizes the case of symmetric electron density distributions corresponding to formation of Δ_{SAS}. From the first sight it seems natural to expect that the common gaps at $\nu=1,2$ decrease with magnetic field and approach Δ_{SAS} at the balance point (Fig. 3). Yet, for all the filling factors in question the situation is far more sophisticated, because the spin splitting, which is comparable to the hybrid splitting, comes into play. The bilayer spectrum is then determined by their competition, which, in principle, may even lead to the closing of common gaps in some intervals of magnetic field. For example, at $\nu=2$ the actual gap is given by the splitting difference, and so it vanishes for equal splittings. In our experiment, for the simplest case of $\nu=1$ one can expect that over the range of magnetic fields used, the many-body enhanced spin gap is large compared to Δ_{SAS} (Ref. 17). That stands to reason, since it is the smaller splitting that corresponds to $\nu=1$ (Fig. 3). For $\nu=2$ the very similar behavior of the gap with magnetic field hints that at these lower fields the hybrid splitting is dominant. As a result of interchange of the hybrid and spin splittings, odd $\nu>1$ near the balance in our case correspond to spin rather than hybrid gaps.

In summary, we have performed magnetocapacitance measurements on a bilayer electron system in a parabolic quantum well with a narrow tunnel barrier in its center. For asymmetric electron density distributions created by gate depletion in this soft two-subband system we observe two sets of quantum oscillations. These originate from the upper electron subband in the front part of the well and from the gaps in the bilayer spectrum at integer fillings. For the lowest filling factors $\nu=1$ and $\nu=2$, the common gap formation is attributed to magnetic-field-induced hybridization of electron subbands, dependent on the competition between the hybrid and spin splitting.

We gratefully acknowledge J. P. Kotthaus, A. V. Chaplik and M. Shayegan for fruitful discussions of the results. This work was supported in part by Volkswagen-Stiftung under Grant I/71162, Deutsche Forschungsgemeinschaft, AFOSR under Grant F49620-94-1-0158, INTAS under Grant 93-933, the Russian Fund for Fundamental Re-

search under Grant 97-02-16829, and the Program ''Statistical Physics'' from the Russian Ministry of Sciences. The Munich–Santa Barbara collaboration has been also supported by a joint NSF-European Grant and the Max Planck Research Award.

[1] G. S. Boebinger, H. W. Jiang, L. N. Pfeiffer, and K. W. West, Phys. Rev. Lett. **64**, 1793 (1990).
[2] Y. W. Suen, J. Jo, M. B. Santos *et al.*, Phys. Rev. B **44**, 5947 (1991).
[3] A. H. MacDonald, P. M. Platzman, and G. S. Boebinger, Phys. Rev. Lett. **65**, 775 (1990).
[4] L. Brey, Phys. Rev. Lett. **65**, 903 (1990).
[5] S. Q. Murphy, J. P. Eisenstein, G. S. Boebinger *et al.*, Phys. Rev. Lett. **72**, 728 (1994).
[6] T. S. Lay, Y. W. Suen, H. C. Manoharan *et al.*, Phys. Rev. B **50**, 17725 (1994).
[7] Y. W. Suen, L. W. Engel, M. B. Santos *et al.*, Phys. Rev. Lett. **68**, 1379 (1992).
[8] J. P. Eisenstein, G. S. Boebinger, L. N. Pfeiffer *et al.*, Phys. Rev. Lett. **68**, 1383 (1992).
[9] Y. W. Suen, J. Jo, M. B. Santos *et al.*, Phys. Rev. B **44**, 5947 (1991).
[10] Y. W. Suen, H. C. Manoharan, X. Ying *et al.*, Surf. Sci. **305**, 13 (1994).
[11] T. Chakraborty and P. Pietilainen, Phys. Rev. Lett. **59**, 2784 (1987).
[12] D. Yoshioka, A. H. MacDonald, and S. M. Girvin, Phys. Rev. B **39**, 1932 (1989).
[13] H. A. Fertig, Phys. Rev. B **40**, 1087 (1989).
[14] S. He, X. C. Xie, S. Das Sarma, and F. C. Zhang, Phys. Rev. B **43**, 9339 (1991).
[15] A. G. Davies, C. H. W. Barnes, K. R. Zolleis *et al.*, Phys. Rev. B **54**, R17331 (1996).
[16] R. C. Ashoori and R. H. Silsbee, Solid State Commun. **81**, 821 (1992).
[17] V. T. Dolgopolov, A. A. Shashkin, A. V. Aristov *et al.*, Phys. Low-Dimens. Semicond. Struct. **6**, 1 (1996); V. T. Dolgopolov, A. A. Shashkin, A. V. Aristov *et al.*, Phys. Rev. Lett. **79**, 729 (1997).
[18] M. Hartung, A. Wixforth, K. L. Campman, and A. C. Gossard, Solid-State Electron. **40**, 113 (1996).
[19] G. Salis, B. Graf, K. Ensslin *et al.*, Phys. Rev. Lett. **79**, 5106 (1997).
[20] T. Jungwirth and A. H. MacDonald, Phys. Rev. B **53**, 9943 (1996).

Published in English in the original Russian journal. Edited by Steve Torstveit.

Dispersion of the Voigt effect in the magnetic semiconductors $Cd_{1-x}Mn_xTe$

B. B. Krichevtsov, R. V. Pisarev, A. A. Rzhevskiĭ, and V. N. Gridnev
A. F. Ioffe Physicotechnical Institute, Russian Academy of Sciences, 194021 St. Petersburg, Russia

H.-J. Weber
Physics Department, Dortmund University, 44221 Dortmund, Germany

(Submitted 17 March 1998)
Pis'ma Zh. Éksp. Teor. Fiz. **67**, No. 8, 569–573 (25 April 1998)

Spectral measurements of the Voigt birefringence Δn were performed for the cubic magnetic semiconductor $Cd_{1-x}Mn_xTe$ ($0 \leqslant x \leqslant 0.52$) in order to investigate how the exchange interaction of Mn^{2+} ions with itinerant electrons depends on the electron wave vector. It was determined that $\Delta n/x^2$ is independent of x and the magnetic field direction, i.e., the effect is due to the Mn^{2+} ions and is isotropic. Below the band gap edge the dispersion of the birefringence Δn can be described well in all samples by the unusual dependence $\Delta n \sim (E_g - \hbar\omega)^{-3.5}$. This can be explained by a decrease of the exchange interaction of Mn^{2+} ions with itinerant electrons with increasing distance from the center of the Brillouin zone. © *1998 American Institute of Physics.*
[S0021-3640(98)01008-1]

PACS numbers: 75.50.Pp, 78.20.Fm, 78.20.Ls

The Voigt effect — birefringence induced by an external magnetic field **B** — is quadratic in **B** and therefore invariant under time reversal, or T-even. This makes it insensitive to the sign of T-odd quantum numbers characterizing the state of the experimental object. In consequence, spectral measurements of the Voigt effect are ordinarily less informative than measurements of the Faraday effect (which is linear in the magnetic field), if the problem is the investigation of electronic excitation spectra. Together with the relative smallness of the induced birefringence, this greatly narrows the range of application of the Voigt effect as compared with the Faraday effect.

However, going beyond the bounds of the problem of determining the electronic excitation spectrum in the narrow sense, the quadratic dependence of the Voigt effect on the magnetic field can be an advantage under certain conditions. We encountered just such a situation while investigating the microscopic nature of magnetooptic effects in the magnetic semiconductors (also called semimagnets) $Cd_{1-x}Mn_xTe$.[1] Such investigations are necessary in connection with the difficulties arising in the interpretation of the Faraday effect under conditions when the contribution of transitions between valence band Γ_8 and the conduction band Γ_6 predominates,[2] since the spectral dependence of the rotation angle $\phi \sim (E_g - \hbar\omega)^{-3/2}$ in the frequency range $\hbar\omega < E_g$ is sharper than the theoretically

predicted and observed dependence $\phi \sim (E_g - \hbar\omega)^{-1/2}$ in cubic nonmagnetic semiconductors (see, for example, Ref. 3). In Ref. 2 it was shown that this discrepancy between theory and experiment can be eliminated by assuming, on the basis of experimental results on magnetoreflection[4,5] and subsequent theoretical analysis,[6,7] that the splittings of the Γ_6 and Γ_8 bands in a magnetic field depend on the wave vector $\mathbf{k}$ of the itinerant electrons and decrease strongly with distance from the center of the Brillouin zone. As is well known,[8] in $Cd_{1-x}Mn_xTe$ these splittings are determined mainly by the exchange interaction of Mn^{2+} ions with itinerant carriers and, at the center of the Brillouin zone, are given by the relations $\Delta E_r = 3rA$ and $\Delta E_s = sB$, where $r = \pm 1$ and $s = \pm 1, \pm 3$ enumerate the states of the Γ_6 and Γ_8 bands, respectively. The parameters A and B describe the exchange interaction of Mn^{2+} ions with itinerant electrons:[8] $A = \frac{1}{6} N_0 \alpha(\mathbf{k}=0)\langle S_z^{Mn}\rangle x$ and $B = \frac{1}{6} N_0 \beta(\mathbf{k}=0)\langle S_z^{Mn}\rangle x$, where N_0 is the number of unit cells per unit volume, $\langle S_z^{Mn}\rangle$ is the average spin of the Mn^{2+} ions which is induced by the magnetic field ($\mathbf{B} \| z$), and $\alpha(\mathbf{k})$ and $\beta(\mathbf{k})$ are exchange integrals for the conduction and valence bands, respectively.

A decrease of $\Delta E_{rs} = \Delta E_r - \Delta E_s$ with increasing k results in an increase of the relative contribution of the interband transitions with small k to magnetooptic effects and, in consequence, a sharper frequency dependence of these effects for $\hbar\omega < E_1 < E_g$, where E_1 is an energy parameter which depends on the character of the k dependence of ΔE_{rs}: The smaller the size k_0 of the region near the center of the Brillouin zone in which the exchange integrals $\alpha(\mathbf{k})$ and $\beta(\mathbf{k})$ do not vary much, the closer E_1 is to E_g. So, a change of the exponent ν in the dispersion of the Faraday rotation $\phi \sim (E_g - \hbar\omega)^{\nu}$ from $\nu = -1/2$ to $-3/2$ in a wide range of frequencies $\hbar\omega < E_g$ is possible only under the condition that k_0 is sufficiently small, at least an order of magnitude less than the size k_B of the Brillouin zone.[2]

We note that there is nothing surprising about the k dependence of the splittings of the energy bands in itself, since the effective Hamiltonians of the itinerant electrons depend on k. However, the change in ΔE_{rs} as a result of this factor[6,7] is much smaller than that observed experimentally,[4,5] and for this reason it was suggested in Ref. 7 that the main reason for the decrease of ΔE_{rs} with distance from the center of the Brillouin zone is the k dependence of the exchange integrals α and β. As was noted in Ref. 7, the calculation of the functions $\alpha(\mathbf{k})$ and $\beta(\mathbf{k})$ in a realistic model is a difficult problem. These considerations show that experimental investigations of this problem, including studies by magnetooptic methods, are now timely.

To obtain more-reliable information about the character of the wave vector dependence of the exchange integrals it is natural to investigate the effects where such a dependence would be most strongly manifested. The Voigt effect is such an effect, since it is a quadratic function of the exchange integrals. This circumstance dictated our choice of the Voigt effect for investigating the problem set forth above. We note that in Ref. 9 the Voigt birefringence measurements in $Cd_{1-x}Mn_xTe$ were performed at low temperatures in a narrow spectral region near the excitonic resonance and for this reason can be described well by the exchange interaction parameters referring to the center of the Brillouin zone. Dispersion of the exchange integrals can appear only at frequencies not too close to the excitonic transition or the band gap edge in the case when interband transitions make the dominant contribution to the effect. For this reason, we undertook

the investigation of the dispersion of Voigt birefringence in $Cd_{1-x}Mn_xTe$ in the region $\hbar\omega < E_g$.

For the birefringence measurements we used an experimental apparatus whose main elements are: a light source (He–Ne laser, $\lambda = 0.633$ μm and 1.15 μm, and a Al_2O_2:Ti laser, $\lambda = 0.7$–0.83 μm), a polarizer, a Glan prism, a sample in the gap of an electromagnet $\mathbf{B} \perp \mathbf{q}$ ($\mathbf{q}$ is the wave vector of the light), a tunable quarter-wave plate, a Faraday modulator, an analyzer, and a photodiode. When measuring birefringence the polarization of the light after the polarizer must be parallel to one of the axes of the quarter-wave plate and make an angle of 45° with the principal directions of a section through of the optical indicatrix of the crystal. The value of the birefringence is determined from the relation $\Delta n = \lambda\alpha/\pi d$, where α is the analyzer rotation angle corresponding to extinction, equal to half the phase shift between the linearly polarized normal waves, and d is the thickness of the sample. We employed a geometry in which the polarization of the incident light and the axis of the quarter-wave plate made an angle of 45° with $\mathbf{B}$. The crystal could rotate in the gap of the electromagnet in the range of azimuthal angles $0 < \theta < 360°$ around an axis pointing in the direction $\mathbf{q}$. The magnetic field varied in the range ± 1.5 T. The linear birefringence due to internal stresses in the crystal and to the Lorentz birefringence was measured in the absence of a magnetic field. The sensitivity of the measurements of the angle of rotation of the plane of polarization was equal to 10″. The measurements were performed at temperature $T = 294$ K. In all crystals the dispersion of the refractive index was measured by measuring the rotation of the plane of polarization of light reflected from the surface of the crystal for different angles of incidence. The refractive index n was calculated according to the Fresnel formulas.

The measurements were performed on $Cd_{1-x}Mn_xTe$ single crystals with Mn^{2+} ion density $x = 0$, 0.25, 0.35, 0.42, and 0.52. The band gap E_g was calculated using the formulas presented in Ref. 1. The samples were cut out in planes of the type (110), (111) and consisted of polarized plates with dimensions of about $2 \times 3 \times 0.7$ mm. The orientation of the samples was set using x-ray diffraction by the Bragg reflection method. The Laue diffraction patterns of the crystals were investigated in reflection in order to check the degree of crystal perfection and the presence of twins and intergrowths in the crystals. The spontaneous birefringence of the experimental samples did not exceed $\Delta n \simeq 5 \times 10^{-6}$.

Since the $Cd_{1-x}Mn_xTe$ crystals are noncentrosymmetric (point group T_d), the measured angle α is determined not only by the Voigt effect, which is quadratic in the magnetic field $\mathbf{B}$, but also by the magnetically induced spatial dispersion that is linear in $\mathbf{B}$ and which is associated with bilinear terms of the type $\Delta\epsilon_{ij} = \gamma_{ijkl} q_k B_l$ in the permittivity tensor ϵ_{ij}. This effect also leads to birefringence, and therefore the field dependences $\alpha(B)$ in all experimental samples are nonsymmetric relative to the value $\mathbf{B} = 0$ and can be described by the sum of the contributions that are quadratic and linear in the magnetic field. The different character of the $\mathbf{B}$ dependence of these contributions makes it possible to distinguish them simply and reliably. The measurement results and the analysis of the magnetically induced spatial dispersion linear in $\mathbf{B}$ are of interest in their own right and were published in Ref. 10. In the present letter we examine only the Voigt effect which is quadratic in $\mathbf{B}$.

In all crystals the contribution that is quadratic in the magnetic field is independent of the direction of $\mathbf{B}$ within the limits of experimental error. This attests to the isotropy of

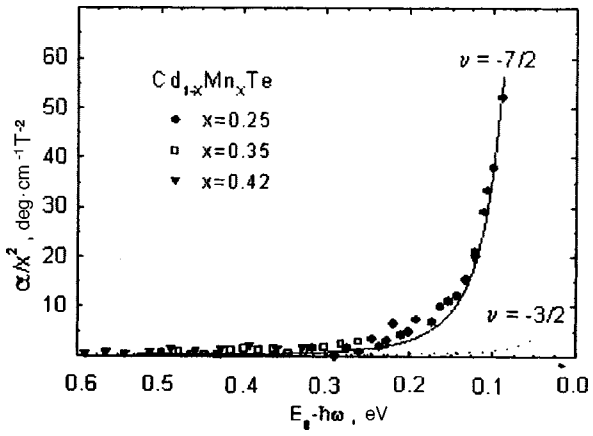

FIG. 1. Spectral dependence of the normalized values of the Voigt effect α/x^2 versus $(E_g-\hbar\omega)$ in crystals with different concentrations of magnetic ions Mn^{2+}. The solid and dashed lines correspond to the computed dependences with the indicated values of the exponent ν.

the effect. We note that for (110)-type samples the cubic symmetry admits anisotropy of the Voigt effect.

Figure 1 shows the spectral dependences of the normalized values of the Voigt effect α/x^2 for all the experimental samples. As one can see from the figure, these dependences are universal, i.e., they do not depend on x. Therefore, the Voigt effect is quadratic in x. Such a dependence attests to the fact that the Mn^{2+} ions make the dominant contribution to the Voigt effect. The dispersion of the Voigt effect in different samples is described well by the function $(E_g-\hbar\omega)^{-3.5}$.

The measured frequency dependence $\alpha(\omega)\sim\omega\Delta n(\omega)$ was found to be much sharper than the theoretically predicted dependence in nonmagnetic semiconductors, where $\Delta n\sim(E_g-\hbar\omega)^{-3/2}$ (see, for example, Ref. 11). Since, as was noted in Ref. 2, the sharper spectral dependence of linear magnetooptic effects could be due to k dependence of the exchange integrals, we shall calculate the contribution of transitions from the valence band Γ_8 into the conduction band Γ_6 with allowance for k dependence in the quadratic Voigt effect.

Expanding the permittivity tensor $\epsilon_{ij}(\omega,\mathbf{B})$ in the magnetic field $\mathbf{B}$ and retaining only the resonance term, which varies most rapidly with frequency near E_g, we obtain the following expression for the tensor β_{ijkl} which determines the Voigt effect in the phenomenological relation $\Delta\epsilon_{ij}=\beta_{ijkl}B_kB_l$:

$$\beta_{ijkl}=\frac{4\pi\hbar e^2}{\omega V}\frac{\partial}{\partial B_l\partial B_k}\sum_{r,s,\mathbf{k}}\frac{v^i_{s\mathbf{k},r\mathbf{k}}v^j_{r\mathbf{k},s\mathbf{q}}}{E_{r\mathbf{k},s\mathbf{k}}(E_{r\mathbf{k},s\mathbf{k}}-\hbar\omega)}\bigg|_{\mathbf{B}\to 0}, \tag{1}$$

where V is the volume of the crystal; $E_{r\mathbf{k},s\mathbf{k}}$ is the transition energy between the states of the valence band ($s=\pm1,\pm3$) and the conduction band ($r=\pm1$); and, $\mathbf{v}$ is the electron velocity operator. In the group T_d the tensor β_{ijkl}, which is symmetric in the indices i,j and k,l, has three linearly independent components β_{11}, β_{12}, and β_{44}. Since Δn does

not depend on the direction of **B** in the spectral interval which we investigated, the isotropic medium approximation, in which $2\beta_{44}=\beta_{11}-\beta_{12}$ and $\Delta n=2\beta_{44}B^2/n$, can be used.

Since we are interested primarily in the frequency dependence of Δn near E_g, i.e., the most singular part of Δn, to evaluate the quantity in Eq. (1) we shall make a number of simplifications. We shall neglect the dependence of the velocity matrix elements on **B** and **k**, i.e., we shall assume that they are constants. Moreover, we shall neglect the anisotropy of the spectrum, both the crystalline anisotropy and the anisotropy due to the magnetic field. These factors are important only for calculating the absolute value of Δn, which can be done only by numerical calculation of the spectrum and matrix elements of the velocity operator followed by numerical integration in Eq. (1). Further, as was shown in Ref. 2, the contribution of light holes to magnetooptic effects in $Cd_{1-x}Mn_xTe$ is small compared with the contribution of heavy holes. This also introduces a large simplification in the calculation of Δn. Then, with **k**-independent exchange integrals α and β, we obtain the well-known[11] dependence $\Delta n\sim(E_g-\hbar\omega)^{-3/2}$. If the k dependence of the exchange integrals α and β is now taken into account, assuming, as in Ref. 2, that $\alpha,\beta\sim k_0^2/(k_0^2+k^2)$, then in the photon energy range determined by the parameter

$$\kappa=m_{ch}E_g/\hbar^2k_0^2(1-\hbar\omega/E_g)\sim 1, \quad m_{ch}^{-1}=m_c^{-1}+m_{hh}^{-1},$$

the character of the behavior of Δn changes from $\Delta n\sim(E_g-\hbar\omega)^{-3/2}$ for $\kappa\ll 1$ to $\Delta n\sim(E_g-\hbar\omega)^{-7/2}$ for $\kappa\gg 1$. If it is assumed, as done in Ref. 2, that the parameter k_0 is small compared with the size of the Brillouin zone, then the spectral interval investigated in this work corresponds to the condition $\kappa\gg 1$, which leads to the dependence $\Delta n\sim(E_g-\hbar\omega)^{-7/2}$, in agreement with the dependence obtained in our experiment.

In summary, the spectral dependence obtained in the present work for Voigt birefringence below the interband absorption edge agrees with the conjecture made in Ref. 2 that the exchange interaction of Mn^{2+} ions with itinerant electrons decreases rapidly with distance from the center of the Brillouin zone. We underscore that the results of our work indicate new possibilities for using the Voigt effect for investigating the microscopic mechanisms of magnetooptic phenomena and the exchange interaction in a wide class of semiconductor materials doped with magnetic ions.

This work was supported by the Russian Fund for Fundamental Research under the program ''Fundamental Spectroscopy'' and by Deutsche Forschungsgemeinschaft.

[1] J. K. Furdyna, J. Appl. Phys. **64**, R29 (1988).
[2] S. Hugonnard-Bruyère, C. Buss, F. Vouilloz *et al.*, Phys. Rev. B **50**, 2200 (1994).
[3] J. G. Mavroides, in *Optical Properties of Solids*, edited by F. Abelès, North Holland, Amsterdam, 1972.
[4] E. Dudziak, J. Brzezinski, and L. Jedral, in *Physics of Semiconducting Compounds*, Polish Academy of Sciences, Warsaw, 1982, p. 166.
[5] D. Coquillat, J. P. Lascaray, M. C. Desjardins-Deruelle *et al.*, Solid State Commun. **59**, 25 (1986).
[6] J. Ginter, G. A. Gay, and Le Dang, Solid State Commun. **48**, 849 (1983).
[7] A. K. Bhattacharjee, Phys. Rev. B **41**, 5696 (1990).
[8] J. A. Gaj, in *Semiconductors and Semimetals*, edited by J. K. Furdyna and J. Kossut, Academic Press, Boston, 1988, Vol. 25, p. 275.
[9] Eunsoon Oh, D. U. Bartholomew, A. K. Ramdas *et al.*, Phys. Rev. B **44**, 10551 (1991).
[10] B. B. Krichevtsov, R. V. Pisarev, A. A. Rzhevsky *et al.*, Phys. Rev. B (1998), at press.
[11] M. Cardona, Helv. Phys. Acta **34**, 796 (1961).

Translated by M. E. Alferieff

Exchange interaction effects in inter-Landau level Auger scattering in a two-dimensional electron gas

E. Tsitsishvili
Institute of Cybernetics, 380086 Tbilisi,Georgia

Y. Levinson
Department of Condensed Matter Physics, The Weizmann Institute of Science, 76100 Rehovot, Israel

(Submitted 17 March 1998)
Pis'ma Zh. Éksp. Teor. Fiz. **67**, No. 8, 574–579 (25 April 1998)

We consider the influence of spin effects on the inter-Landau level electron-electron scattering rate in a two-dimensional electron gas. Because of exchange spin splitting, the Landau levels are not equidistant. This leads to the suppression of Auger processes and a nonlinear dependence of the lifetime on the concentration of excited electrons even at very low excitation levels. © *1998 American Institute of Physics.* [S0021-3640(98)01108-6]

PACS numbers: 71.70.Di, 71.70.Gm, 72.10.−d

A considerable amount of work has been done[1–5] on the determination of the electron lifetime in the excited Landau levels (LL) in a two-dimensional electron gas (2DEG). It has been found that electron–electron (ee) scattering is the dominant relaxation mechanism off the magnetophonon resonance conditions, when the emission of LO phonons is suppressed.[6,7] In this case the electron lifetime is determined by Auger processes, in which two excited electrons in the same LL are scattered, deexciting one to a lower LL, and exciting the second to a higher LL. The decrease of the measured lifetimes with increasing *excited* electron concentration, $n_{\rm exc}$, has proved a convincing argument for this conclusion.

One might think that the probability for an Auger process to occur, τ_{ee}^{-1}, increases linearly with $n_{\rm exc}$. However, the experiments do not confirm this conclusion.[4] We will show that this ''naive'' picture is not complete, and that the nonlinear dependence of τ_{ee}^{-1} on $n_{\rm exc}$ is due to spin effects.

In a 2DEG the LLs are equally spaced if one neglects spin effects (and nonparabolicity). The exchange interaction breaks the equidistant LL spacing. The exchange energy in the Landau level $N\sigma$ ($\sigma=\uparrow,\downarrow$) is usually written as $-\Sigma_{N\sigma}$, where $\Sigma_{N\sigma}=E_0\nu_{N\sigma}$, with $E_0>0$, and $\nu_{N\sigma}$ is the corresponding filling factor.[8] The observed values of E_0 are of the order of several meV (e.g., in GaAs one has $E_0=3$–6 meV at 10 T).[9–12] The Zeeman spin splitting is important for the empty LLs only, since it is much smaller (~ 0.2 meV at 10 T) than the exchange energy.

We will consider a situation that is similar to the experiment of Ref. 4, in which the

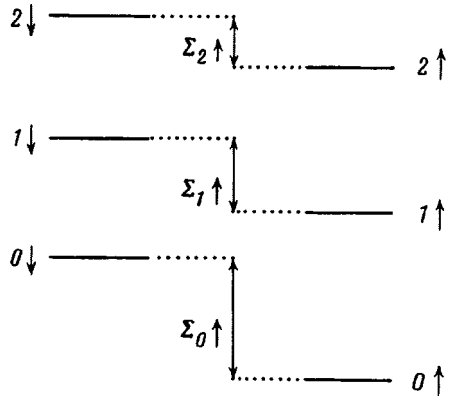

FIG. 1. The Landau level ladder in the spin polarized case.

2DEG is spin polarized. At equilibrium the electrons occupy the lowest LL, $0\uparrow$, with a filling factor $\nu_{0\uparrow}=\nu<1$. Due to cyclotron absorption some of the electrons are excited to the higher LLs, $N\uparrow$. Since the Auger processes preserve the initial spin orientation due to total spin conservation during the scattering event, the LLs $N\downarrow$ are empty. They coincide with the ''bare'' levels and are equally spaced (see the left-hand part of Fig. 1). The LLs $N\uparrow$ are occupied with filling factors $\nu_{0\uparrow}>\nu_{1\uparrow}>\nu_{2\uparrow}>\ldots$, and $\nu=\nu_{0\uparrow}+\nu_{1\uparrow}+\nu_{2\uparrow}+\ldots$. Due to the exchange interaction the LLs $N\uparrow$ are shifted downward, depending on the level occupation, by an energy $\Sigma_{N\uparrow}=E_0\nu_{N\uparrow}$ (see the right-hand part of Fig. 1). If the excitation is not very strong, and also on account of nonparabolicity, one can consider a three-level model with $\nu_{0\uparrow}+\nu_{1\uparrow}+\nu_{2\uparrow}=\nu$, as is shown in Fig. 1. Since $\nu_{0\uparrow}>\nu_{1\uparrow}>\nu_{2\uparrow}$, the energy shifts $\Sigma_{0\uparrow}>\Sigma_{1\uparrow}>\Sigma_{2\uparrow}$, and hence, the LLs $0\uparrow$, $1\uparrow$, and $2\uparrow$ are nonequidistant.

The lifetime of the photoelectrons in level $1\uparrow$ is governed by the Auger process $1\uparrow+1\uparrow\rightarrow 0\uparrow+2\uparrow$. It is clear that since the LLs are not equidistant this process is forbidden by energy conservation and can happen only due to the LL broadening. Hence it is clear that the Auger transitions are well suppressed if the unevenness in the LL spacing $\Sigma=(\Sigma_{0\uparrow}-\Sigma_{1\uparrow})-(\Sigma_{1\uparrow}-\Sigma_{2\uparrow})=E_0(\nu-3\nu_{1\uparrow})$ is larger than the LL width Δ. In this case only the tails of the density of states (DOS) of the LLs are effective. One can suppose that the greatest possibility for energy conservation occurs when the scattering partners are situated in the middle between the centers of the lowest and highest LLs, $0\uparrow$ and $2\uparrow$. At very low excitation, one can assume that in first approximation Σ is independent of the excitation intensity. Then the probability of the Auger process $1\uparrow+1\uparrow\rightarrow 0\uparrow+2\uparrow$ is $\tau_{ee}^{-1}\sim\nu_{1\uparrow}$. When $\nu_{1\uparrow}$ is increased further the exchange energy $\Sigma_{0\uparrow}$ decreases, while $\Sigma_{1\uparrow}$ and $\Sigma_{2\uparrow}$ increase, and hence the unevenness Σ decreases. This obviously causes an increase in the scattering rate, resulting in a superlinear dependence of τ_{ee}^{-1} on $\nu_{1\uparrow}$. One can expect that the nonlinear enhancement of the scattering rate will be essential when the change in the unevenness, $\delta\Sigma=3E_0\nu_{1\uparrow}$, approaches the LL width Δ, and hence, the crossover filling factor is $\nu_{1\uparrow}^{*}\simeq\Delta/3E_0$. Since the LL width, $\Delta\lesssim 1$ meV,[13] is appreciably smaller than the exchange energy E_0, one finds $\nu_{1\uparrow}^{*}\ll 1$. Thus, the nonlinear dependence of the scattering rate τ_{ee}^{-1} on $\nu_{1\uparrow}$ can be pronounced even at low concentrations of the excited electrons.

As an illustration we calculate the scattering rate τ_{ee}^{-1} of the Auger process

$1\uparrow+1\uparrow\rightarrow 0\uparrow+2\uparrow$ using the approaches given in Refs. 14 and 15. We consider a 2DEG in a strong magnetic field and a random statistically homogeneous potential with a correlator: $\langle U(y)U(0)\rangle=\Delta^2\exp(-y^2/\Lambda^2)$, where the correlation length Λ is much larger than the magnetic length $l_B=(eB/\hbar c)^{1/2}$. The correlation length is of the order of the spacer $\Lambda\simeq d$, while typical values of the magnetic length for fields B between 5 and 15 T are ~ 100 Å. Hence the random potential can be considered as a smooth one in samples with a spacer $d\geqslant 200$ Å.

We assume that the LLs follow the random potential in space, and that the DOS $\rho(\varepsilon)=(\sqrt{2\pi}\Delta)^{-1}\exp(-\varepsilon^2/2\Delta^2)$, where the energy ε is reckoned from the LL center and renormalized by the exchange energy. In the calculation of the scattering rate only relative coordinates of the interacting electrons are important. We choose the gauge $A=(-By,0,0)$. Let $y_1=l_B^2k_1$ and $y_2=l_B^2k_2$ be the guiding centers before scattering, and $y_1'=l_B^2k_1'$ and $y_2'=l_B^2k_2'$ the guiding centers after scattering; k_1,k_2,k_1',k_2' are the corresponding momenta. The shifts of the electrons in the scattering event are $(y_1'-y_1)=q$ and $(y_2'-y_2)=-q$, and the ''average'' distance between the scattering partners is $[(y_2'+y_2)/2-(y_1'+y_1)/2]=p$. These quantities define the scattering probability. The averaged scattering rate of a test electron in the $1\uparrow$ LL with an energy ε reckoned from its center is

$$\left\langle \frac{1}{\tau_{ee}} \right\rangle_{\varepsilon} = \int \int_{-\infty}^{+\infty} \frac{dpdq}{2\pi\hbar l_B^2} |M(p,q)-\overline{M}(p,q)|^2 (S_\varepsilon(p,q)+S_\varepsilon(q,p)), \tag{1}$$

where $M(p,q)$ and $\overline{M}(p,q)$ are the scattering matrix elements for the direct and exchange electron collisions, respectively. The functions $S_\varepsilon(p,q)$ and $S_\varepsilon(q,p)$ are due to the statistical factors and energy conservation. $S_\varepsilon(p,q)$ is related to the ''deexciting'' Auger transition, in which the test electron is deexcited to the lower level $0\uparrow$ and its partner is excited to the upper level $2\uparrow$, while $S_\varepsilon(q,p)$ corresponds to the ''exciting'' transition, in which the test electron is excited to the upper level $2\uparrow$, and its partner is deexcited to the lower level $0\uparrow$.

It is easy to check that $\overline{M}(p,q)=M(q,p)$, and

$$M(p,q)=\frac{1}{l_B^2}\int_{-\infty}^{+\infty} d\eta\ V(q,\eta)F(q,p-\eta), \tag{2}$$

where

$$V(q,\eta)=\int_{-\infty}^{+\infty} d\xi\ V(\sqrt{\xi^2+\eta^2})\exp\left(\frac{iq\xi}{l_B^2}\right) \tag{3}$$

is the Fourier transform of the ee interaction potential $V(r)$. The ee interaction is chosen as $V(\sqrt{x^2+y^2})=V_0\exp\{-(x^2+y^2)/l_{sc}^2\}$, where l_{sc} is the screening length, $V_0\simeq e^2/\kappa l_B$, and κ is the dielectric constant. The function $F(q,p)$ is defined as follows:

$$F(q,p)=\frac{1}{4}\exp\left(-\frac{p^2}{2l_B^2}-\frac{q^2}{2l_B^2}\right)\int_{-\infty}^{+\infty} dz e^{-2z^2} H_1(z+s)H_1(z-s)H_2(z-r), \tag{4}$$

where $s=(p+q)/2l_B$, $r=(p-q)/2l_B$, and $H_n(y)$ is an Hermite polynomial. Since the initial and final states must overlap, the electron shift in the scattering event is of the

order of or smaller than the magnetic length l_B, and hence $q \lesssim l_B$. Thus, the Auger transitions are quasivertical in space. The ''average'' distance between interacting electrons is limited by the screening length l_{sc} of the ee interaction, $p \lesssim l_{sc}$. In the situation we consider l_{sc} is defined by the electrons in the $0\uparrow$ LL, and since this level is only partially occupied, the screening is strong and $l_{sc} \simeq l_B$ (Ref. 16). In this case, the matrix elements $M(p,q)$ and $\overline{M}(p,q)$ that enter Eq. (1) are exponentially small if $p,q \gg l_B$ (Ref. 15), and therefore the main contribution to the integrals in Eq.(1) arises from $p,q \lesssim l_B$. Note also that due to the spatial homogeneity, $M(p,q)=M(-p,-q)$ and $S_\varepsilon(p,q) = S_\varepsilon(-p,-q)$, and one can restrict the integration over p in Eq. (1) to $p>0$.

We will consider the low-excitation limit, such that $\nu_{1\uparrow} \ll \nu_{0\uparrow}$, and $\nu_{2\uparrow}=0$. In this case the electron concentration in the $0\uparrow$ LL changes only slightly with pumping, and one can assume that the initial Fermi distribution in this level is not perturbed. The energy distribution of the photoelectrons in level $1\uparrow$ depends on the relation between the inter- and intra-LL relaxation times. In order to simplify the calculations we will consider the case in which the inter-LL relaxation is faster, and thus the excited electrons are not at equilibrium. We suppose that they are distributed uniformly in space and are excited in a rather wide spectral interval, thus their occupation numbers are assumed to be constant and equal to $\nu_{1\uparrow}$.

With this in mind the function $S_\varepsilon(p,q)$ in Eq. (1) is

$$S_\varepsilon(p,q)=\nu_{1\uparrow}\langle \delta(\varepsilon+\Sigma+U(p+q)-U(q)-U(p))[1-f(U(q))]\rangle, \tag{5}$$

where $\langle \ldots . \rangle$ stands for the statistical average,[14] and $f(\varepsilon)$ is the Fermi distribution in the LL $0\uparrow$. Performing in Eq.(5) the average over realizations of the random potential[15] at the limit of zero temperature, $T=0$, one obtains

$$S_\varepsilon(p,q)=\frac{\nu_{1\uparrow}}{8\sqrt{\pi}\Delta}\frac{\Lambda^2}{|pq|}\exp\left\{-\frac{1}{4\Delta^2}\left[\varepsilon-\frac{\Lambda^2\Sigma}{2pq}\right]^2\right\}\left\{1-\Phi\left[-\frac{\Lambda}{2\Delta|q|}\left(\varepsilon-\varepsilon_F-\frac{\Sigma q}{2p}\right)\right]\right\}, \tag{6}$$

where $\Phi(x)=(2/\sqrt{\pi})\int_0^x e^{-t^2}dt$ is the probability integral,[17] and ε_F is the Fermi energy reckoned from the center of the $0\uparrow$ LL.

The factor $\{1-\Phi\}$ in Eq. (6) is due to the occupation of the $0\uparrow$ LL. Let us introduce the Fermi-level replica (FLR), which is given by $\varepsilon_F+\hbar\omega_B-\Sigma_{1\uparrow}$ and is thus pinned to the level $1\uparrow$ (see Fig. 2). The energy difference $\varepsilon-\varepsilon_F$ in Φ is the test electron energy reckoned from the FLR. Consider first the Auger transitions with $q>0$, i.e., when the scattering partners are closer in space after scattering. The factor $\{1-\Phi\}$ shows that these transitions are strong if the test electron is above the FLR by an energy $\simeq\Sigma/2$, i.e., at $\varepsilon-\varepsilon_F \gtrsim \Sigma/2$, and weak if $\varepsilon-\varepsilon_F \lesssim \Sigma/2$ (see the left-hand part of Fig. 2). Similarly, the Auger transitions with $q<0$ (i.e., when the scattering partners are closer in space before scattering) are strong at $\varepsilon-\varepsilon_F \gtrsim -\Sigma/2$, and weak if $\varepsilon-\varepsilon_F \lesssim -\Sigma/2$ (see the right-hand part of Fig. 2). In both cases the crossover scale is $\Delta(l_B/\Lambda)\equiv\Delta_B \ll \Delta$, much smaller than the LL width. Thus, due to the occupation of the lowest LL, $0\uparrow$, all Auger processes for large negative energies of the test electron are quenched.

The origin of the exponential factor is as follows. During the scattering event the total momentum and energy are conserved, i.e., $[\varepsilon+U(p+q)-2\Sigma_{1\uparrow}]-[U(p)+U(q)-\Sigma_{0\uparrow}]=0$. Since the Auger transitions are quasivertical ($q \ll \Lambda$), the random potential

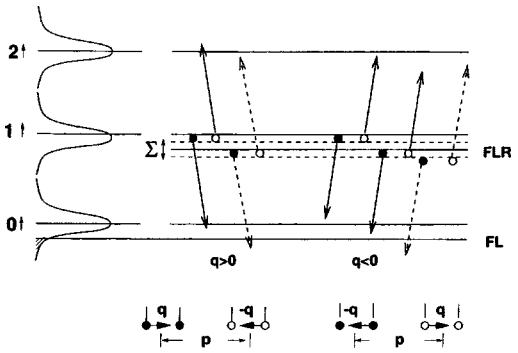

FIG. 2. The Auger process: $1\uparrow + 1\uparrow \rightarrow 0\uparrow + 2\uparrow$. The suppressed processes are shown with dashed arrows.

$U(y)$ can be expanded in powers of q and p. Assuming the test electron is at $y=0$, i.e., $\varepsilon = U(0)$, one obtains $U''(0)pq = -\Sigma$, where $\Sigma = \Sigma_{0\uparrow} - 2\Sigma_{1\uparrow}$ is the unevenness in the LL spacing. The exponential factor in Eq. (6) is proportional to the conditional probability $\mathrm{Probc}\{U(0)=\varepsilon | U''(0) = -\Sigma/pq\}$ that if the random potential $U(y)$ at $y=0$ is $U(0)=\varepsilon$, then its second derivative at the same point is $U''(0) = -\Sigma/pq$. Typical magnitudes of the second derivative of the random potential at energies $|\varepsilon| \lesssim \Delta$ are $|U''| \simeq \Delta/\Lambda^2$, which is much smaller than Σ/l_B^2 for typical Σ. Hence energy conservation can not be satisfied for $|\varepsilon| \lesssim \Delta$, and can be obeyed only in the tails of the DOS, where the probability of finding large $|U''|$ is not small. This can be seen from the exponential factor in Eq. (6), which has its maximum values at $\varepsilon = \pm\varepsilon_s \simeq (\Lambda/l_B)^2\Sigma \gg \Delta$, i.e., in the tails of the DOS.

Note that the results obtained in the case of a smooth random potential differ from the general predictions given above. Namely, the scattering rate in this case is very sensitive to unequal distances between the LLs, and is suppressed not only when the unevenness in the LL spacing is comparable to the LL width, but also at much smaller $\Sigma \gtrsim \Delta(l_B/\Lambda)^2 \equiv \Delta_s$ with $\Delta_s \ll \Delta$. In addition when the occupation of the excited LL $1\uparrow$ increases, the scattering rate responds to a much smaller change of the unevenness than predicted, $\delta\Sigma \simeq \Delta$. Indeed, as follows from the exponential factor in Eq. (6), the scattering rate τ_{ee}^{-1} is sensitive to the decrease in Σ, when $\delta\Sigma \simeq 8\Delta_s^2/\Sigma \ll \Delta$. The crossover filling factor is also much smaller, $\nu_{1\uparrow}^* \simeq \Delta_s^2/\Sigma E_0 \ll \Delta/E_0$. For example, at $\Delta_s \simeq 0.1$meV, $E_0 \simeq 2$meV, and $\Sigma \simeq 0.5$ meV, $\nu_{1\uparrow}^* \simeq 0.01$.

The dependence of the scattering rate on the concentration of the excited electrons at the test electron energy $\varepsilon = \varepsilon_F$ is shown in Fig. 3. The magnetic field is $B = 6$ T, and the curves correspond to two different electron concentrations: $n = 4.5\times 10^{10}$ cm^{-2}, i.e., $\nu = 0.31$ (curve 1), and $n = 7.3\times 10^{10}$ cm^{-2}, i.e., $\nu = 0.5$ (curve 2). The other parameters are as follows: $\kappa = 12$, $\Delta = 1$ meV, $\Lambda = 300$ Å, and $E_0 = 2$ meV.[12] From Fig. 3 it can be seen that in both cases the scattering rate τ_{ee}^{-1} changes linearly with the filling factor $\nu_{1\uparrow}$ only at very small $\nu_{1\uparrow}$. The arrows in Fig. 3 indicate the crossover values of $\nu_{1\uparrow}^*$, when the deviation from the linear law amounts to about 100%. For a given $\nu_{1\uparrow}$, the scattering rate τ_{ee}^{-1} is more suppressed at larger electron concentrations, because of the greater unevenness in the LL spacing.

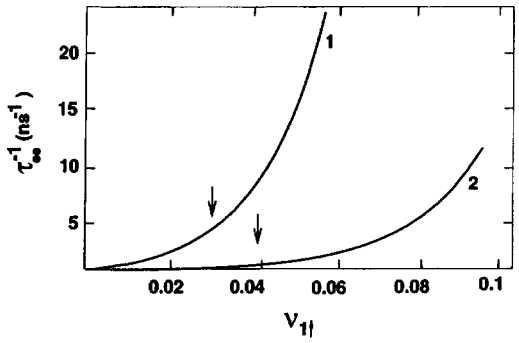

FIG. 3. The Auger scattering rate, τ_{ee}^{-1}, for the process: $1\uparrow+1\uparrow\rightarrow 0\uparrow+2\uparrow$ at $\varepsilon=\varepsilon_F$, $\nu=0.31$ (curve 1), and $\nu=0.5$ (curve 2), versus the filling factor $\nu_{1\uparrow}$. The arrows indicate the crossover filling factors $\nu_{1\uparrow}^{*}$ (see also text).

We are grateful to E. Gornik for fruitful discussions. This work is supported by the MINERVA Foundation.

[1] H. Sakaki, K. Hirakawa, J. Yoshino *et al.*, Surf. Sci. **142**, 306 (1984).
[2] M. Helm, E. Gornik, A. Black *et al.*, Physica B & C **134**, 323 (1985).
[3] C. J. G. M. Langerak, J. Singleton, P. J. van der Wel *et al.*, Phys. Rev. B **38**, 13133 (1988).
[4] I. Maran, W. Seidenbusch, E. Gornik *et al.*, Semicond. Sci. Technol. **9**, 700 (1994).
[5] W. Heiss, P. Auer, E. Gornik *et al.*, Appl. Phys. Lett. **67** (8), 1100 (1995).
[6] T. A. Vaughan, R. J. Nicholas, C. J. G. M. Langerak *et al.*, Phys. Rev. B **53**, 16 481 (1996).
[7] B. N. Murdin, C. M. Ciesal, C. J. G. M. Langerak *et al.*, *International Conference on Nonequilibrium Carrier Dynamics in Semiconductors*, Berlin, Germany, 1997.
[8] T. Ando and Y. Uemura, J. Phys. Soc. Jpn. **37**, 1044 (1974).
[9] A. Usher, R. J. Nicholas, J. J. Harris, and C. T. Foxon, Phys. Rev. B **41**, 8829 (1992).
[10] K. von Klitzing and Th. Englert, Surf. Sci. **73**, 70 (1978).
[11] R. J. Nicholas, R. J. Haug, K. von Klitzing, and G. Weimann, Phys. Rev. B **37**, 1294 (1988).
[12] V. T. Dolgopolov, A. A. Shashkin, A. V. Aristov *et al.*, Phys. Rev. Lett. **79**, 729 (1997).
[13] I. V. Kukushkin and V. B. Timofeev, Adv. Phys. **45**, 147 (1996), and references therein.
[14] Y. Levinson, Phys. Rev. B **51**, 16 898 (1995).
[15] E. Tsitsishvili and Y. Levinson, Phys. Rev. B **56**, 6921 (1997).
[16] I. S. Gradshteyn and I. M. Ryzhik, *Table of Integrals, Series and Products*, Academic Press, New York, 1980.
[17] A. L. Efros, Phys. Rev. B **45**, 11 354 (1991).

Published in English in the original Russian journal. Edited by Steve Torstveit.

Interwell radiative recombination in the presence of random potential fluctuations in GaAs/AlGaAs biased double quantum wells

V. B. Timofeev, and A. V. Larionov
Institute of Solid State Physics Russian Academy of Sciences, 142432 Chernogolovka, Moscow Region, Russia

A. S. Ioselevich
Landau Institute of Theoretical Physics, Russian Academy of Sciences, 142432 Chernogolovka, Moscow Region, Russia

J. Zeman and G. Martinez
High Field Magnetic Laboratory, MPI-FKF and CNRS, 38042 Grenoble, France

J. Hvam and K. Soerensen
Microelectronic Centre, Lyngby, Denmark

(Submitted 23 March 1998)
Pis'ma Zh. Éksp. Teor. Fiz. **67**, No. 8, 580–585 (25 April 1998)

The interwell radiative recombination from biased double quantum wells (DQW) in *pin* GaAs/AlGaAs heterostructures is investigated at different temperatures and external electrical fields. The luminescence line of interwell recombination of spatially separated electron–hole pairs exhibits systematic narrowing with temperature increase from 4.5 to 30 K. A theoretical model is presented which explains the observed narrowing in terms of lateral thermally activated tunneling of spatially separated $e-h$ pairs localized by random potential fluctuations in the quantum wells. © *1998 American Institute of Physics.*
[S0021-3640(98)01208-0]

PACS numbers: 78.66.Fd, 73.20.Dx

INTRODUCTION

Biased double quantum wells (DQWs) have attracted considerable interest in the last decade.[1–4] These structures provide a unique possibility of optically exciting electrons and holes which are spatially separated in adjacent quantum wells. These electrons and holes can be bound into interwell excitons by the Coulomb interaction. The interwell excitons have long lifetimes compared to intrawell ones, because their recombination requires tunneling through the interwell barrier. The interwell excitons can therefore be accumulated to rather high densities and cooled down to low temperatures. Existing theories predict an interesting collective behavior of interwell excitons at high densities and low enough temperatures.[5–8]

In this letter we point out that in real biased DQWs, *pin* or *nin* structures, a random potential arising due to charged residual impurities and other imperfections can modify

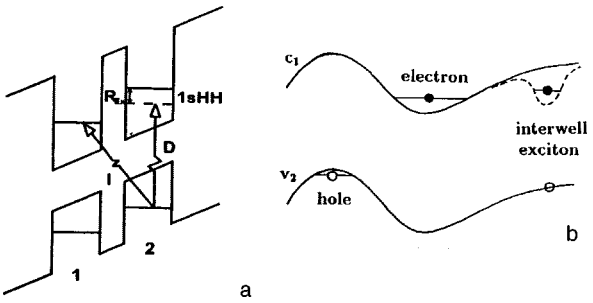

FIG. 1. a — Direct (D) and indirect (I) radiative transitions in a biased double quantum well. b — An electron and a hole, laterally localized at extrema of a random potential. c_1 and v_2 are the profiles of the bottom of the conduction band in the first quantum well, and the top of the valence band in the second quantum well, respectively. An interwell exciton is also shown.

the interwell radiative process quite dramatically. At low temperatures and reduced excitation rates the photoexcited electrons and holes, besides having a *vertical* spatial separation in adjacent wells, are strongly *laterally* localized by random potential fluctuations in quantum wells (see Fig. 1). Under conditions of such lateral localization the interwell luminescence spectrum should involve a distribution function of random ''wells'' and ''hills'' of the fluctuating potential, which are occupied by electrons and holes, respectively. The interwell radiative probability in this case is controlled not only by vertical tunneling through the interwell barrier but also by lateral tunneling of electrons and holes localized at randomly distributed extrema of the fluctuating potential in the respective quantum wells. One can expect the interwell luminescence spectrum of localized e–h pairs to be a rather broad line, with a width that depends on the amplitude of the random potential fluctuations, on the filling of these fluctuations by electrons and holes, and on the (thermally activated) lateral tunneling. In this letter we report both experimental and theoretical studies of the interwell luminescence line shape and its evolution with temperature at low excitation levels.

EXPERIMENTAL STRUCTURES

In the experiments we used GaAs/AlGaAs pin DQW structures with the following architecture: a substrate of n-type GaAs (Si-doped to 10^{18} cm^{-3}) is covered by a buffer layer of GaAs (Si-doped to 10^{17} cm^{-3}) followed by a layer of n-type $Al_{0.35}Ga_{0.65}As$ (Si-doped to 10^{18} cm^{-3}) with a width of 0.5 μm. The intrinsic part of the samples consists of a 0.3 μm thick undoped layer of $Al_{0.35}Ga_{0.65}As$ followed by the first well (undoped GaAs layer 80 Å wide), an undoped $Al_{0.35}Ga_{0.65}As$ barrier layer 50 Å wide, the second well (undoped GaAs layer 80 Å wide), and by a 0.3 μm thick undoped $Al_{0.35}Ga_{0.65}As$ barrier. Then comes the p-type part of the structure, consisting of a 0.5 μm thick layer of p-type $Al_{0.35}Ga_{0.65}As$ doped with Be to 10^{18} cm^{-3}, covered by a 40 Å undoped GaAs cap layer. A 1×1 cm^{-2} rectangular structure with Ohmic contacts to the p- and n-type regions was made for applying external bias to the structure. The structures used exhibited typical I–V characteristics for pin diodes in the dark and at low excitation powers. The photoluminescence (PL) spectra were excited either with a He–Ne laser (6328 Å) or with a semiconductor injection laser (6750 Å).

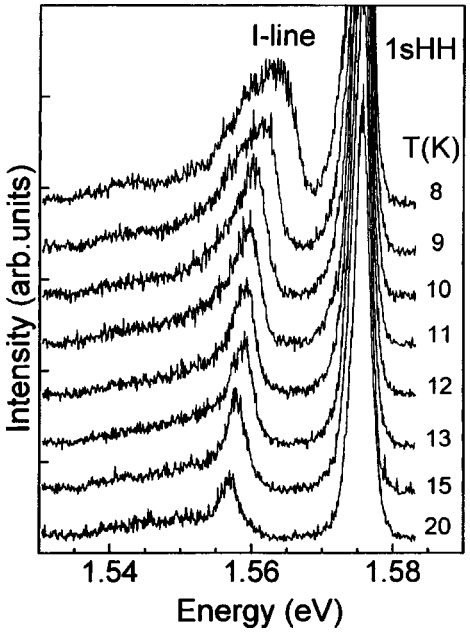

FIG. 2. Photoluminescence spectra measured at forward bias $U=+0.4V$ and different temperatures under CW excitation (6328 Å) of ~ 5 mW/cm^2.

EXPERIMENTAL RESULTS

Figure 2 illustrates the PL spectra of the pin DQWs measured at a given external field applied to the structure (forward bias $U=+0.4$ V) under cw excitation (6750 Å) at different temperatures. Besides the narrow line $1sHH$, corresponding to the ground state of the intrawell exciton with a heavy hole, one can see at low T a several-times-broader line (the I line), corresponding to interwell recombination. The I line is linearly tuned on the spectral scale under variation of the applied bias, a property which is characteristic of interwell luminescence in pin DQWs (see Fig. 3). From Fig. 2 one can see a strong narrowing of the interwell luminescence line as the temperature increases. The violet tail of this line is close to exponential, with a width equal to T. A systematic narrowing of the interwell luminescence line (by around a factor of four) with increasing temperature was observed at low excitation power for different external bias, forward or reverse, and in the built-in-field. Therefore this is a general property of interwell PL which, in our opinion, has to do with the random potential fluctuations.

The phenomenon of strong lateral localization of photoexcited electrons and holes at random potential fluctuations is confirmed independently by direct measurements of the interwell luminescence kinetics.[9] First of all, this kinetics is nonexponential within the I line at low T. The kinetics exhibit shorter decay times at the violet boundary and longer ones (a few hundred nanoseconds) on the red side of the I line. At higher T, when the FWHM of the I line approaches $2T$, the luminescence decay kinetics becomes, to high accuracy, exponential.

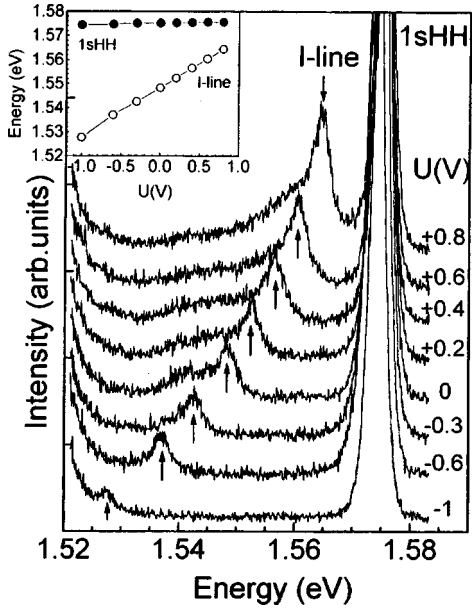

FIG. 3. Photoluminescence spectra measured at temperature 20 K and different bias under cw excitation (6328 Å) of $\sim$1.5 mW/cm^2. The inset shows the evolution of the positions of the 1sHH and I lines.

THEORY

Let us discuss the theory of the interwell luminescence in the presence of a random potential. We estimate the luminescence intensity within the ''exponential approximation,'' totally disregarding all pre-exponential factors, and neglect the Coulomb interaction (i.e., the effects of the interwell excitons), which do not qualitatively change the results. Consider two quantum wells, the energy difference between the averaged (with respect to the random potential) position of the bottom of the conduction band in the first well and that of the top of the heavy hole band in the second well being ω_0. We assume that a smooth Gaussian random potential energy $u(\rho)=-|e|\varphi(\rho)$ (ρ is a lateral coordinate) is present in the wells, so that the local positions of the bottom of the conduction band and the top of the valence band depend on ρ. If the correlation radius r_c of the random potential is larger than the distance ($\sim$150 Å) between the wells, then $u(\rho)$ is identical in both wells. The assumption that r_c is large looks plausible, since charged impurities are localized relatively far from the quantum wells. It is also supported by the magnetic field dependence of the luminescence spectrum.[9] The temperature T is much lower than the characteristic amplitude u_0 of the random potential, so that the photoexcited electrons (holes) are normally localized near the minima (maxima) of the random potential $u(\rho)$ (Fig. 1a).

From the very low excitation power used (5 mW/cm^2) and the value of the interwell decay time (100 ns) measured directly from the luminescence kinetics under pulsed excitation, one can estimate an upper bound on the average density of nonequilibrium e–h pairs as 10^9 cm^{-2}. Therefore in this experiment the filling of potential fluctuations by electrons (holes) (i.e., the average number of photoexcited carriers per area $\sim r_c^2$) is

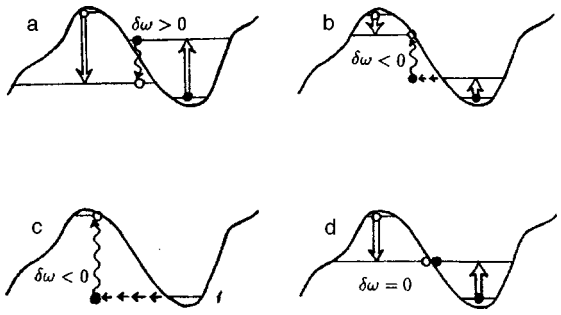

FIG. 4. Recombination processes for different energies of the emitted photon. The curves c_1 and v_2 of Fig. 1b are vertically shifted to coincide. Double arrows show activation, broken arrows show tunneling, and wavy arrows show recombination. a — $\delta\omega > 0$; b — $\delta\omega < 0$; c — The dominant process for low T: pure tunneling, $\delta\omega = U_i - U_j < 0$; d — The dominant process for high T: pure activation, $\delta\omega \approx 0$.

much less than unity if the correlation length r_c of the random potential is around 1000 Å or less. Thus at such low excitations the classical Boltzmann distribution is likely to be established in the vicinity of each extremum (i.e., minimum i or maximum j):

$$n_i^{(e)}(\epsilon_e) = \exp\{-(\epsilon_e - \mu_i^{(e)})/T\}, \quad n_j^{(h)}(\epsilon_h) = \exp\{-(\mu_j^{(h)} - \epsilon_h)/T\}, \tag{1}$$

where the energies of electrons (holes) $\epsilon_e(\epsilon_h)$, and their local chemical potentials $\mu_i^{(e)} \times(\mu_j^{(h)})$ are reckoned from the average position of the bottom of the conduction band (top of the valence band). The interwell luminescence intensity can be written in the form ($\hbar = 1,\ k_B = 1$)

$$I(\omega) \propto \left\langle \sum_{ij} \int n_i^{(e)}(\epsilon_e)\, \nu_i^{(e)}(\epsilon_e) d\epsilon_e n_j^{(h)}(\epsilon_h)\, \nu_j^{(h)}(\epsilon_h) d\epsilon_h \right.$$

$$\left. \times w_{ij}[\epsilon_e, \epsilon_h, \{u\}] w_0 \delta[(\epsilon_h - \epsilon_e) + \delta\omega] \right\rangle, \tag{2}$$

where $\delta\omega \equiv \omega - \omega_0$, and $\nu_i^{(e)}(\epsilon_e)$ and $\nu_j^{(h)}(\epsilon_h)$ are the densities of states for electrons near the ith minimum and for holes near the jth maximum of the random potential, respectively. Since the probability of recombination is proportional to the square modulus of the overlap integral of the envelope wave functions of an electron and a hole, expression (2) involves two factors: w_0 is the probability of tunneling between the two quantum wells (vertical tunneling), and $w_{ij}[\epsilon_e, \epsilon_h, \{u\}]$ is the the square modulus of the overlap integral of the lateral envelope functions of an electron and a hole. The latter factor is exponentially small if the classically accessible regions for the electron and the hole do not overlap: then it involves the probability of lateral tunneling (Fig. 4). The sum in (2) runs over the pairs of adjacent minima (i) and maxima (j) of the random potential, and the angle brackets stand for the average over the random potential.

In the main part of the present paper we adopt the assumption of *global equilibrium*: $\mu_i^{(e)} = \mu^{(e)}$, $\mu_j^{(h)} = \mu^{(h)}$, which means that the photocarriers escape from the quantum wells (due to recombination, leakage to the leads through the bulk, or whatever) so slowly that an equilibrium between different local extrema has time to be established. Under this assumption one can rewrite (2) in the form:

$$I(\omega)\propto e^{-\delta\omega/T}\left\langle \sum_{ij}\int_{U_i}^{\infty} d\epsilon_e \int_{-\infty}^{U_j} d\epsilon_h w_{ij}[\epsilon_e,\epsilon_h,\{u\}]\delta[(\epsilon_h-\epsilon_e)+\delta\omega]\right\rangle, \tag{3}$$

where $U_i(U_j)$ is the value of the ith (jth) minimum (maximum). In writing the expression (3) we have omitted all ω-independent (although possibly T-dependent) factors such as w_0 and the average concentration of carriers: These factors do not affect the line shape we are interested in.

In principle, the average (3) may be evaluated for general $\delta\omega$ with the aid of the optimal fluctuation method. In this letter, however, we restrict consideration to several simple limiting cases, in which the calculations are transparent and elementary.

VIOLET TAIL

For $\delta\omega>0$ the classically accessible regions for the electron and the hole overlap (Fig. 4a); therefore the function $w_{ij}[\epsilon_e,\epsilon_h,\{u\}]$ does not introduce any exponential factor into the integrand of (3); the only exponential factors come from the Boltzmann distribution functions. As a result, for $\delta\omega>0$ one obtains

$$I(\omega)\propto\exp(-\delta\omega/T), \tag{4}$$

in accordance with experimental observations.

FAR RED TAIL

For large negative $\delta\omega$ the dependence of the lateral tunneling probability w on the realization of the random potential is of only secondary importance: the bottleneck of the process is finding a proper ''antisymmetric'' fluctuation of the random potential with sufficiently high maximum and deep minimum (namely, $U_j-U_i>\hbar|\delta\omega|$ is required). The probability P for such a fluctuation to occur can be estimated as $P\approx P(U_j=|\delta\omega|/2,U_i=-|\delta\omega|/2)\approx P(u=|\delta\omega|/2)P(u=-|\delta\omega|/2)=\exp\{-(\hbar|\delta\omega|/2u_0)^2\}$, where $u_0^2=\langle u^2(\rho)\rangle$. Thus, in the case of large negative $\delta\omega$ one can, roughly, write:

$$I(\omega)\propto\exp\{-\delta\omega/T-(\delta\omega/2u_0)^2\}. \tag{5}$$

Taking into account the lateral tunneling introduces only a relatively small correction to the exponential in (5); we do not consider this correction in the present letter.

NEAR RED TAIL

If $|\delta\omega|$ is small (smaller than u_0), then the tunneling path is shorter than the correlation radius r_0. This means that the lateral tunneling proceeds, basically, in the constant field $\mathbf{F}(\rho)=\nabla u(\rho)$, and we can write

$$w_{ij}[\epsilon_e,\epsilon_h,\{u\}]\propto\exp\{-4\sqrt{2m}|\delta\omega|^{3/2}/3|\mathbf{F}(\rho)|\}, \tag{6}$$

so that, for a Gaussian random potential, the averaging procedure in (3) can be reduced to an integration over the fields $\mathbf{F}$ with a Gaussian weight $\propto\exp\{-(\mathbf{F}/F_0)^2\}$, where $F_0^2=\langle\mathbf{F}^2(\rho)\rangle$. Performing the integration by the method of steepest descent, we finally arrive at

$$I(\omega)\propto\exp\{-\delta\omega[(1/T)-(1/T_c)]\},\quad T_c=(F_0^2/24m)^{1/3}\equiv u_0(\Delta/24u_0)^{1/3}, \tag{7}$$

where $\Delta = F_0^2/mu_0^2 \sim 1/mr_0^2$ is a typical level spacing for the size-quantized electronic levels in the random potential. Thus the semiclassical condition $\Delta \ll u_0$ for the random potential ensures that $T_c \ll u_0$.

THE OVERALL LINE SHAPE

Combining all the results obtained in the above limiting cases, we can draw the following conclusions concerning the shape of the I line:

(i) For $T \ll T_c$ the spectrum of the I line should have a broad symmetric Gaussian peak having a full width $\Gamma = \sqrt{2}u_0$ and centered at $\delta\omega = 2u_0^2/T$.

(ii) For $T \approx T_c$ (more specifically, for $|T - T_c| < T_c^2/u_0$) the spectrum should be highly asymmetric: the red tail is Gaussian with a width $\Gamma_r = u_0/\sqrt{2}$, while the violet tail is exponential with a width $\Gamma_v \sim T$.

(iii) For $T > T_c$ the spectrum should show a quite narrow peak centered at $\delta\omega = 0$; the red wing is exponential with a width $\Gamma_r \sim TT_c/(T - T_c)$, while the violet wing is exponential with a width $\Gamma_v \sim T$.

DISCUSSION

The physical mechanism underlying the narrowing of the I line is a switching between the tunneling mode and the activational mode of barrier penetration, a phenomenon which is common to all systems where thermally activated tunneling plays a part (see, e.g., Ref. 10). At low temperatures $T < T_c$ the optimal mode of barrier penetration for the system (in our case penetration of the lateral potential barrier for electrons) is tunneling: the electrons and holes take the energetically most favorable positions (minima and maxima of $u(\rho)$, respectively); the electron starts tunneling from the very bottom U_i of the potential minimum and meets a hole only upon reaching a nearby potential maximum U_j (Fig. 4c). Such a process contributes to luminescence with energy $\delta\omega = U_i - U_j$, and therefore at low temperatures the I line is subject to inhomogeneous broadening, with a width $\Gamma \sim u_0$. At high temperatures $T > T_c$ the optimal mode of barrier penetration is activation: the system prefers to wait for a thermal fluctuation such that both the electron and hole are excited from their equilibrium positions at the extrema of $u(\rho)$, while the classically accessible regions for the electron and hole overlap in this excited state, so that no lateral tunnel is required (Fig. 4d). Such a process contributes most to luminescence with an energy $\delta\omega \approx 0$, and therefore the inhomogeneous broadening of the I line does not occur at $T > T_c$. Note that the switching takes place at $T_c \ll u_0$, so that most of the photocarriers are still localized near the extrema of $u(\rho)$.

The above physical picture predicts the high-T narrow I peak to appear at the violet edge of the broad low-T I band. Experimentally, however, this peak arises roughly at the center of the I band. One reason for this discrepancy might be a systematic shift of the I line, due to different screening conditions for the external electric field at different temperatures. The other reason might be lack of *global* equilibrium at low T. Under certain (rather general) conditions the *local* equilibrium is characterized by there being a roughly equal number of electrons (holes) captured by different minima (maxima). This means that $\mu_i^{(e)} \approx U_i + \text{const}$, $\mu_j^{(h)} \approx U_j + \text{const}$ at local equilibrium. A detailed analysis of this

nonequilibrium case will be published elsewhere; here we only mention that under the above conditions, an intermediate T-independent near violet tail of luminescence arises at low temperatures:

$$I(\omega) \propto \exp\{-(\delta\omega/2\tilde{u}_0)^2\} \quad \text{for} \quad 2\tilde{u}_0 < \delta\omega < 4\tilde{u}_0^2/T, \tag{8}$$

where $\tilde{u}_0 \sim u_0$. This tail should, however, be easily destroyed with increase of temperature, because of the efficient onset of global equilibrium for the relevant fluctuations. The above suppression of the violet wing of the I band might be partly responsible for the shift of the position of the narrow high-T I line towards the middle of the broad low-T band.

V. B. T. and A. V. L. acknowledge the partial support of INTAS, RFFR, and Physics of Nanostructures grants.

[1] Y. J. Chen, E. S. Koteles, B. S. Elman and C. A. Armiento, Phys. Rev. B **36**, 4562 (1987).
[2] T. Fukuzava, E. E. Mendes and J. M. Hong, Phys. Rev. Lett. **64**, 3066 (1990).
[3] J. A. Kash, M. Zachau, E. E. Mendes *et al.*, Phys. Rev. Lett. **66**, 2247 (1991).
[4] L. V. Butov, A. Zrenner, G. Abstreiter *et al.*, Phys. Rev. Lett. **73**, 304 (1994).
[5] Yu. E. Lozovik and V. I. Yudson, Zh. Éksp. Teor. Fiz. **71**, 738 (1976) [Sov. Phys. JETP **44**, 389 (1976)].
[6] D. Yoshioka and A. H. MacDonald, J. Phys. Soc. Jpn. **59**, 4211 (1990).
[7] X. M. Chen and J. J. Quinn, Phys. Rev. Lett. **67**, 895 (1991).
[8] H. Chu and Y. C. Chang, Europhys. Lett. **35**, 535 (1996).
[9] V. B. Timofeev, A. I. Filin, A. V. Larionov *et al.*, , Europhys. Lett. **41**, 535 (1998).
[10] A. S. Ioselevich, E. I. Rashba, in *Quantum Tunneling in Condensed Media*, edited by Yu. Kagan and A. J. Leggett, North-Holland, Amsterdam, 1992, Chapter 7, pp. 347–425.

Published in English in the original Russian journal. Edited by Steve Torstveit.

Extension of the spin–statistics theorem to nonlocal fields

M. A. Solov'ev[a)]
P. N. Lebedev Physical Institute, Russian Academy of Sciences, 117924 Moscow, Russia

(Submitted 16 March 1998)
Pis'ma Zh. Éksp. Teor. Fiz. **67**, No. 8, 586–591 (25 April 1998)

A new and more general derivation of the connection between spin and statistics that is applicable to nonlocal quantum fields with arbitrarily singular ultraviolet behavior is proposed. The derivation employs the concept of the analytical wave front of a distribution and makes it possible to characterize precisely the admissible degree of breakdown of locality for which there exists in the theory a Klein transformation which reduces the fields to normal commutation relations. © *1998 American Institute of Physics.* [S0021-3640(98)01308-5]

PACS numbers: 05.30.−d

1. INTRODUCTION

The locality condition plays a central role in the derivation of the experimentally observed connection between spin and statistics from the basic assumptions of quantum field theory.[1,2] As was noted long ago by Pauli,[3] if locality is rejected, it becomes permissible to quantize a scalar field by means of the relation $[\varphi(x_1),\ \varphi(x_2)]_+ = \Delta^{(1)}(x_1 - x_2)$, where $\Delta^{(1)}$ is an even solution of the free equation which decays exponentially $\sim \exp(-m|\mathbf{x}_1 - \mathbf{x}_2|)$ at spatial infinity. However, this does not mean that strict local commutativity is necessary for the normal connection between spin and statistics. The aim of this letter is to show that the admissible degree of locality breakdown for which this connection is preserved can be characterized with the aid of the concept of the wave front of a distribution. This concept was introduced into mathematics comparatively recently and has become central in the spectral analysis of singularities in the modern theory of differential equations.[4] In brief, it will be proved that anomalous commutation relations are impossible if the commutators and anticommutators of the fields fall off with spacelike separation of the arguments more rapidly than any linear exponential. Since quantum fields are scalar (generalized) functions of the space–time coordinates, this decay property requires an exact definition, which is given below.

We will not impose any restrictions on the singularity of a field, and we assume that the theory can contain nonlocal expressions in the form of series in derivatives of δ functions of all orders. Accordingly, the high-energy restrictions imposed on the behavior of the vacuum averages by the demands of microcausality need not hold.[5,6] The quantum theory of highly singular interactions is the best-developed area of nonlocal field theory and has interesting connections with string theory (see Refs. 7 and 8). As was shown in Ref. 9, the standard way of deriving the connection between spin and statistics, employ-

ing the analytic properties of vacuum averages in x space, remains in force in the presence of moderate nonlocality, which corresponds to exponential growth in momentum space. The case of a higher-order singularity, where the region of analyticity is empty, was studied in Refs. 10 and 11, where the extension of the spin–statistics theorem involves the construction of envelopes of holomorphy in p space. I shall show that enlisting the concept of the wave front of a distribution gives an alternative and complete solution of the problem.

From a technical standpoint the absence of high-energy restrictions means that the Fourier transforms of the test functions with which the fields are averaged must belong to a Schwartz space $\mathcal{D}$ of smooth functions with compact support. In the coordinate representation they are entire analytic functions with the property

$$|f(z)| \leqslant C_N(1+|x|)^{-N} e^{b|y|}, \tag{1}$$

where $N=1,2,\ldots$, and the positive constants C_N and b depend on f. The space of functions satisfying the inequality (1) with fixed b is designated as $S^{0,b}$, while in nonlocal field theory the union $\cup_{b>0} S^{0,b}$, which is nothing more than $\tilde{\mathcal{D}}$, is designated as S^0. Together with $S^0(\mathbf{R}^n)$, we shall use related spaces corresponding to cones in $\mathbf{R}^n$. If U is an open cone, then $S^0(U)$ is determined by the inequality

$$|f(z)| \leqslant C_N(1+|x|)^{-N} e^{b|y|+bd(x,U)}, \tag{2}$$

where $d(\cdot,U)$ is the distance between the point represented by the dot and U. If K is a closed cone, then

$$S^0(K) \stackrel{\text{def}}{=} \bigcup_{U \supset K\setminus\{0\}} S^0(U). \tag{3}$$

As usual, conjugate spaces are denoted by a prime. The closed cone K is said to be the support cone of the generalized function $w \in S'^0$ if w admits a continuous linear continuation to the space $S^0(K)$, i.e., if $w \in S'^0(K)$. The reader is referred to Refs. 8 and 12 for a justification of this definition. Here we note only that if w is an ordinary function that decreases in the complementary cone $\mathbf{R}^n \setminus K$ more rapidly than a linear exponential and that grows no more rapidly than as a power law in all other directions, then the cone K is a support cone for it. The condition $w \in S'^0(K)$ is actually the correct extension of this decay property to the case of an arbitrary singularity.

2. ASYMPTOTIC COMMUTATIVITY

Let us consider the theory of a finite number of fields $\varphi, \psi, \ldots$, that are operator-valued generalized functions on the space $S^0(\mathbf{R}^4)$ and transform according to finite-dimensional representations of the proper Lorentz group $L_+^\uparrow$ or its covering group $SL(2,\mathbf{C})$. We assume that all the standard assumptions of the general theory of quantum fields,[1,2] with the exception of locality, hold. We denote the general invariant domain of definition of fields in the Hilbert space of states by D and the vacuum by Ψ_0. We will call the Lorentzian components φ_j and ψ_k asymptotically commutative (anticommutative) for a space-like separation of the arguments if for any $\Phi, \Psi \in D$ the matrix element $\langle \Phi, [\varphi_j(x_1), \psi_k(x_2)]_{(+)}^{-} \Psi \rangle$ possesses a support cone $\{(x_1,x_2) \in \mathbf{R}^4 \times \mathbf{R}^4 : (x_1-x_2)^2 \geqslant 0\}$. We replace the locality axiom by the condition of asymptotic commutativity, which means that any two field components either asymptotically commute or asymptotically

anticommute. As usual, we assume that the $-$ or $+$ sign in this condition depends only on the type of field but not on the Lorentzian components, so that in what follows we will omit the Lorentzian indices j,k.

3. GENERALIZATION OF THE SPIN–STATISTICS THEOREM

The first step in the standard derivation of this theorem[1,2] is a proof of the fact that if a field φ possesses different commutation relations with ψ and ψ^*, then either $\varphi(x)\Psi_0=0$ or $\psi(x)\Psi_0=0$. This proof directly transfers to nonlocal fields, since it is based on a weak cluster property of vacuum averages, which follows from the existence and uniqueness of the vacuum without the use of locality axioms (see Ref. 2, Sec. 7.2.B). The second step establishes that an anomalous commutation relation between φ and the conjugate quantity φ^* leads to $\varphi(x)\Psi_0=0$. This step employs the property of analyticity of the vacuum averages in x space; it is the generalization of this property that presents the main difficulty.

For definiteness, we assume that φ is a nonlocal field with integer spin, and we employ the notation

$$W(x_1-x_2)=\langle\Psi_0,\varphi(x_1)\varphi^*(x_2)\Psi_0\rangle,\quad W^{\mathrm{tr}}(x_1-x_2)=\langle\Psi_0,\varphi^*(x_1)\varphi(x_2)\Psi_0\rangle. \tag{4}$$

An anomalous asymptotic commutation relation means that

$$W(\xi)+W^{\mathrm{tr}}(-\xi)\in S'^0(\overline{V}), \tag{5}$$

where $\overline{V}$ is a closed light cone. We regularize the ultraviolet behavior by multiplying $\tilde{W}(p)$ by the cutoff factor $h(p^2/M^2)$, where $h\in\mathcal{D}(\mathbf{R})$ and $h(t)=1$ for $|t|\leqslant 1$. The regularized vacuum average W_M is a Lorentz-covariant distribution with moderate growth and the Bargmann–Hall–Wightman theorem (BHW theorem), according to which $W_M(\xi)=W_M(-\xi)$ for $\xi^2<0$, is applicable to it. Therefore the difference $T_M\overset{\mathrm{def}}{=}W_M(\xi)-W_M(-\xi)$ admits a continuous continuation onto the space $S^0(\overline{V})$, which can be given by the formula $(\hat{T}_M, f)=(T_M, \chi f)$, where χ is a multiplier in the Schwartz space S, identically equal to 1 in an ϵ-neighborhood of $\overline{V}$. It is important that these continuations be consistent with each other, specifically,

$$\hat{T}_M|S^{0,b}(U)=\hat{T}_{M'}|S^{0,b}(U), \tag{6}$$

if $U\supset\overline{V}\setminus\{0\}$ and M, M' are sufficiently large compared to b. Indeed, $(W_M, g)=(W, g)$ for $g\in S^{0,M}$, since then supp $\tilde{g}$ is contained in a sphere of radius M. For $M>8neb$, according to Theorem 5 in Ref. 13, the space $S^{0,M}$ is dense in $S^{0,b}(U)$ according to the topology of $S^{0,M}(U)$, whence Eq. (6) follows. Therefore the unregularized difference $W(\xi)-W(-\xi)$ also admits a continuous continuation to $S^0(\overline{V})$, which makes it possible to rewrite formula (5) as

$$W(\xi)+W^{\mathrm{tr}}(\xi)\in S'^0(\overline{V}). \tag{7}$$

But this is compatible with the spectral condition $\mathrm{supp}(\tilde{W}+\tilde{W}^{\mathrm{tr}})\subset\overline{V}^+$ only if

$$W(\xi)+W^{\mathrm{tr}}(\xi)\equiv 0, \tag{8}$$

since the following theorem is valid.

UNIQUENESS THEOREM

If the support of the distribution $u \in \mathcal{D}'$ is contained in a sharp cone, while the support cone of its Fourier transform is different from $\mathbf{R}^n$, then u is identically equal to zero.

The proof of this theorem will be given in the next section. Here we note that in the local theory the distributions $\widetilde{W}$ and $\widetilde{W}^{\mathrm{tr}}$ possess (inverse) Laplace transforms, whose domain of analyticity contains real space-like points, and the vanishing of the sum $W + W^{\mathrm{tr}}$ at these points implies that it equals zero identically on account of the uniqueness of the analytical continuation. My theorem shows that not only the vanishing of $W + W^{\mathrm{tr}}$ for $\xi^2 < 0$ but also the more-rapid-than-linear-exponential decay of $W + W^{\mathrm{tr}}$ in space-like directions are incompatible with the positivity of energy–momentum. After averaging with a test function of the form $\overline{f}(x_1) f(x_2)$ formula (8) goes over to the equality $\|\varphi^*(f)\Psi_0\|^2 + \|\varphi(f)\Psi_0\|^2 = 0$ and implies that $\varphi(x)\Psi_0 = 0$, since f is arbitrary. Moreover, in consequence, any vacuum average containing at least one operator φ equals zero. For example, let φ stand in the next-to-last place. The vacuum average $\langle \Psi_0, \psi_1, \ldots, \psi_{n-1}\varphi\psi_n\Psi_0\rangle$ considered in the relative coordinates $\xi_j = x_j - x_{j+1}$ has a spectrum in a sharp cone $\overline{V^+} \times \ldots \times \overline{V^+}$ and is identical to the generalized function $\langle \Psi_0, \psi_1, \ldots, \psi_{n-1}[\varphi, \psi_n]_{\mp}\Psi_0\rangle \in S'^0(\mathbf{R}^{4(n-1)} \times \overline{V})$. Hence it equals zero once again on account of the uniqueness theorem. Next we use induction.

If φ possesses half-integer spin, then these same considerations forbid the anomalous relation $W(\xi) - W^{\mathrm{tr}}(-\xi) \in S'^0(\overline{V})$, since in this case $W(\xi) + W(-\xi) \in S'^0(\overline{V})$ follows from the BHW theorem, which once again leads to Eq. (8). Further analysis of the commutation relations between different fields in a theory with a finite number of finite-component fields is similar. Ultimately, it can be asserted that the condition of asymptotic commutativity allows for the existence of a Klein transformation, which transforms the initial set of fields into a new set possessing a normal connection between spin and statistics, where fields with integral spin commute asymptotically with all other fields with space-like separation of the arguments, while fields with half-integral spin anticommute asymptotically with one another.

4. PROOF OF THE UNIQUENESS THEORM

Actually, we will obtain a stronger result, from which the required assertion follows as a corollary. A similar uniqueness theorem also holds for a broader class of generalized functions, called ultradistributions and defined on Gel'fand–Shilov spaces $S_0^\alpha, \alpha > 1$. The Fourier dual to S_0^α space is denoted by S_α^0. The space $S_\alpha^0(U)$, where U is an open cone, is given by a formula similar to (2) with $(1+|x|)^{-N}$ replaced by $\exp(-|x/a|^{1/\alpha})$ and is a union of normalized spaces $S_{\alpha,a}^{0,b}(U)$ over $a > 0$, $b > 0$. The spaces $S_\alpha^0(K)$ corresponding to closed cones possess better topological properties than $S^0(K)$, and the following equality can be easily established[14] for spaces conjugate to them:

$$S'^0_\alpha\left(\bigcup_{j=1}^{n} K_j\right) = \sum_{j=1}^{n} S'^0_\alpha(K_j). \tag{9}$$

Moreover, as was shown in Ref. 13, if the cone K is sharp (this is equivalent to the interior region of the conjugate cone $K^* = \{q : qx \geqslant 0, \forall x \in K\}$ being nonempty), then w

$\in S_\alpha'^0(K)$ possesses a Laplace transform $(w,\ e^{i(p+iq)x})$, which is analytic in the region $\mathbf{R}^n+i(\text{int } K^*)$, with the Fourier transform of w being its limiting value in the limit $q \to 0$, $q \in \text{ int } K^*$.

Let $u \in S_0'^\alpha$. Recall[4] that the analytical wave front $WF_A(u)$ consists of pairs (p,ξ), where p runs through the set of points where u is not an analytic function, while ξ is a cone of the directions of ''poor'' behavior of $\tilde{u}$ which are responsible for the appearance of a singularity at the point p.

LEMMA

If $u \in S_0'^\alpha$ and $\tilde{u} \in S_\alpha'^0(K)$, then $WF_A(u) \subset \mathbf{R}^n \times K$.

Indeed, cover K by a finite number of closed sharp convex cones K_j and construct the decomposition $\tilde{u}=\Sigma w_j$, $w_j \in S_\alpha'^0(K_j)$ according to formula (9). Next, take the (inverse) Laplace transform of each w_j. Then u will be a sum of the limiting values of analytic functions from the regions $\mathbf{R}^n+i(\text{int } K_j^*)$, and according to Theorem 9.3.3 in Ref. 4

$$WF_A(u) \subset \mathbf{R}^n \times \bigcup_{j=1}^{n} K_j^{**}. \tag{10}$$

By virtue of closure and convexity one has $K_j^{**}=K_j$. Refining and contracting the covering to K gives the indicated inclusion.

Let us now prove the uniqueness theorem. Let $u \in S_0'^\alpha$ and supp $u \subset V$, where V is a sharp cone. If the support of u contains the point 0, then any vector $\xi \in -V^*$ serves as an outer normal to supp u at this point. According to the Kasiwara theorem (see Ref. 4, Theorem 9.6.6), all nonzero elements of the linear span of the set of normals is contained in $WF_A(u)_0$. Since $\text{int } V^* \neq \emptyset$, this span covers $\mathbf{R}^n$. Hence, by virtue of the lemma, $\tilde{u} \notin S_\alpha'^0(K)$ for $K \neq \mathbf{R}^n$, i.e., only $\mathbf{R}^n$ can be a support cone of $\tilde{u}$. Now let $0 \notin$ supp u. Assume that $\tilde{u} \in S_\alpha'^0(U)$, where $\overline{U} \neq \mathbf{R}^n$, and let $\|\cdot\|_{U,a,b}$ be the norm of the Banach space conjugate to $S_{\alpha,a}^{0,b}$, and let us construct the series $\Sigma_{\nu=1}^{\infty} a_\nu u_\nu$, where $u_\nu(p)=u(\nu p)$. If

$$0 < a_\nu < 1/(\nu^2 \|\tilde{u}_\nu\|_{U,\nu,\nu}), \tag{11}$$

then the series $\Sigma a_\nu \tilde{u}_\nu$ converges in $S_\alpha'^0(U)$, and, moreover, the series $\Sigma a_\nu u_\nu$converges in $S_0'^\alpha$. Let $\mathcal{U}$ denote its sum. It is easy to choose coefficients a_ν so that the support $\mathcal{U}$ will contain the point zero. Indeed, let the distance from supp u to 0 equal 1, and let p_0 be the point of supp u closest to 0. For each $\mu=1,2,\ \ldots$ choose a test function $g_\mu \in S_0^\alpha$, with support in the sphere $|p-p_0/\mu| < (1/2)(1/\mu - 1/(\mu+1))$, such that $(u_\mu, g_\mu)=1$. Note that $(u_\nu, g_\mu)=0$ for $\nu < \mu$. Specify the coefficients a_ν successively, imposing besides (11) the condition $a_\nu|(u_\nu, g_\mu)| \leqslant a_\mu/2^\nu$ for $\mu < \nu$. Then for each μ

$$(\mathcal{U}, g_\mu) = a_\mu + \sum_{\nu>\mu} a_\nu (u_\nu, g_\mu) \neq 0,$$

since $\Sigma_{\nu>\mu} a_\mu/2^\nu \leqslant a_\mu/2$. Thus $0 \in$ supp $\mathcal{U}$, and we have returned to the situation considered above. This completes the proof.

5. CONCLUDING REMARKS

The relation established in Sec. 4 between the analytical wave front of a distribution (ultradistribution) and the support cone of its Fourier transform makes it possible to approach differently other problems of the theory of nonlocal interactions, including the extension of the CPT theorem to them, the expansion of the Borchers equivalence classes, the construction of superpropagators, and others. The derivation, based on the uniqueness theorem, of the necessary and sufficient conditions for CPT symmetry will be given in a companion paper. The spaces $S^0_\alpha(K)$ were invoked in order to circumvent the difficulties connected with the derivation of the analog of formula (9) for $S'^0(K)$. However, the fields could have been assumed from the very beginning to be given on S^0_α — this gives not only a broader framework for constructing a theory but also a convenient operational calculus, the principles of which are set forth in Refs. 12–14. The space S^0 has been used in many works on nonlocal theory of fields primarily because $\tilde{S}^0$ is identical to the Schwartz space $\mathcal{D}$ appearing in the standard arsenal of the theoretical physicist. I followed tradition, but there is no need for this. The topological structure of the spaces $S^0(K)$ is very complicated, and even the proof of completeness for them is a serious problem, whose solution requires the use of homological methods. I note also that in the present letter I adhered to the standard Bose–Fermi alternatives and I did not consider intermediate statistics. However, the condition of asymptotic commutativity can also be formulated for nonlocal parafields, after which the question of the connection between spin and parastatistics actually reduces to the analysis set forth above.

I am grateful to Professor V. Ya. Faĭnberg for a helpful discussion. I am also grateful the Russian Fund for Fundamental Research for funding under Grant 96-02-16117 and to INTAS for funding under Grant 96-0398.

[a)]e-mail: soloviev@td.lpi.ac.ru

---

[1] R. F. Streater and A. S. Wightman, *PCT, Spin and Statistics and All That*, Benjamin, Reading, 1964 [Russian translation, Nauka, Moscow, 1966].
[2] N. N. Bogolyubov, A. A. Logunov, A. I. Oksak *et al.*, *General Principles of Quantum Field Theory* [in Russian], Nauka, Moscow, 1987.
[3] W. Pauli in *Niels Bohr and the Development of Physics*, Pergamon, London, 1955 [Russian translation, IL, Moscow, 1958].
[4] L. Hörmander, *The Analysis of Linear Partial Differential Operators*, Vol. 1, Springer, Berlin, 1983 [Russian translation, Mir, Moscow, 1986].
[5] N. N. Meĭman, Zh. Éksp. Teor. Fiz. **47**, 1966 (1964) [Sov. Phys. JETP **20**, 1320 (1965)].
[6] A. Jaffe, Phys. Rev. **158**, 1454 (1967).
[7] V. Ya. Fainberg and A. L. Filkov, JETP Lett. **58**, 870 (1993).
[8] V. Ya. Fainberg and M. A. Soloviev, Teor. Mat. Fiz. **93**, 514 (1992).
[9] M. Z. Iofa and V. Ya. Faĭnberg, Zh. Éksp. Teor. Fiz. **56**, 1644 (1969) [Sov. Phys. JETP **29**, 880 (1969)].
[10] W. Lücke, Commun. Math. Phys. **65**, 77 (1979).
[11] W. Lücke, Acta Phys. Austriaca **55**, 213 (1984).
[12] M. A. Soloviev, in *Developments in Mathematics: The Moscow School*, Chapman and Hall, London, 1993.
[13] M. A. Soloviev, Commun. Math. Phys. **184**, 579 (1997).
[14] M. A. Soloviev, Lett. Math. Phys. **33**, 49 (1995).

Translated by M. E. Alferieff

Noise-induced hypersensitivity to weak alternating signals

S. L. Ginzburg and M. A. Pustovoĭt[a)]
B. P. Konstantinov St. Petersburg Institute of Nuclear Physics, Russian Academy of Sciences, 188350 Gatchina, Leningrad Region, Russia

(Submitted 10 March 1998)
Pis'ma Zh. Éksp. Teor. Fiz. **67**, No. 8, 592–596 (25 April 1998)

An example of the helpful role of noise in information transmission processes is the well-known phenomenon of stochastic resonance. This letter examines another such example — parametric-noise-induced giant amplification of ultraweak signals in a system with on–off intermittency. © *1998 American Institute of Physics.*
[S0021-3640(98)01408-X]

PACS numbers: 05.40.+j, 07.50.Qx, 07.50.Hp

Until recently the role of noise in information transmission processes was considered to be purely destructive. However, not too long ago the phenomenon of stochastic resonance was discovered, i.e., signal amplification and improvement of the signal/noise ratio accompanying the transmission of a signal to which noise with the optimal intensity is added. It has been shown experimentally and theoretically that stochastic resonance can exist in the most diverse systems, ranging from ice ages to SQUIDs (see, for example, Ref. 1). This demonstrates that noise can play an important constructive role in the signal transmission process.

In the present letter we shall demonstrate this constructive role for another example — a simple stochastic model demonstrating the property of on–off intermittency. Systems with on–off intermittency have been attracting increasing the attention of investigators in recent years.[2–4] These systems are characterized by giant fluctuations of the physical quantities, which can assume finite values with close probability and become vanishingly small in the laminar phase. We shall describe below an unusual phenomenon we discovered in these systems, which appears as a result of the presence of parametric noise with the optimal intensity in them — a giant response of a system to very small actions (hypersensitivity), when perturbations of the order of 10^{-20}, for example, give rise to a response of the order of 1.

The simplest equation capable of demonstrating on–off intermittency is the equation of an overdamped Kramers oscillator:[5,6]

$$dx/dt=\lambda x+\beta\xi(t)x-Ux^3+\sigma\varphi(t)+AR(t),$$

$$\langle\xi(t)\xi(t')\rangle=\langle\varphi(t)\varphi(t')\rangle=\delta(t-t'),\quad \langle\xi(t)\varphi(t')\rangle=0, \tag{1}$$

$$R(t+T)=R(t)=\begin{cases}1, & 0<t\leqslant T/2\\ -1, & T/2<t\leqslant T.\end{cases}$$

Here $\xi(t)$ and $\varphi(t)$ are Gaussian white noise; λ, β, U, σ, and A are constants; and, $R(t)$ is a periodic square-wave signal. Equation (1) is to be understood in the Stratonovich sense. We can see that noise appears in this equation both additively and multiplicatively, and, as will be seen below, the latter noise gives rise to hypersensitivity. We note that the case $A=\sigma=0$ was studied in detail in Ref. 5.

In the absence of noise ($\beta=\sigma=0$) and for $A\ll 1$ Eq. (1) can be easily solved, and it can be shown that the amplitude of the output signal $\Delta x\sim A/|\lambda|$, i.e., there is no signal amplification.

The Fokker–Planck equation (FPE) for Eq. (1) has the form

$$\frac{\partial F}{\partial t}=-\frac{\partial}{\partial x}\left\{\left[\left(\lambda+\frac{\beta^2}{2}\right)x-Ux^3+AR(t)\right]F\right\}+\frac{1}{2}\frac{\partial^2}{\partial x^2}\{(\beta^2x^2+\sigma^2)F\}. \tag{2}$$

It is quite difficult to solve Eq. (2) in general form. For this reason, we shall employ the following approximation. The signal $R(t)$ in Eq. (1) assumes two values: ± 1. Let T_0 be the transient relaxation time after the signal is switched from one value to another. Let the signal satisfy the adiabaticity condition

$$T\gg T_0. \tag{3}$$

The FPE in this case can be easily solved. We obtain for $(A,\sigma)\ll(\lambda,\beta,U)$

$$F(x)=C\left(x^2+\frac{\sigma^2}{\beta^2}\right)^{(\alpha-1)/2}\exp\left\{\frac{2AR(t)}{\beta\sigma}\arctan\frac{\beta x}{\sigma}-\frac{Ux^2}{\beta^2}\right\}, \tag{4}$$

$$\alpha=2\lambda/\beta^2,$$

where C is a normalization constant.

In what follows we shall have everywhere β, $U\sim 1$, $\lambda\sim 0.01$, A, $\sigma\sim 10^{-n}$, $n\gg 1$. Then, in a very wide range $10^{-n}\ll x\ll 1$, we obtain from Eq. (4) a scaling distribution density

$$F(x)\sim x|^{\alpha-1}, \tag{5}$$

which, according to Refs. 6–8, is a criterion for the existence of on–off intermittency. Let us examine the limit $\sigma\to 0$ (the weak signal is much stronger than the additive noise). Assuming

$$\arctan\frac{\beta x}{\sigma}\overset{\sigma\to 0}{\to}\frac{\pi}{2}\operatorname{sign}x-\frac{\sigma}{\beta x},$$

we obtain

$$F(x)=C|x|^{\alpha-1}\exp\left\{\frac{A\pi R(t)}{\beta\sigma}\operatorname{sign}x-\frac{2AR(t)}{\beta^2x}-\frac{Ux^2}{\beta^2}\right\}. \tag{6}$$

The large first term in the exponential in Eq. (6) means that in the case of a positive signal R the distribution density is different from zero only for positive x, while for a negative signal it is different from zero only for negative x, i.e.,

$$F(x)=C|x|^{\alpha-1}\theta(\text{sign } AR(t)x)\exp\left\{-\frac{2AR(t)}{\beta^2 x}-\frac{Ux^2}{\beta^2}\right\}, \tag{7}$$

where $\theta(x)$ is the Heaviside unit step function. The normalization factor C cannot be calculated exactly, but its asymptotic expressions for $|\alpha|\ll 1$, $U/\beta^2\sim 1$ are

$$C=\begin{cases}\alpha;\ \alpha>0, & z\gg 1,\\ 1/\ln\dfrac{1}{A}; & z\ll 1,\\ |\alpha|A^{|\alpha|}; & \alpha<0,\quad z\gg 1,\end{cases} \tag{8}$$

$$z=|\alpha|\ln\frac{1}{A}.$$

The changeover in the asymptotic behavior in Eq. (8), i.e., crossover, occurs when the parameter z becomes of the order of 1, i.e., at a signal amplitude

$$A_0=\exp(-1/r|\alpha|). \tag{9}$$

Thus, for small values of α a very weak signal is capable of radically altering the distribution density.

To estimate the amplitude of the output signal we shall calculate the moments of $F(x)$ for $z\ll 1$. Using the explicit form of $R(t)$ we obtain

$$\langle x(t)\rangle=\frac{\beta}{2}\sqrt{\frac{\pi}{U}}\frac{1}{\ln(1/A)}R(t),\quad \langle x^2(t)\rangle=\frac{\beta^2}{2U}\frac{1}{\ln(1/A)}, \tag{10}$$

$$\frac{\langle x(t)\rangle^2}{\langle x^2(t)\rangle}=\frac{\pi}{2\ln(1/A)}\ll 1.$$

The signal gain equals

$$I=\frac{\langle x(t)\rangle}{AR(t)}=\sqrt{\frac{\pi}{4UA}}\frac{\beta}{\ln(1/A)}. \tag{11}$$

For example, for $\beta=0.7$, $U=1$, and $A=10^{-11}$ we obtain $I=2.5\times 10^9$. Therefore, on account of the multiplicative noise, our model of an overdamped Kramers oscillator possesses the property of hypersensitivity to weak signals. A similar phenomenon — sensitivity of a system to a weak *constant perturbation* as a result of the noise added to the perturbation — was studied earlier (see Ref. 9 and references cited therein) for the example of the chiral selectivity of a chemical reaction. In our case, aside from the fact that the noise that induces the sensitivity is parametric, the system can amplify a signal that is *time-dependent*. Even though the variance of x is large compared with the signal, the phenomenon can be easily observed by standard statistical methods. For example, Fig. 1 displays the time series of $\langle x(t)\rangle$ for $A=10^{-11}$, $\lambda=-0.01$ and 0.01, $\beta=1.0$, $U=1$ as averages over an ensemble of 4100 time series of $x(t)$ with the same phase of

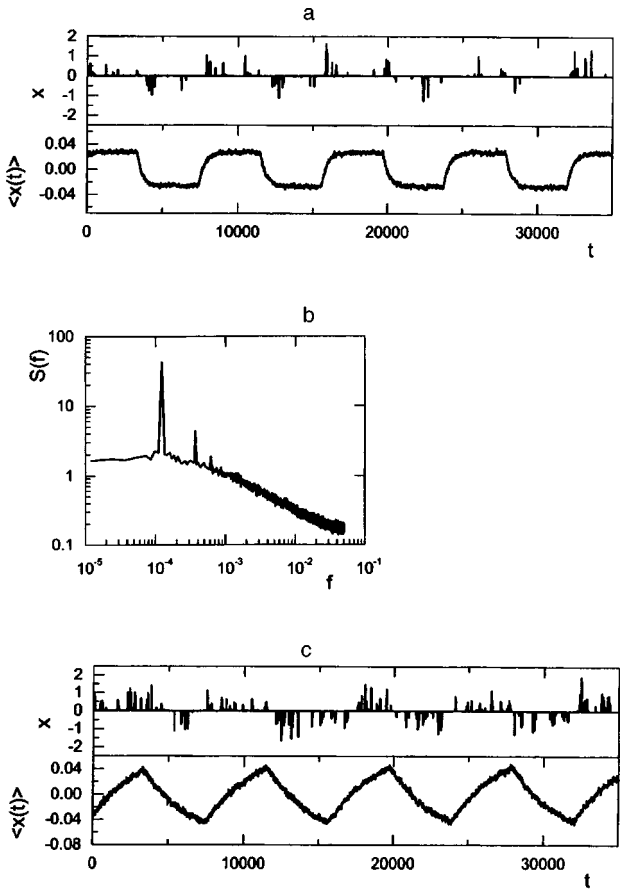

FIG. 1. a) Time series of the output signal x and of the average $\langle x(t)\rangle$ over an ensemble of 4100 time series with the same phase of the input signal for $\beta=1.0$ and $\lambda=-0.01$. b) Power spectrum of the signal x in part (a), obtained by averaging over 200 time series with a random phase; c) Same as a but with $\lambda=0.03$. The amplitude of the input signal $A=10^{-11}$, the period $T=8192$.

the input signal. We note that for comparatively small *average* magnitudes of the signal, the *instantaneous* values of the amplitude can reach values of the order of 1, making it possible to observe an ultraweak signal with a low-sensitivity detector. If the adiabaticity condition holds, then according to Eq. (10) $\langle x(t)\rangle = yR(t)$, and the gain $I=y/A$. However, if the adiabaticity condition does not hold, then I can be determined from the formula

$$I^2=\frac{1}{T}\int_0^T\frac{\langle x(t)\rangle^2}{A^2}dt. \tag{12}$$

Since, as one can see from Fig. 1, $\langle x(t)\rangle$ remains a stochastic function even after averaging over a large number of time series, the coefficient I in Eq. (12) is most conveniently calculated by a different method. In Ref. 10 it is shown that if we have a set of time series with a random phase, then their spectral density equals

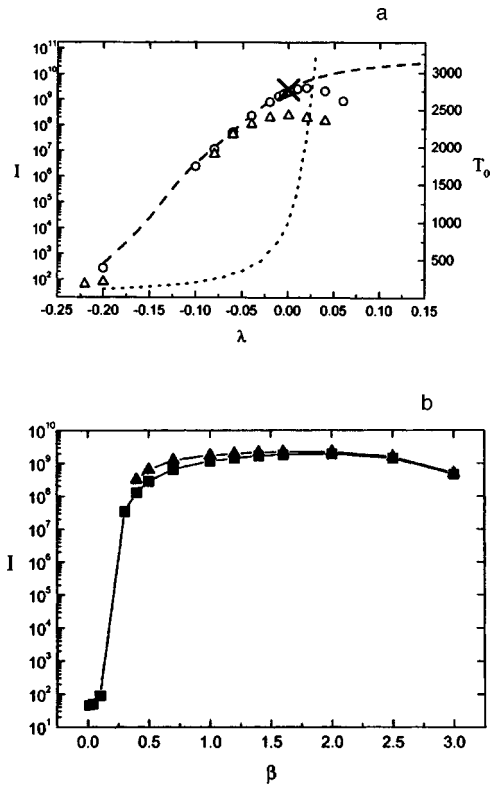

FIG. 2. a) Gain I with signal period $T=819$ (Δ) and $T=8192$ ($\bigcirc$) and relaxation time T_0 (dotted line) versus the parameter λ for fixed $\beta=0.7$. The dashed line shows the results obtained with a static input signal. Cross — estimate (11). b) I versus the intensity β of multiplicative noise for $\lambda=-0.01$ ($\blacksquare$) and 0.01 ($\blacktriangle$). The parameters of the input signal are the same as in Fig. 1.

$$S(\omega)=2\pi\sum_k |x_k|^2\delta(\omega-k\Omega)+S_{\text{noise}}(\omega),$$

where x_k are the Fourier coefficients of the periodic function $\langle x(t)\rangle$, while S_{noise} is the noise contribution to the spectral density. From Eq. (12) it is evident that

$$I^2=\sum_k |x_k|^2/A^2, \text{ i.e., } \quad I^2=\frac{\delta f}{A^2}\sum_i (S_i-S_{\text{noise}}),$$

where S_i is the ith harmonic of the signal in the spectrum and δf is the spectral band width. Figure 2a displays I as a function of the parameter λ for fixed noise $\beta=0.7$. One can see that the estimate (11) written for the case $|\alpha|\approx 0$ is in excellent agreement with the calculations. The dashed line in the figure shows the results obtained with a constant input signal ($R(t)=1$). The gain drops below the static value when the relaxation time T_0 (dotted line in Fig. 2a; an analytical estimate is $T_0\sim A^{-\alpha}$) becomes comparable to the period of the signal, i.e., the condition of adiabaticity breaks down. As the period of the signal increases, the region of adiabaticity increases, as one can see in Fig. 2a. Figure 2b

demonstrates the dependence of the gain on the magnitude of the controlling (multiplicative) noise. This dependence has a maximum, just as in the case of the standard stochastic resonance, the difference being that in our system the signal is additive while the noise is parametric.

In summary, we have demonstrated analytically and by computer simulation that at small absolute values of the parameter α a simple stochastic system with on–off intermittency possesses noise-induced hypersensitivity to weak alternating signals. This is an example of the constructive role of noise in nature.

This work was supported by the State Program ''Physics of Quantum and Wave Processes,'' subprogram ''Statistical Physics,'' Project VIII-3, and by the State Program ''Neutron Investigations of Matter.''

[a)]E-mail: markp@hep486.pnpi.spb.ru

[1] L. Gammaitoni, P. Hänggi, P. Jung, and F. Marchesoni, Rev. Mod. Phys. **70**, 223 (1998).
[2] N. Platt, E. A. Spiegel, and C. Tresser, Phys. Rev. Lett. **70**, 279 (1993).
[3] J. F. Heagy, N. Platt, and S. M. Hammel, Phys. Rev. E **49**, 1140 (1994).
[4] N. Platt, S. M. Hammel, and J. F. Heagy, Phys. Rev. Lett. **72**, 3498 (1994).
[5] W. Horsthemke and R. Lefever, *Noise-Induced Phase Transitions*, Springer, New York, 1984.
[6] H. L. Yang and E. J. Ding, Phys. Rev. E **54**, 1361 (1996).
[7] A. S. Pikovsky, Phys. Lett. A **165**, 33 (1992).
[8] A. S. Pikovsky and P. Grassberger, J. Phys. A **24**, 4567 (1991).
[9] D. K. Kondepudi, I. Prigogine, and G. W. Nelson, Phys. Lett. A **111**, 29 (1985).
[10] P. Jung, Phys. Rep. **234**, 175 (1993).

Translated by M. E. Alferieff

ERRATA

Erratum: Optical phonons in quantum-wire structures [JETP Lett. 67, No. 2, 120–134 (25 January 1998)]

A. Milekhin, Yu. Pusep, Yu. Yanovskiĭ, V. Preobrazhenskiĭ, and B. Semyagin

Institute of Semiconductor Physics, 630090 Novosibirsk, Russia
Pis'ma Zh. Eksp. Teor. Fiz. **67**, No. 8, 597 (25 April 1998)

[S0021-3640(98)01508-4]

PACS numbers: 63.22.+m, 78.30.Fs, 99.10.+g

The first two sentences of the body of the paper should read as follows:

Progress in molecular-beam epitaxy (MBE) technology has made it possible to grow perfect GaAs/AlAs superlattices (SLs) on high-index GaAs surfaces, such as (011),[1] (112),[2,3] and (311).[2–4] The lower symmetry of these SLs as compared with SLs on (100)-oriented GaAs/AlAs leads to optical anisotropy in the plane of the SL layers.[2–6]

Also, Eq. (1) should read

$$q_m = m\pi/\{(n+\delta)d\}, \quad d = a/\sqrt{11}. \tag{1}$$

